SELF-DAMPING CHARACTERISTICS OF TRANSMISSION LINE CONDUCTORS SUBJECTED TO FREE AND FORCED VIBRATION

Molungoa Samuel Mokeretla

Dissertation submitted in fulfilment of the
requirements for the degree

MAGISTER TECHNOLOGIAE:
ENGINEERING: MECHANICAL
in the

School of Mechanical Engineering and Applied Mathematics

Faculty of Engineering and Information Technology
at the

Central University of Technology, Free State

Supervisor: Prof. M.A.E. Kaunda (Pr Eng, PhD)

BLOEMFONTEIN
February 2011

DECLARATION OF INDEPENDENT WORK

DECLARATION WITH REGARD TO INDEPENDENT WORK

I, MOLUNGOA SAMUEL MOKERETLA, identity number [redacted] and student number 20423756, do hereby declare that this research project submitted to the Central University of Technology, Free State for the degree MAGISTER TECHNOLOGIAE: ENGINEERING: MECHANICAL, is my own independent work and complies with the Code of Academic Integrity, as well as other relevant policies, rules and regulations of the Central University of Technology, Free State, and has not been submitted before to any institution by myself or any other person in fulfilment (or partial fulfilment) of the requirements for the attainment of any qualification.

_____ _____

SIGNATURE OF STUDENT **DATE**

ABSTRACT

The objectives of this research were to investigate and establish a procedure to determine the self-damping characteristics of transmission line conductors subjected to free and forced vibrations. The TERN and Aero-Z IEC62219-REV240609 conductor cables were the transmission line conductors that were readily available at the Vibration Research and Testing Centre (VTRC) of the University of KwaZulu-Natal (UKZN).

The question to be answered was whether the self-damping characteristics of the TERN and Aero-Z IEC62219-REV240609 conductors were adequate to suppress Aeolian or wake-induced vibrations. In other words, is it necessary for external damping mechanisms to be used with these conductors? This study confirmed that the self-damping characteristics of conductors are not adequate to suppress Aeolian or wake-induced vibrations.

Governing partial differential equations describing the characteristics of the catenary and parabolic cable conductors were developed to validate the experimental results.

The experimental tests involved both conductors being subjected to an impulse function (a free vibration method) and also to a harmonic function (a forced vibration method). Measurements were carried out using accelerometers, and the recording equipment consisted of oscilloscopes and the PUMA system.

With both the free and forced vibration methods, the damping factor of the TERN conductor was confirmed to be $\zeta \leq 0.05,$ whereas the damping factor of the Aero-Z IEC62219-REV240609 was confirmed to be $\zeta \leq 0.2$.

A procedure for determining the self-damping characteristics of the TERN and Aero-Z IEC62219-REV240609 conductors was developed, with the damping factor found to be

$\zeta \leq 0.2$ for both conductors. These methods can assist in the implementation of procedural analysis of the self-damping behaviour of different types of transmission conductors and in finding the most suitable mass absorber (damper) to use in reducing the rate of failure of transmission line conductors. The results of this study can be used to improve the mathematical modelling of Aeolian and wind-induced vibrations where both self-damping properties and a mass absorber are incorporated.

ACKNOWLEDGEMENTS

I would like to thank the following individuals for their valuable assistance and support:

My supervisor, Prof. M.A.E. Kaunda, for his guidance and advice;

Pravesh Moodley of the University of KwaZulu-Natal's Vibration Research and Testing Centre, for providing valuable information and the necessary laboratory facilities for testing purposes;

My friends and colleagues at the Central University of Technology, Free State; and

My parents; Marake and Mamolungoa Mokeretla, for their unfailing moral support and encouragement when I needed it most.

I would also like to acknowledge the generous financial support of the Central University of Technology, Free State, the Vibration Research and Testing Centre at the University of KwaZulu-Natal, as well as the Tertiary Education Support Programme (TESP) of Eskom.

TABLE OF CONTENTS

LIST OF FIGURES

LIST OF TABLES

List of symbols

c	Wave speed
f	Frequency
l	Loop length
L	Span length
ρA	Conductor mass/unit length
n	Number of loops
p	Wave number
T	Conductor tension
w	Weight of each conductor / unit length
λ	Wavelength
ω	Angular velocity
ζ	Damping factor
ς	Damping factor
δ	Viscous damping
c	Damping coefficient
D	Conductor diameter
EI	Flexural rigidity
EI_0	Undamped flexural rigidity
η	Loss factor
r	Mode number
$\hat{Y}_\tau$	Antinodes' displacement amplitude
Y^a	Fourier analysis
F_{sd}	Self-damping force for single-mode vibration
F_{ad}	Self-damping force during Aeolian vibration
$f(t) = \delta(t)$	Impulse function
$f(t) = F \sin \omega t$	Sinusoidal or harmonic function
S	Cable length
$T_{\max}$	Maximum tension
T_o	Uniform horizontal distribution of load
h	Sag
R	Resultant
ρ	Density

A	Cross-Sectional area
$y(t,x)$	Deflection
t	Function of time
x	Distance along cable
μ	Weight per unit length
c	Wave propagation velocity
A	Amplitude
k	Wave number
Q	Quality factor
ω_n	Resonant frequency (rad/s)
f_n	Resonance frequency (Hz)
f_1 and f_2	Half-power
Δf	Bandwidth
G	Accelerations (m/s^2)
d	Displacement (mm)
τ	Period
F_o	Amplitude
h	Non-dimensional damping

Chapter 1

INTRODUCTION

Many countries that use transmission lines have discovered that failure on the transmission lines is often caused by Aeolian and wake-induced vibration, which can have a major impact on the structural lifetime and service of transmission lines. Quite often, the presence of vibration is not desirable, and the interest lies in the reduction thereof. The increasing demand for the improvement of existing methods and the development of new techniques for controlling vibration on transmission line conductors is a major concern. In the case of unacceptable vibration and acoustics, there is a need to understand the overall nature of the problem, including the internal and external damping characteristics of the conductor. This dissertation describes the researcher's mission to investigate and establish a procedure to determine the self-damping (internal damping) of transmission line conductors due to free and forced vibration.

1.1 Background

Conductor vibration: Overhead transmission and distribution line designs need to be analysed to ensure that wind-produced vibration will not cause failures or damage to the conductor (PLP, 2008). Almost every rural distribution line will experience some Aeolian vibration at times. Certain locations and prevalent weather conditions may affect certain line designs and produce amplitude and vibration frequencies that will cause fatigue failure of the conductor or structural components. Because so many factors are involved, it is extremely difficult to establish a single set of guidelines applicable to all conductor designs.

Aeolian vibration: This is the most common type of vibration and results from vortex shedding under laminar flow of wind. This is a low-amplitude vibration with a maximum frequency of 3-60 Hz for wind speeds of 1-8 m/s). Sometimes, additional sinusoidal waves

of differing frequencies arise on the line, corresponding to a higher mode of vibration. This vibration lies on the vertical plane, exerts continuous alternating bending stresses on the conductor strands, and may eventually lead to fatigue failure of the conductor (PLP, 2008).

Conductor galloping: Also known as long-wave vibration, this is characterised by low frequencies of 0.1-1 Hz. This phenomenon is most common when there is sleet covering the cable, because this coating of ice creates irregular edges and surfaces, disturbing the air flow, which breaks away at these points to induce a certain self-excitation. Thus the system becomes susceptible to vibration subject to resonance. The conditions most conducive to galloping are low pressure with high winds and a temperature of between 0 and -5 ^{0}C (PLP, 2008).

Wake-induced oscillation: This type of vibration occurs when bundled conductors are exposed to moderately strong crosswinds, and arises from the shielding effect that windward sub-conductors have on leeward ones. The wake proceeding downwind from a stationary windward sub-conductor can subject the leeward sub-conductor to a complex and variable set of forces, which, depending on the relative magnitude, may suppress the motion of the leeward sub-conductor or may cause it to move in an elliptical and irregular orbit. This complicates both the aerodynamic and mechanical forces acting upon the leeward sub-conductor. At worst, wake-induced oscillation may cause suspension hardware failure or crushing of the conductor strands due to clashing. In most cases, damage is limited to rapid wear in suspension hardware, or fatigue of spacers or other accessories (PLP, 2008).

Damping: This is of great importance in the dynamic design of engineering structures, especially for response prediction and vibration control. The two major mechanisms of vibration control are energy dissipation and vibration isolation Inman, 2001).

Self-damping: According to Vecchiarelli, Currie and Havard (1995), "When a conductor flexes, the strands of the conductor slip against each other; this relative motion generates frictional forces that provide damping. In addition, internal losses are incurred at the microscopic level within the core and individual strands of the conductor; this is known as metallurgical or material damping. The combination of these dissipative effects is referred to as conductor self-damping." Conductor self-damping can be a major source of energy dissipation during Aeolian vibration. However, as conductor tension increases, the strands tend to lock and slippage is reduced. As a result, conductor self-damping decreases and the severity of Aeolian vibration increases, thereby raising the potential for fatigue damage. It is for this reason that the tension of an undamped conductor is kept relatively low.

Free vibration: This is the natural response of a structure to a particular impact or displacement and is wholly determined by the structure's mechanical properties (Inman, 2001).

Forced vibration: This is the response of a structure to a repetitive forcing function that causes the structure to vibrate at the frequency of the excitation (Inman, 2001).

1.2 Problem statement

By means of this study, the researcher sought to develop a procedure for determining conductor self-damping, including damping factors, oscillation decay, travelling wave, and resonant frequencies. This also involved further investigation into the internal damping of a conductor (self-damping) to determine the necessity of external dampers. This required the use of laboratory test methods to measure the self-damping properties of conductors.

1.3 Scope

This research is limited to the self-damping characteristics of transmission line conductors subjected to free and forced vibration methods.

1.4 Hypothesis

The increasing demand for the improvement of existing methods and the development of new techniques for controlling the vibration of transmission line conductors is a major concern. Various researchers (including Noiseux, 1992) have studied the phenomenon of self-damping, but there is a lack of empirical procedures for the analysis of the self-damping behaviour of a conductor. Moreover, manufacturers do not provide specific standards relating to the internal damping of a conductor, which might explain the prevalence of failure in transmission line conductors. It is therefore necessary to firstly understand the self-damping characteristics of transmission line conductors before considering other factors that may have an influence on transmission lines. The use of mass absorbers without considering the influence of self-damping disregards the true behaviour of the conductor.

The self-damping characteristics of conductors are not supplied by the manufacturers and must therefore be determined by means of research so that they can be incorporated in mathematical modelling. The damping of conductors is usually done by means of the addition of mass absorbers, but since the self-damping characteristics are not known, mathematical modelling cannot be effectively implemented.

1.5 Methodology

There are several methods that can be used to measure the self-damping of transmission line conductors, but this research focused on two main methods, namely "free vibration" and "forced vibration".

The test was applied to a conductor subjected to an impulse function, which is a free vibration method, and also to a harmonic function, which is a forced vibration method (see Figure 1 below).

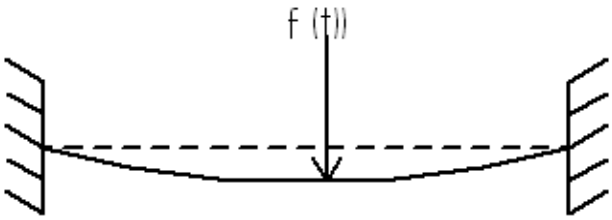

Figure 1: Conductor under functional load

Test case 1: Free vibration: $f(t) = \delta(t)$ - impulse function
Test case 2: Forced vibration: $f(t) = F \sin \omega t$ - sinusoidal or harmonic function

Free vibration method: The theory relating to the free vibration method is discussed in Chapter 3 of this dissertation. The procedure relating to the free vibration method is discussed in Chapter 5 of this dissertation. The conductor was subjected to an impulse function whereby a hammer was used to introduce an impulse force. Accelerometers were used as measuring instruments from which an oscilloscope recorded the data. Using the data captured by the oscilloscope, the log decrement method developed in Chapter 3 (Section 3.7: Measurement of damping) was used to calculate the log decrement (δ) and the corresponding damping factor (ς).

Forced vibration method: The theory and procedure relating to the forced vibration method are discussed in Chapter 4 of this dissertation. The conductor was subjected to a harmonic function whereby an electrodynamics exciter motor or shaker was employed. Measurements were carried out by accelerometers from which data was recorded onto the PUMA system, which incorporated the control system of the electrodynamic shaker. A sweep test was done to locate the natural frequencies, the details of which were used to calculate the quality factor (Q) to obtain the damping factor (ζ) (see Section 4.2: Quality factor as a measure of damping).

The results: Chapter 6 of this dissertation details the results for the free vibration method (Section 6.2) and the forced vibration method (Section 6.3). In Chapter 7, the results found

for the free vibration method of TERN conductor are compared with the results found for the free vibration method of Aero-Z IEC62219-REV240609 conductor (Sections 7.2. and 7.3). In Chapter 8, the results found for the forced vibration will be compared with the results found in Chapter 7 for the free vibration method. Furthermore, the self-damping (internal damping) results are compared with the external damping results to check whether the self-damping characteristics of a transmission line conductor are adequate to suppress Aeolian and wind-induced vibrations (Sections 7.3 and 8.3.).

1.6 Structure of the dissertation

Chapter 1 of the dissertation forms the introduction.

Chapter 2 contains the literature review.

Chapter 3 is dedicated to the free vibration method, discussing the theoretical background.

Chapter 4 is dedicated to the forced vibration method, discussing the theoretical background.

Chapter 5 contains the apparatus and experimental procedure used on free vibration method and forced vibration method.

Chapter 6 presents the results for both the free and the forced vibration methods.

Chapter 7 discusses the analysis of results for free vibration method.

Chapter 8 discusses the analysis of results for forced vibration method.

Chapter 9 contains the discussion of the results.

Chapter 10 provides the conclusions of this study.

Chapter 11 lists the recommendations arising from this study.

Chapter 12 contains the list of references used in this study.

The appendices follow at the end of the dissertation.

Chapter 2

LITERATURE REVIEW

2.1 Introduction

The purpose of this Chapter is to reflect the background knowledge gathered from other researchers and link it with the research conducted for purposes of this dissertation. The author's deductions are shown in italics. The literature review outlines conductor vibrations, the importance of studying the self-damping characteristics of transmission line conductors, the methods used by other researchers and their findings, as well as the conclusion.

2.2 Conductor vibrations

For purposes of this dissertation, overhead transmission and distribution line designs were analysed in order to determine a method to prevent wind-produced conductor vibration from causing line failures or damage (PLP, 2008). Almost every rural distribution line included in the study would have experienced some Aeolian vibration. Different locations and prevalent weather conditions had affected certain line designs, producing amplitude and vibration frequencies that had caused fatigue failure of the conductor or structure components. Since so many factors were involved, it was extremely difficult to establish a single set of guidelines applicable to all conductor designs. *It therefore became clear that certain properties of the conductors, such as self-damping, would have to be analysed in an effort to limit failure caused by vibration.*

2.3 Reasons for studying the self-damping characteristics of transmission line conductors

The increasing demand for the improvement of existing methods and the development of new techniques for controlling vibration on transmission line conductors is a major

concern. A number of researchers [Noiseux, 1992; Vecchiarelli *et al.*, 1995) have examined the topic of self-damping, but there is a lack of empirical information on conductor damping forces, as well as a lack of an empirical procedure to determine the self-damping characteristics of transmission line conductors. Manufacturers also do not provide specific standards relating to the internal damping of conductors, which might cause them to fail. *The author therefore identified the need to understand the self-damping characteristics of transmission line conductors before considering other aspects that could have an influence on the functioning of transmission lines. The use of mass absorbers without considering the influence of self-damping does not provide a true picture of the functioning of the conductor, and certain procedures would have to be developed for this purpose*.

Previous studies have focused on reducing vibration by means of the dissipation of the vibration energy. Many laboratory studies on conductor self-damping have been performed, but in such cases it was found that determining the energy dissipated due to conductor self-damping was not a straightforward process (Vecchiarelli *et al.*, 1995). Significant discrepancies in experimental results could occur as a result of extraneous sources of damping, such as aerodynamic resistance. *This shows that more advanced technology is needed in determining the internal damping of a conductor*.

2.4 Other researchers' methods and results

Boltezar and Otrin (2007) studied the lateral vibrations of straight and curved cables with no axial preload. The finite element used was based on the Euler-Bernoulli theory, and the researchers studied the dissipation of energy with viscous and structural damping models. They also identified the Rayleigh coefficients and the frequency dependence of the loss factor. Using equality between measured and computed natural frequencies; the estimated-frequency depended on the dynamic modulus of elasticity and was used for all cables studied. The experimental measurements were based on mathematical models, and the support excitation was achieved by the use of an electrical shaker. The amplitude force was measured at the fixed support with a dynamometer. For the curved cable, the mathematical

model was verified for in-plane and out-of-plane vibrations. Their results appear below (Boltezar & Otrin, 2007).

Table 1: Difference of the damping ratios for the two identification methods, for length $l = 0.253\,m$

Mode number	1	2	3
LSM_t	0.0323	0.0106	0.0103
NY_f	0.029	0.0135	0.012

Table 2: Difference of the damping ratios for the two identification methods, for length $l = 0.328\,m$

Mode number	1	2	3	4
LSM_t	0.024	0.00984	0.0097	0.0098
NY_f	0.021	0.011	0.014	0.012

Table 3: Difference of the damping ratios for the two identification methods, for length $l = 0.4\,m$

Mode number	1	2	3	4	5
LSM_t	0.071	0.028	0.0342	0.0315	0.027
NY_f	0.062	0.039	0.035	0.0318	0.034

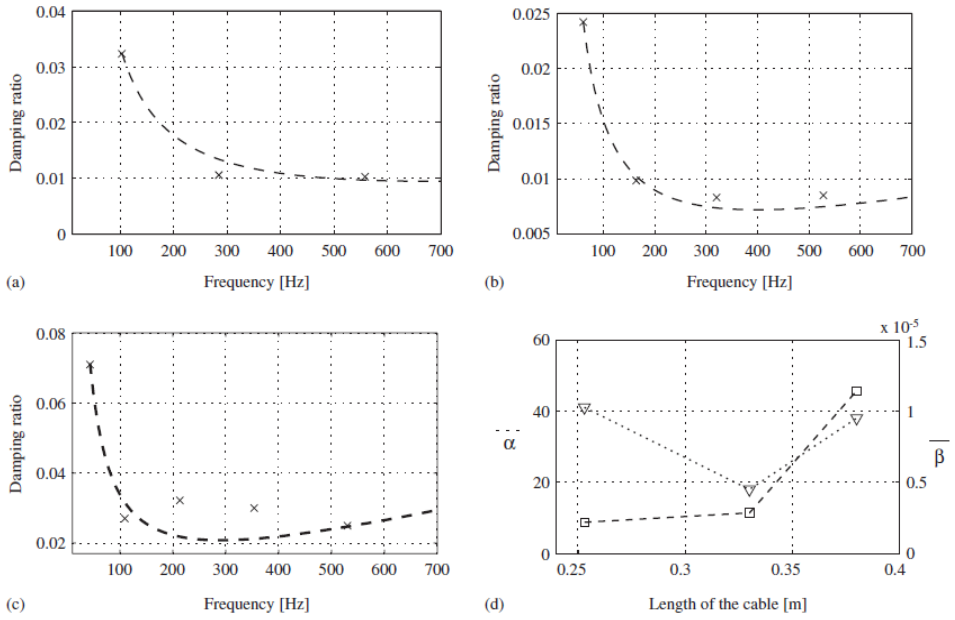

Figure 2: Approximated Rayleigh function (- - -) for measured damping ratios at natural frequencies (ς) for straight cable lengths: (a) 0.253 m, (b) 0.328 m and (c) 0.4 m; (d) changes if Rayleigh coefficients α(. . .) and β(- - -) with different lengths of cables.

Boltezar and Otrin (2007) did not include tension in their experimental data, and different results might have been achieved if tension had been included. The research conducted for purposes of this dissertation did include tension. The method of analysis, using Rayleigh damping, is classical, and the graph of the frequency versus damping ratio might be applicable to this work.

Adhikari (2006) proposed a damping method suitable for structural elements, stating: "A method for identification of damping matrix using experimental modal analysis has been proposed. The method is based on generalized proportional damping. The generalized proportional damping expresses the damping matrix in terms of smooth continuous functions involving specially arranged mass and stiffness matrices so that the system still possesses classical normal modes. This enables one to model variations in the modal damping factor with respect to the frequency in a simplified manner. Once a scalar

function is fitted to model such variations, the damping matrix can be identified very easily using the proposed method. This implies that the problem of damping identification is effectively reduced to the problem of a scalar function fitting. The method is simple and requires the measurement of damping factors and natural frequencies only. The proposed method is applicable to any linear structures provided accurate mass and stiffness matrices are available and the modes are not significantly complex. If a system is heavily damped and modes are highly complex, the proposed identified damping matrix can be a good starting point for more sophisticated analyses."

The graph of model damping versus frequency was adapted for use in this study.

Furthermore, Adhikari and Woodhouse (2001) proposed certain methods to identify damping from experimentally identified complex modes. The method for the identification of a non-proportional viscous damping matrix in vibrating systems was included. The method was explored by applying it to simulated data from a simple problem, in which a linear array of spring-mass oscillators was damped by non-viscous elements over part of its length. The results were illustrated by two particular damping models and representative parameter values. Symmetry breaking of the fitted viscous damping matrix depended on the value of the characteristic time constant θ of the damping model – when θ was short compared to the natural vibration period, the damping was electively viscous and the fitting procedure gave a physically sensible symmetric matrix. When θ was longer, however, the memory of the damping function influenced the detailed behaviour.

The approach of using experiments was taken for purposes of this dissertation.

McClure and Lapointe (2003) found that "internal damping mainly comes from the cables and the structures. When a cable is subjected to longitudinal shock loads, internal damping arises from the axial friction between the strands and friction induced by bending of the wire. Little research has been carried out on the subject and cable manufacturers do not supply this information. Furthermore, most of the research done on cable self-damping

relates to the study of Aeolian vibrations and galloping in intact spans, two instability phenomena dominated by transverse rather than longitudinal motion." *There were no results produced for the internal damping of the conductor.* McClure and Lapointe (2003) went on to state that all analyses performed in their case study assumed linear elastic materials. This was certainly an unrealistic assumption if analyses were carried out to explain failure of the mechanisms.

For short time spans $(l \leq 1m)$ transverse effects dominate, whereas for long time spans $(\geq 1m)$ such as those considered in this research, the tension effect may dominate. See Beards (1995), for example, as well as the following equations (Chapter 3):

$$EI\frac{\partial^4 y(t,x)}{\partial x^4} - T\frac{\partial^2 y(t,x)}{\partial x^2} + \rho A\frac{\partial^2 y(t,x)}{\partial t^2} = 0$$

$$\omega_n^2 = \left(\frac{n\pi}{l}\right)^2 \cdot \frac{T}{\rho A} + \left(\frac{n\pi}{l}\right)^4 \cdot \frac{EI}{\rho A}$$

The natural frequency is inversely proportional to the length of the conductor and therefore $\frac{1}{l^2} \geq \frac{1}{l^4}$ for $l \geq 1m$.

Rawlins (2009) determined "self-damping" through measurements in the laboratory, which proved difficult and time-consuming under standard laboratory procedures, *in this regard a suitable analytical model of conductor self-damping mechanics is required.* He further proposed a model used as a tool for exploring and better understanding the variations in the characteristics of the conductor samples. *This work will add or contribute to methods based on the standard recommended procedures.*

Sorokin and Rega (2007) developed a theory to describe the linear time-harmonic behaviour of an arbitrarily sagged inclined cable under heavy fluid loading by a viscous

fluid. The ensuing evaluated added mass and viscous damping coefficients were shown to be highly dependent on the type of mode. The Figure below, taken from Sorokin and Rega (2007), shows the damping coefficient versus frequency in Hertz, which may be applicable to this dissertation. *The theory of free linear vibration of arbitrarily sagged inclined cables in a viscous fluid presented in the framework of the heavy fluid loading concept, as used by Sorokin and Rega (2007), was not applied in this study.*

Diana, Falco, Cigada and Manenti (2000) stated that their experimental method for testing the self-damping of overhead transmission lines on laboratory spans was in accordance with international standards. Two testing procedures were developed, namely the power method and the inverse standing wave ratio (ISWR) method. The differences found between the two were assumed to be caused by dead-end losses, which were a function of the non-dimensional damping (h), as shown in the Figure below (Diana *et al.*, 2000).

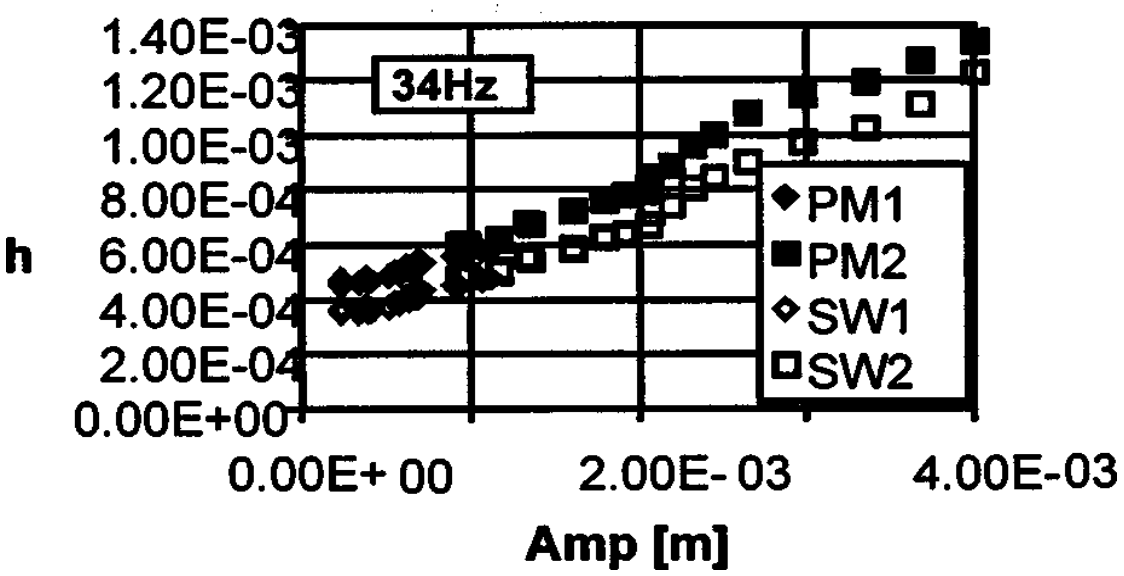

Figure 3: Comparison power method-ISWR method: 34 Hz (1, 2 different test runs; ACST cable, diameter 24.15 mm).

The two methods fixed the way in which data was to be presented in measurement reports, although there were comments about the advantages and disadvantages of both methods, which required further investigation. The ISWR method was based on the measuring of amplitude of vibration in two nodes along the span at constant frequency. *In this dissertation, the changing of the damping ratio coefficient is recorded in respect of the frequency in order to show the effect of frequency on damping.* The Std 664-1993 span methods prescribed by the Institute of Electrical and Electronics Engineers (IEEE) were used (Pon, 2009):

Inverse standing wave ratio (ISWR) method

Power method

Logarithmic decay method

These methods used span to test conductor and damper together to obtain a combined total power dissipation due to self-damping of the conductor, plus damping due to an external damper, used in conjunction with IEEE Std 563-1978. The power dissipation due to conductor self-damping was subtracted from the combined total damping to obtain the power dissipation of the external damper. It was further stated that IEEE Std 664-1993 status (as of summer 2009) had not been revised since last being reaffirmed in 2007 and was due for maintenance reaffirmation, revision or withdrawal in 2012. *In this regard, the self-damping characteristics of conductors were researched further in order to affiliate these standards.*

Yamaguchi, Alauddin and Poovarodom (2001) conducted an experimental procedure to analyse the dynamic characteristics of a structure using a fixed-fixed beam with 10 randomly placed masses. The shaker was used as an impact hammer to ensure a consistent force and location for all the tests. The ruler was used to minimise error in measuring the mass locations in the beam experiment. The grid system and nodal points were employed to minimise error in measuring the oscillator. The hammer was located in the plate experiment, and the magnets were used as attached masses for ease of placement in the

beam experiment. The magnets were attached to the oscillators in the plate experiment, and the hard steel tip and small brass plate on the flexible beam were used to obtain virtually noise-free data up to 4.5 kHz. The statistics of the frequency response functions measured at different points were obtained for low, medium and high frequency. The variability in the amplitude of the measured frequency response functions was compared with numerical Monte Carlo simulation results. The data obtained in these experiments was to be used for validation of the uncertainty quantification and propagation methods in structural dynamics. Yamaguchi and Adhikari (1995) and Adhikari, Friswell, Lonkar and Sarkar (2009) analysed the dynamic characteristics of a structure with free and forced response of a cable system using an energy-based method of damping. Evaluation was applied to analyse the characteristics of system modal damping. An energy-based method was derived in the form of the product of modal strain energy ratio and loss factor whereby numerical results were obtained with the finite element method.

Cooper and Nuckles (1996) performed Aeolian vibration tests on four distinct sample constructions of "705 kcmil 26/7 Drake" overhead transmission conductors to determine their self-damping characteristics. They discovered that "the vibration behavior for the conventional construction versus the trap wire (TW) design was very similar for a given tension and frequency." Normally, if the size of longitudinal length of a conductor increased, the self-damping capabilities also increased. In this case, there was only a .098 inch reduction in diameter for the TW design. *This was not sufficient to make a significant difference in the power dissipation*. Furthermore, the test results of Cooper and Nuckles (1996) were plotted on the graphs of power dissipation versus frequency. *This is closely related to showing damping versus frequency and was therefore considered for purposes of this study.*

The identified damping ratios (Boltezar, Slavic & Simonovski, 2003; Boltezar & Otrin, 2009) for the spatially curved steel wires with a casing were identified with the wavelet-based technique, while the loss factor came from the "Nyquist" plot.

Barbieri, Junior and Barbieri (2004) studied the dynamical behaviour of the electrical cables of transmission lines using theoretical and experimental methods as shown (Barbieri *et al.* 2004).

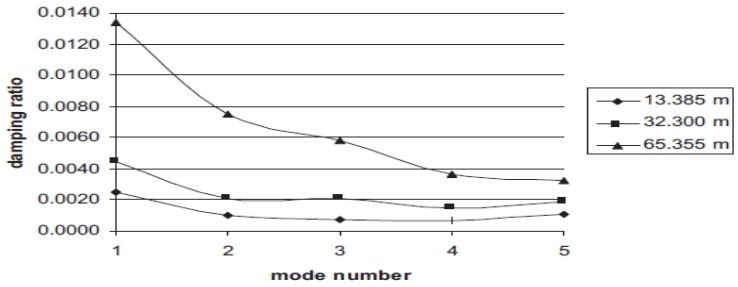

Figure 4: Damping ratio (14.78% RTS cable load).

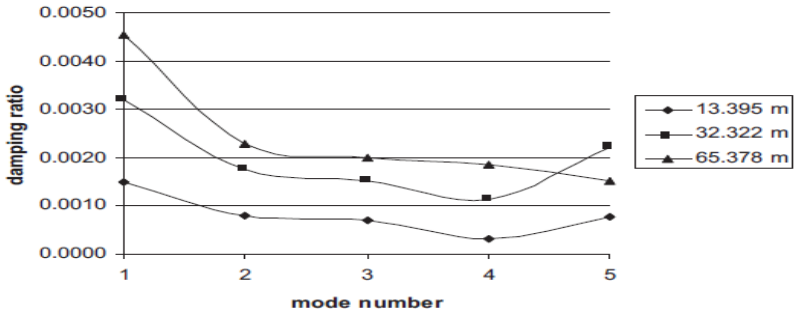

Figure 5: Damping ratio (21.91% RTS cable load).

Table 4: Eigenvalues (10 700 N cable load)

Mode number	Experimental	Reduced model
1	−0.11 ± i27.13	−0.11 ± i26.93
2	−0.05 ± i53.98	−0.05 ± i53.87
3	−0.06 ± i80.76	−0.06 ± i80.82
4	−0.07 ± i108.35	−0.07 ± i107.80
5	−0.15 ± i135.20	−0.15 ± i134.77

The numerical analyses were conducted using the finite element method. For validation of the mathematical models, the simulated results were compared with experimental data

obtained in an automated testing system for overhead line cables. The modal parameters were optimised through a gradient search routine, the complex envelope technique, and the single-degree-of-freedom method. The estimated values for the eigenvalues and eigenvectors through analytical and experimental methods presented consistent values for all situations of mechanical load and sample length. It proved possible to estimate the damping ratio for the first five eigendata through the search and complex envelope techniques. Furthermore, Barbieri *et al.* (2004) established a procedure to identify damping of transmission line cables in order to estimate in a simple (proportional) way the system damping matrix. The procedure was based on experimental and simulated data where experimental data was collected through five accelerometers and the simulated data was obtained using the finite element method. The system damping matrix was estimated through different procedures whereby three sample lengths and two different mechanical loads were applied. The experimental and simulated results presented good approximates. *The free vibration method is also considered in this dissertation.*

Ceballos and Prato (2008) presented a procedure to measure the axial force acting on a cable from free vibration tests. Their analysis was carried out through analytical solutions, and the axial force was derived by optimising the correspondence between measured and analytical natural frequencies considering, as simultaneous adjustment variables, the axial force and the bending stiffness of the cable. It was discovered that the influence of the rotational stiffness at the cable ends on the estimation of the axial force increased with the bending stiffness of the cable. For cables with deviator collars near the ends, an analytical solution was proposed to derive the rotational stiffness at the supports, while an experimental procedure was proposed in the case of cables without deviators. *In this report, the free and forced vibration tests with clamped boundary conditions are considered. The experimental tests are further analysed by means of theoretical calculations*.

In past laboratory studies of conductor self-damping, the main focus was on energy dissipation due to conductor self-damping. Although several investigators have carried out

various tests on a variety of conductors, determining the energy dissipated due to conductor self-damping has proven not to be a straightforward process Vecchiarelli, Currie & Havard, 2000). Furthermore, significant discrepancies in experimental results could be caused by extraneous sources of damping, such as aerodynamic resistance. The method proposed by Vecchiarelli *et al.* (2000) was the energy balance method, which is simple but limited, as it does not account for the effects of travelling waves, contributions from other spatial modes of vibration, conductor flexural rigidity, and damper mass. *This emphasises the need for further investigational methodologies for determining the self-damping characteristics of transmission line cables.*

The finite element method was used by Barbieri *et al.* (2004) to obtain numerical models, after which the simulated results were compared with the experimental data obtained in an automated testing system for overhead line cables. The forced response was obtained through an impulsive excitation (impact hammer) or electromechanical shaker, and the vibration signals were collected through accelerometers placed along the half sample. The Irvine parameter was used to analyse the eigenbehaviour. Barbieri *et al.* (2004) discovered that the numeric and experimental dynamical behaviour is a function of the excitation frequency.

Kahla (1995) used a numerical method for analysing the dynamics of single guy cables on both windward and leeward conductors. The results of this method were compared to those of analytical formulae. The natural frequencies and mode shapes were determined for both windward and leeward conductors. *Whereas Kahla (1995) used wind to excite the motion of both windward and leeward conductors, this researcher used the shaker to excite the motion of a single conductor.* The following graphs, taken from Kahla (1995), reflect some of his results.

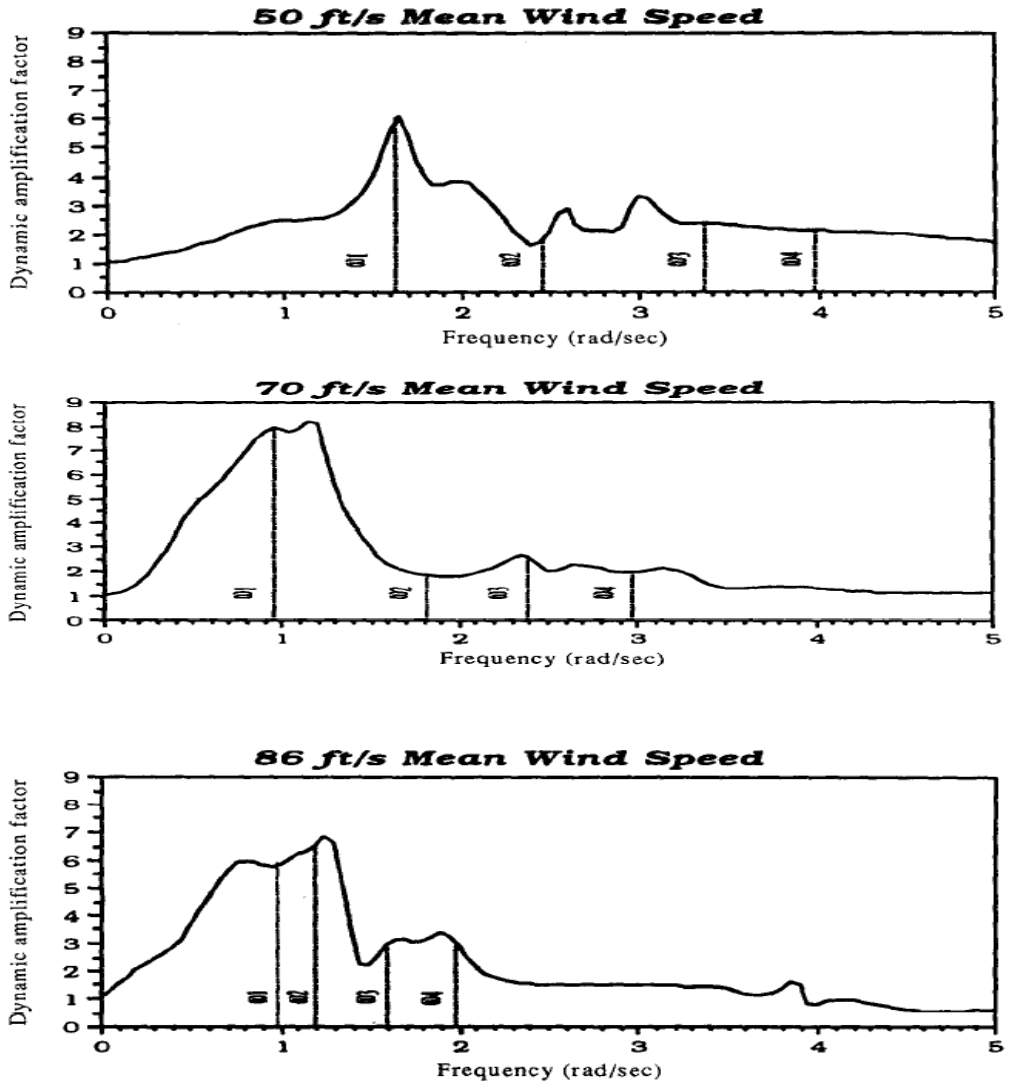

Figure 6: Variation of the leeward guy dynamic amplification factor as a function of the wind fluctuating frequency.

Koh and Rong (2004) presented a paper on the dynamic analysis of three-dimensional cable motion, accounting for axial, flexural and torsion deformations, as well as geometric non-linearity due to large displacements and rotations. Their comprehensive study covered analytical formulation and a numerical strategy based on an iterative finite difference scheme, as well as experimental verification by means of shaking Table tests. A specific

problem of cable motion due to support excitation was used to illustrate the asymmetry and sensitivity of the dynamic tension response associated with geometric non-linearity of large-displacement cable motion. The shaking Table tests validated the accuracy of the numerical results obtained for both two-dimensional and three-dimensional cases.

Brennan, Carrella, Waters and Lopes (2008) described the free and forced dynamic behaviour of a single-degree-of-freedom system in cases where the damper is elastically supported (Zener model). Optimum values of the damping were determined for cases where the mean square displacement response of the mass and the mean square force transmitted to the rigid base were of interest. It was shown that having the spring in series with the damper affords no benefits, and the best option is to have the damper rigidly connected. *The theoretical work is applicable to this study, but the results for a conductor with a mass absorber damper are compared with the results for a conductor without a mass absorber damper in order to determine the effects of internal damping of the transmission line conductor.*

Diana, Bruni, Cheli, Fossati and Manenti (1998) carried out a dynamic analysis of the high-voltage overhead transmission line crossing known as Lago de Maracaibo in Venezuela. This entailed the evaluation of the dynamic response of the overhead transmission line when subjected to vortex-induced and wake-induced vibrations, as well as the buffeting effects of wind action in particular. Mathematical models were used to reproduce the interaction between wind and structure, taking into account the aerodynamic non-linear forces acting on the cables, while the structural model was generally liberalised in the neighbourhood of the equilibrium configuration. In these cases, a frequency domain analysis was mostly performed by means of the modal approach, while linear finite element models were used for time domain analysis. Methodologies were presented to simulate the different problems, producing some results in terms of choice of damping system, the minimum inter-phase distances, and the parameters related to the dynamic design of the towers. These processes excluded the internal damping characteristics of the conductors.

Fang and Lyons (1996) presented an expression for modal damping (loss factor or logarithmic decrement) that was obtained analytically for tensioned pipes where the material damping was the only source of damping. The dependence of modal damping on axial tension, which was well known from general experience with cables, was explained. The expression was extended to give an equivalent modal loss factor when there were other forms of damping such as dry friction, as in the cases of cables and marine risers. Test results on vertical tensioned pipes with pivoted ends and fixed ends were presented. When pivoted joints were used, Coulomb damping in these joints dominated the structural damping behaviour. When the pivoted ends were replaced by fixed ends, the damping values were greatly reduced and were of a similar level to those measured when the pivots stopped moving in the tests with pivoted ends. It was shown that these low damping values were in part caused by the dry friction force between the pipe specimen and metal shafts in the push-fixings used in the tests. The material damping was predicted by the expression developed to be only a small part of the structural damping in all the tests.

Hagedorn, Mitra and Hadulla (2002) proposed the energy-balance method to estimate the vibration amplitudes of the vortex-excited vibrations of single conductors in overhead transmission lines with dampers, but also to determine the strains at critical points in the span. In modelling the vortex-excited oscillations in this manner, it was assumed that the conductor was always in resonance. The discrete spectrum of the free conductor vibrations was thus replaced by a continuous spectrum. This could be justified by the fact that the resonance frequencies were very closely spaced, and there was little sense to physically distinguish between the individual resonances, which depend on parameters that were not well determined. Conductors both with and without mass absorber dampers were used in this work to check whether the self-damping characteristics of the transmission line conductors were adequate to suppress Aeolian or wake-induced vibrations.

Pon (2009) presented a model formulation capable of analysing large-amplitude free vibrations on a suspended cable in three dimensions. The virtual work-energy functional

was used to obtain the non-linear equations of three-dimensional motion. The formulation was also to be used on cables having small sag-to-span ratios in a convenient specified applied end tension. Based on the multi-degrees-of-freedom model, numerical procedures were implemented to solve both spatial and temporal problems.

Chucheepsakul, Srinil and Rega (2004) determined the self-damping of a conductor experimentally whereby a length of conductor was forced to vibrate at a single mode of vibration, while the total energy dissipated along the entire span of the conductor was measured. Different laboratory experiments had been done, but there was a lack of empirical information on the self-damping force of a conductor and this had to be modelled in the study. A theoretical analysis of conductor self-damping was developed in which the underlying force was assumed to be of the hysteretic type. *This clearly shows the need for further investigation of relevant methods, as done in this study.*

A number of researchers have studied the vibration of cables and damping mechanisms (Adhikari *et al.*, 2009; Barbieri, Novak & Barbieri, 2004; Cornila, Capolungoa, Qua & Jairazbhoy, 2007; Fekr & McClure, 1998; Hagedorn *et al.*, 2002; Hardy & Leblond, 1993; Ni, Ko & Zheng, 2002; Park, Lyu & Lee, 2008; Rawlins, 2000; Vecchiarelli *et al.*, 1995). Several books on vibration theory (Beards, 1995; EPRI, 1979; Inman, 2008; James, Smith, Wolford & Whaley, 1989; Meirovitch, 2001; Meriam, 2008Oliveira & Preire, 1994; Thomson & Dahleh, 1998) have also covered techniques of evaluating damping characteristics and energy dissipation. This dissertation looks closely at the fundamentals of damping characterisation and experimental techniques based on published books and some new papers.

2.5 Conclusions

From the literature review, there is compelling evidence of the need to investigate and establish procedures to determine the self-damping characteristics of transmission line conductors.

Chapter 3

THEORETICAL BACKGROUND ON THE FREE VIBRATION METHOD

3.1 Introduction

This Chapter covers the theory related to free vibration of a transmission line conductor, as used for the analysis of results (see Chapter 7).

The theory is formulated in Section 3.2. The parabolic cable is considered in Section 3.3 and the catenary cable in Section 3.4. The governing differential equation for the eigenvalue problem is presented in Section 3.5 while Section 3.6 reflects the wave equation and Section 3.7 the measurement of damping.

3.2 Theory

This Section looks at cable static and dynamic equations (EPRI, 1979; Oliveira & Preire, 1994). If the intensity of the variable and continuous load applied to the cable (see Figure 7) is expressed as ω units of a force per unit of horizontal length x, then the resultant R of the vertical loading is

$$R = \int dR = \int \omega \, dx \tag{3.1}$$

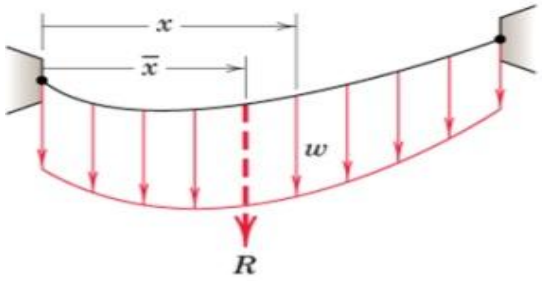

Figure 7: Cable under load

where the integration is taken over the desired interval. We find the position $\bar{x}$ of R from the moment principle, so that

$$R\bar{x} = \int x\, dR \qquad \bar{x} = \frac{\int x\, dR}{R} \tag{3.2}$$

The equilibrium condition of the cables will be satisfied if each infinitesimal element of the cable is in equilibrium. The free-body diagram of a differential element is shown in Figure 8.

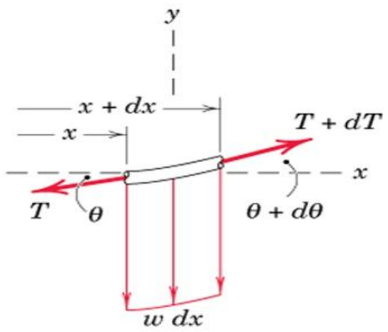

Figure 8: Free-body diagram

At the general position x the tension in the cable is T and the cable makes an angle θ with the horizontal x direction. At the Section $x+dx$ the tension is $T+dT,$ and the angle is $\theta+d\theta$. Note that the changes in both T and θ are taken positive with positive change in $x.$ The vertical load $\omega\, dx$ completes the free-body diagram. The equilibrium of vertical and horizontal forces requires, respectively, that

$$(T+dT)\sin(\theta+d\theta) = T\sin\theta + \omega\, dx$$

$$(T+dT)\cos(\theta+d\theta) = T\cos\theta$$

The equilibrium equation may be written in the form

$$\frac{d^2y}{dx^2} = \frac{w}{T_0} \tag{3.3}$$

Equation (3.3) is the differential equation for the flexible cable. The solution to the equation is that functional relation $y = f(x)$, which satisfies the equation and also satisfies the conditions at the fixed ends of the cable, called boundary conditions. These relationships define the shape of the cable.

3.3 Parabolic cable

When the intensity of vertical loading ω is constant, the description closely approximates a suspension bridge where the uniform weight of the roadway may be expressed by the constant ω. The mass of the cable is not distributed uniformly with the horizontal, but is relatively small and its weight is neglected. For this limiting case it will be proven that Figure 9 shows such a suspension bridge of span L and sag h with origin of co-ordinates taken at the midpoint of the span.

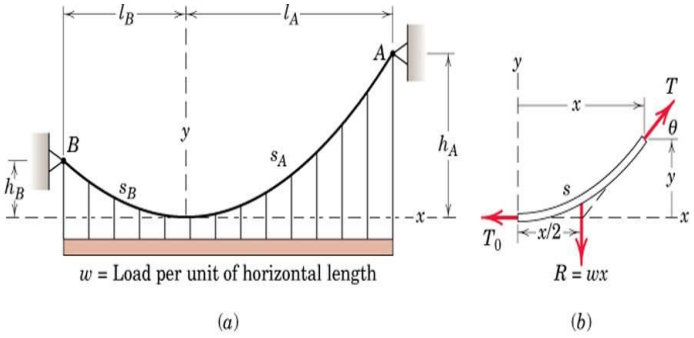

Figure 9: Cables hanging in a parabolic arc

Referring to Figure 9, the integration of equation (3.3) once with respect to x gives

$$\frac{dy}{dx} = \frac{wx}{T_0} + C \tag{3.4}$$

where C is a constant of integration. For the co-ordinate axes chosen, $dy/dx = 0$ when $x = 0,$ so that $C = 0.$ Thus,

$$\frac{dy}{dx} = \frac{wx}{T_0} \tag{3.5}$$

which defines the slope of the curve as a function of x. One further integration yields

$$\int_0^y dy = \int_0^x \frac{wx}{T_0} dx \quad or \quad y = \frac{wx^2}{2T_0} \tag{3.6}$$

Equation (3.6) gives the shape of the cable, which we see is a vertical parabola. The constant horizontal component of cable tension becomes the cable tension at the original.

Inserting the corresponding values $x = l_A$ and $y = h_A$ in equation (3.6) gives

$$T_0 = \frac{w{l_A}^2}{2h_A} \tag{3.7}$$

(3.8)

so that $y = h_A(x/l_A)^2$

The tension T is found from a free-body diagram of a finite portion of the cable, shown in Figure 9. From the Pythagorean Theorem

$$T = \sqrt{{T_0}^2 + w^2x^2} \tag{3.9}$$

with elimination of T_o gives

$$T = \omega\sqrt{\chi^2 + ({l_A}^2/2h_A)^2} \tag{3.10}$$

The maximum tension occurs where $x = l_A$ and is

$$T_{\max} = wl_A\sqrt{1 + (l_A/2h_A)^2} \tag{3.11}$$

The length s_A of the complete cable is obtained from the differential relations by integrating the expression for a differential length $ds = \sqrt{(dx)^2 + (dy)^2}$. This gives us

$$s_A = l_A \left[1 + \frac{2}{3}\left(\frac{h_A}{l_A}\right)^2 - \frac{2}{5}\left(\frac{h_A}{l_A}\right)^4 + ... \right] \tag{3.12}$$

The relationships that applies to the cable Section from the origin to point B can be easily obtained by replacing h_A, l_A and s_A with h_B, L_B and s_B, respectively.

3.4 Catenary cable

Consider now a uniform cable, Figure 10, taken from Oliveira and Preire (1994), suspended at two points in the same horizontal plane and hanging under the action of its own weight only. The free-body diagram of a finite portion of the cable of length s is shown in the right-hand part of Figure 10. This free-body diagram differs from that in Figure 9 in that the total vertical force supported is equal to the weight of the Section of cable of length s in place of the load distributed uniformly with respect to the horizontal.

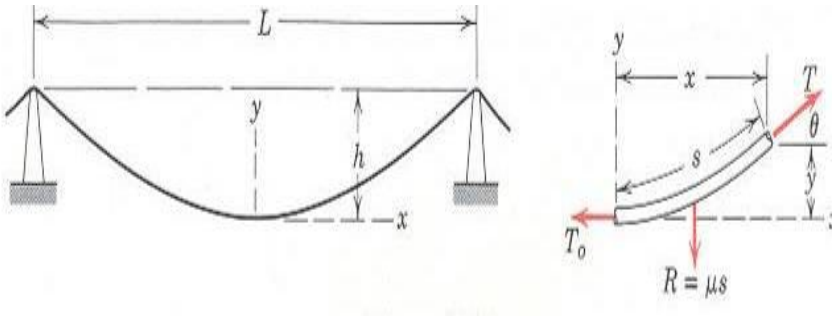

Figure 10: Uniform cable

If the cable has a weight μ per unit of its length, the resultant R of the load is $R = \mu s$, and the incremental load $\omega\, dx$ is replaced by $\mu\, ds$. Thus we may substitute $\omega = \mu\, ds / dx$ into the differential relation for the cable and obtain

$$\frac{d^2y}{dx^2} = \frac{\mu}{T_o}\frac{ds}{dx} \tag{3.13}$$

Since $s = f(x, y),$ it is necessary to change this equation to one containing only two variables.

$$\frac{d^2y}{dx^2} = \frac{\mu}{T_o}\sqrt{1+\left(\frac{dy}{dx}\right)^2} \tag{3.14}$$

Equation (3.11) is the differential equation of the curve (catenary) assumed by the cable.

Solution of this equation is facilitated by the substitution of $\rho = dy/dx,$

$$\frac{dy}{dx} = \frac{e^{\mu x/T_o} + e^{-\mu x/T_o}}{2} = \sinh\frac{\mu x}{T_o} \tag{3.15}$$

The slope may be integrated to obtain

$$y = \frac{T_o}{\mu}\cosh\frac{\mu x}{T_o} + K \tag{3.16}$$

The integration constant K is evaluated from the boundary condition x = 0 when y = 0. This substitution requires that $K = -T_o/\mu$, and hence

$$y = \frac{T_o}{\mu}\left(\cosh\frac{\mu x}{T_o} - 1\right) \tag{3.17}$$

Equation (3.14) is the equation of the curve (catenary) assumed by the cable hanging under the action of its own weight only.

From the free-body diagram in Figure 10 we see that $dy/dx = \tan\theta = \mu s T_o.$ Thus, from the previous expression for the slope,

$$s = \frac{T_o}{\mu}\sinh\frac{\mu x}{T_o} \tag{3.18}$$

The tension T in the cable is obtained from the equilibrium triangle of the forces.

$$T = \cosh \frac{\mu x}{T_o} \tag{3.19}$$

The tension may also be expressed in terms of y with the aid of equation (3.14) which, when substituted, gives

$$T = T_o + \mu x \tag{3.20}$$

3.5 Governing differential equation for the eigenvalue problem

The combined equation for a cable subjected to tension and bending stresses (EPRI, 1979) is given by the following partial differential equation:

$$EI \frac{\partial^4 y(t,x)}{\partial x^4} - T \frac{\partial^2 y(t,x)}{\partial x^2} + \rho A \frac{\partial^2 y(t,x)}{\partial t^2} = 0 \tag{3.21}$$

The symbols are defined as follows: EI is the flexural rigidity, T is the tension, ρ is the density, and A is the cross-Sectional area. The deflection $y(t,x)$ is a function of time t and position x along the cable.

Using the technique of separation of variable, the deflection can be expressed as follows:

$$y(t,x) = f_1(t) \cdot f_2(x) \tag{3.22}$$

Substituting this in the partial differential equation, we obtain the natural-frequency equation measured in rad/s as follows:

$$\omega_n^2 = \left(\frac{n\pi}{l}\right)^2 \cdot \frac{T}{\rho A} + \left(\frac{n\pi}{l}\right)^4 \cdot \frac{EI}{\rho A} \tag{3.23}$$

3.6 Wave equation

A phenomenon intimately related to vibration is wave propagation. In fact, under certain circumstances, vibration and wave propagation are two different representations of the same motion, namely one in terms of standing waves and the other in terms of travelling waves.

The simplest form of wave motion is associated with second-order systems such as strings in transverse vibration, rods in axial vibration, and shafts in torsion, with uniformly distributed parameters. For constant tension and uniform mass distribution, the free vibration of a string can be expressed in the form

$$\frac{\partial^2 y(x,t)}{\partial x^2} = \frac{1}{c^2}\frac{\partial^2 y(x,t)}{\partial t}, \quad c = \sqrt{\frac{T}{\rho}} \tag{3.24}$$

Equation (3.21) represents the one-dimensional wave equation, in which c is the wave propagation velocity. The general solution is

$$y(x,t) = f_1(x-ct) + f_2(x+ct) \tag{3.25}$$

where f_1 and f_2 are arbitrary functions of the arguments $x-ct$ and $x+ct$. A case of particular interest in vibrations is that of sinusoidal waves. One such wave having the amplitude A and travelling in the positive x direction can be expressed as

$$y(x,t) = A\sin\frac{2\pi(x-ct)}{\lambda} \tag{3.26}$$

where λ is the wavelength, defined as the distance between two successive crests. Equation (3.23) can be written in the form

$$y(x,t) = A\sin(2\pi kx - \omega t) \tag{3.27}$$

where

$$k = \frac{1}{\lambda} \tag{3.28}$$

is known as the wave number, defined as the number of waves per unit distance, and

$$\omega = c\frac{2\pi}{\lambda} \tag{3.29}$$

is the frequency of the wave. Moreover,

$$\tau = \frac{2\pi}{\omega} = \frac{\lambda}{c} = \frac{t_n - t_o}{n-1} \tag{3.30}$$

is the period, namely the time necessary for a complete wave to pass through a given point.

Consider a displacement consisting of two identical waves travelling in opposite directions. Recalling that $\sin(\alpha \pm \beta) = \sin\alpha\cos\beta \pm \cos\alpha\sin\beta$, the solution can be written as

$$\begin{aligned} y(x,t) &= A\sin(2\pi kx - \omega t) + A\sin(2\pi + \omega t) \\ &= 2A\sin 2\pi kx\cos\omega t \end{aligned} \tag{3.31}$$

Equation (3.28) states that the combination of two identical waves travelling in opposite directions represents a wave whose profile $2A\sin 2\pi kx$ no longer travels, but oscillates harmonically about the zero position with the frequency ω. Such waves are known as stationary or standing waves. For a string of length L fixed at both ends, equation (3.28) states that the frequency ω_p has a certain value, obtained by solving the differential eigenvalue problem. On the other hand, the frequency ω (equation (3.26)) is arbitrary, which can be attributed to the fact that no boundary conditions have been imposed. However, if we assume that the string experiencing wave motions has nodes at $x = 0$ and $x = L,$ as in the case of the vibrating string, then the wave number must satisfy the relation

$$2kL = r, \quad r = 1,2,..... \tag{3.32}$$

Inserting the above values into equation (3.25) and considering the second of equations (3.24) and (3.29), we obtain the natural frequencies

$$\omega_r = 2\pi kc = r\pi \frac{c}{L} = r\pi \sqrt{\frac{T}{\rho L^2}}, \quad r = 1,2,..... \tag{3.33}$$

which are identical to the natural frequencies of a fixed-fixed string, as can be concluded from the equation. Hence, the normal-mode vibration of a string of finite length can be regarded as consisting of standing waves, where the wave profile corresponding to the rth mode oscillates about the equilibrium position with the natural frequency ω_r.

3.7 Measurement of damping

A convenient measure of the amount of damping in a single-degree-of-freedom system (EPRI, 1979) is the drop in amplitude at the completion of one cycle of vibration. Let t_1 and t_2 be the times corresponding to the first and second peaks and denote the associated peak displacement by x_1 and x_2 respectively, and we obtain

$$\frac{x_1}{x_2} = e^{\zeta\omega_n T} = e^{2\pi\zeta\omega_n} = e^{2\pi\zeta/\sqrt{1-\zeta^2}} \tag{3.34}$$

$$\delta = 1n\frac{x_1}{x_2}. = \frac{2\pi\zeta}{\sqrt{1-\zeta^2}} \tag{3.35}$$

where δ is known as the logarithmic decrement. Equation (3.32) can be solved for damping factor ζ, with the result

$$\zeta = \frac{\delta}{\sqrt{(2\pi)^2 + \delta^2}}. \tag{3.36}$$

For small damping, such that $\zeta << 1,$ equation (3.33) directly yields

$$\zeta \cong \frac{\delta}{2\pi}. \tag{3.37}$$

The damping factor ζ can be determined, perhaps more accurately, by measuring the displacements at two different times separated by a given number of periods. Letting x_1 and x_{j+1} be the peak displacements corresponding to the time t_1 and $t_{j+1} = t_1 + jT$, where j is an integer, and recognising that the value given by the extreme right of equation (3.32) is the same for the ratio of any two consecutive peak displacements, not only for $\frac{x_1}{x_2}$, we conclude that

$$\frac{x_1}{x_{j+1}} = \frac{x_1 x_2}{x_2 x_3} \ldots \frac{x_j}{x_{j+1}} = \left(e^{2\pi\zeta/\sqrt{1-\zeta^2}} \right)^j = e^{j2\pi\zeta/\sqrt{1-\zeta^2}} \tag{3.38}$$

from which we obtain the logarithmic decrement

$$\delta = \frac{2\pi\zeta}{\sqrt{1-\zeta^2}} = \frac{1}{j} 1n \frac{x_1}{x_{j+1}} \tag{3.39}$$

Equation (3.36) bases the calculation of the damping factor on two measurements alone, x_1 and x_{j+1}. While this may be better than using measurements of two consecutive peaks, it can still lead to errors, particularly for small damping, when differences between peak amplitudes are difficult to measure accurately. In such cases, accuracy may be improved by using equation (3.36) and writing

$$1n\ x_j = 1nx_1 - \delta(j-1),\ j = 1,2,\ldots,\ell \tag{3.40}$$

Chapter 4

THEORETICAL BACKGROUND ON THE FORCED VIBRATION METHOD

4.1 Introduction

This Chapter on forced vibration also gives details of a proposed procedure to determine the self-damping characteristics of the TERN and Aero-Z IEC62219-REV240609 conductors. The procedure can be extended to determine characteristics of other overhead transmission line conductors. This Chapter covers the theory of vibration related to forced vibration of the transmission line conductor, as used for the analysis of the results (see Chapter 7). The sweep tests are also described.

In this Chapter, Section 4.2 considers the quality factor as a measure of damping.

4.2 Quality factor as a measure of damping

The quality factor Q is frequently used as a measure of damping (Beards, 1995; EPRI, 1979; Meirovitch, 2001; Meriam, 2008), with Q defined as

$$Q = \frac{1}{2\zeta} \tag{4.1}$$

Since a small damping factor ζ corresponds to a large Q value, a lightly damped system would be referred to as having a high Q factor. Equation (4.1) is associated with the excitation frequencies f_1 and f_2 that correspond to a $magnification\ factor\ of\ 0.707/2\zeta$ as shown in Figure 11. The frequency f_1 is below the resonant frequency f_n, and f_2 is above it.

At resonance $f = f_n$, the magnification factor is

$$\frac{|X|}{F_0/k} = Q = \frac{1}{2\zeta} \tag{4.2}$$

The frequencies f_1 and f_2 are referred to as the half-power points, and $\Delta f = f_2 - f_1$ is referred to as the bandwidth of the system.

By measuring f_n and the bandwidth Δf at the half-power points, an approximate measure of Q can be determined from

$$Q \cong \frac{f_n}{\Delta f} = \frac{f_n}{f_2 - f_1} \text{ or, } Q \cong \frac{\omega_n}{\Delta \omega} = \frac{\omega_n}{\omega_2 - \omega_1}, \text{ therefore} \tag{4.3}$$

$$Q = \frac{1}{2\zeta} \cong \frac{f_n}{\Delta f} \tag{4.4}$$

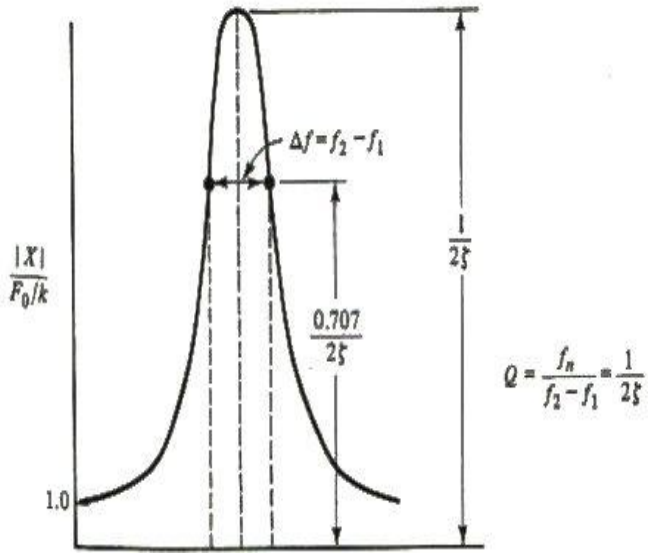

Figure 11: Determination of Q factor

Chapter 5

EXPERIMENTAL PROCEDURE AND THE APPARATUS USED

5.1 Introduction

This Chapter gives more details of proposed procedures to determine the self-damping characteristics of the TERN and Aero-Z IEC62219-REV240609 conductors for both free and forced vibrations methods. The procedure can be extended to determine the characteristics of other overhead transmission line conductors. The apparatus for determining the self-damping characteristics of the TERN and Aero-Z IEC62219-REV240609 conductors were also shown.

The experimental setup of the conductor is presented in Section 5.2. The summary of the free vibration experimental procedure together with the corresponding apparatus is presented in Section 5.3. Lastly, Section 5.4 contains a summary of the free vibration experimental procedure together with the corresponding apparatus.

5.2 Experimental setup of conductor

For steps 1 to 3 of the experimental procedure, as described in Chapter 5 Section 5.3 and Section 5.4, the following measurements were obtained: A conductor with its diameter is selected and clamped between two rigid supports. The conductor is tensioned and the value is recorded from the load cell. Measurements of the heights from floor are carried out at ½ span, ¼ span and ⅛ span away from fixed side and recorded (as shown in Figure 12 and Table5).

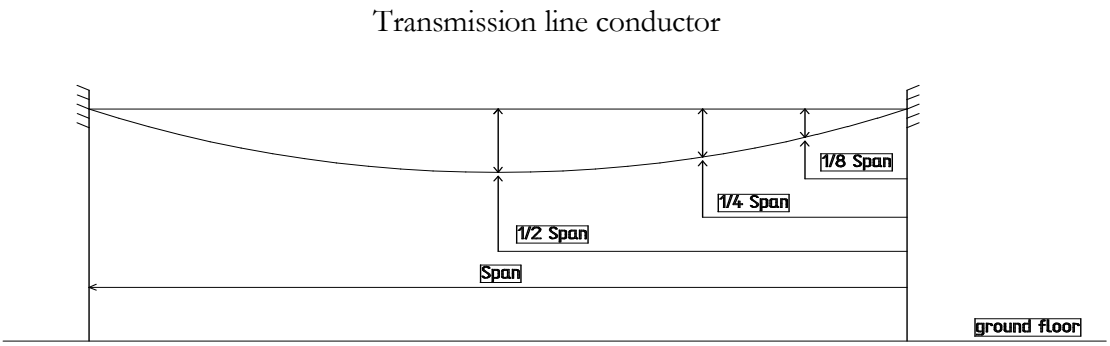

Figure 12: Conductor configuration

Table 5: Initial configurations – Measured results

		Tension		
		T_1: 20.73 kN	T_2: 25.11 kN	T_3: 29.56 kN
Position		Sag (cm)	Sag (cm)	Sag (cm)
1/2 span	42.300 m	55.55	47.35	40.75
1/4 span	21.150 m	40.85	34.95	30.15
1/8 span	10.575 m	22.35	18.20	16.15

Length of conductor: 84.6 m

As shown in Tables 5 and 83, the measured and calculated configurations were in good agreement, with a smallest error of $\varepsilon = 1.00\%$ and largest error of $\varepsilon = 11.22\%$. In general, the difference was smallest at mid-span as the error of $1.00\% \le \varepsilon \le 2.5\%$

5.3 Free vibration experimental procedure and corresponding apparatus

Based on the theory relating to free vibrations, the following procedure was developed:

1. Start with conductor with diameter 1 (e.g. 27 mm for the TERN conductor).
2. Tension the conductor with T_1 and record value of tension from load cell.
3. Measure height from floor at ½ span, ¼ span and ⅛ span away from fixed side.
4. Do free vibration test by hammering conductor at any convenient position x away from non-fixed end.

5. Measure vibration amplitude versus time using piezo-ceramic sensor, accelerometer, etc.
6. Repeat experiment at least six times.
7. Change the tension of conductor to T_2, T_3, T_4, etc. as in step 2 above.
8. Repeat steps 3 to 7 six times.
9. Change conductor with diameter 2, diameter 3, etc. (for example, Aero-Z IEC62219-REV240609 conductor …).
10. Repeat steps 1 to 9 six times.
11. End test.

This procedure is briefly described in Chapter 1, Section 1.5.

5.4 The photographic view of experimental procedures and corresponding apparatus.

The apparatus for determining the self-damping characteristics of the TERN and Aero-Z IEC62219-REV240609 conductors consisted of the 84.6 m span VRTC test rig housed in the Vibration Research and Testing Centre (VRTC) at the University of KwaZulu-Natal (UKZN), which is shown in the photograph below.

VRTC Centre

The TERN or Aero-Z IEC62219-REV240609 conductor is clamped between two rigid supports as shown below. One end is fixed and the other end is the load end.

Inside view of VRTC Centre showing test rig

At 1.2 m position, an impulsive force is introduced by a single blow for the free vibration method. Alternative impulsive forces are also introduced at various positions along the transmission line conductor as detailed in the report.

Inside view of VRTC Centre showing shaker

Measurements are taken using a series of accelerometers positioned at the mid and end points along the transmission line conductor. The recording equipment consists of oscilloscopes.

Inside view of VRTC Centre showing recording equipment

The VRTC lab is in a fully temperature-controlled, enclosed environment. The conductor tension is measured using a load cell.

5.5 Forced vibration experimental procedure and corresponding apparatus

1. Start with conductor with diameter 1 (e.g. 27 mm for the TERN conductor).
2. Tension the conductor with T_1 and record value of tension from load cell.
3. Measure height from floor at ½ span, ¼ span and ⅛ span away from fixed side.
4. Do forced vibration test using the shaker.
5. Locate resonant frequencies by vibrating the conductor from dc frequency to kilohertz.
6. For each of the first four lowest resonant frequencies, vibrate the conductor for a few seconds and record displacement, velocity and acceleration amplitudes, as well as applied shaker force and phase angle between displacement and force.
7. Repeat experiment at least six times.
8. Change the tension of conductor to T_2, T_3, T_4, etc, as in step 2 above.
9. Repeat steps 1 to 8 six times.
10. Change conductor with diameter 2, diameter 3, etc. (e.g. Aero-Z IEC62219-REV240609 conductor …).
11. Repeat steps 1 to 10 six times.
12. End test.

This procedure is briefly described in Chapter 1, Section 1.5.

As for the forced vibration method, the apparatus for determining the self-damping characteristics of the TERN or Aero-Z IEC62219-REV240609 conductor consisted of the 84.6 m span test rig housed in the VRTC of UKZN.

The TERN or Aero-Z IEC62219-REV240609 conductor is clamped between two rigid supports. One end is fixed and the other end is the load end.

An electrodynamic exciter motor or shaker, which is used for the forced vibration method, is positioned 1.2 m from the load-end fixed block, as shown below.

Inside view of VRTC Centre: showing shaker connected to transmission line

Measurements are taken using a series of accelerometers positioned at the mid and end points along the transmission line conductor. The recording equipment consists of oscilloscopes and the PUMA system, which incorporates the control system of the electrodynamic shaker.

The VRTC lab is in a fully temperature-controlled, enclosed environment. The conductor tension is measured using a load cell.

The safety of workers is guaranteed when conducting experiments in that measurement system are separated from the line system by a special guard, which can be removed during the setting up of the experiments. Helmets, goggles and ear protectors are worn at all times during experiments.

Chapter 6

RESULTS

6.1 Introduction

The experimental results presented here consist of the results for the free vibration method, as captured by the Fluke oscilloscope, and the results for the forced vibration method, as captured by the PUMA system.

In this Chapter, Section 6.2 presents the results for the free vibration method, while Section 6.3 presents the results for the forced vibration method.

6.2 Results for free vibration method

The results for the free vibration method using the TERN conductor and also the Aero-Z IEC62219-REV240609 conductor are presented below. The Fluke Scope Meter was used to capture or store the results from the accelerometer for both conductors.

6.2.1 Results of free vibration for the TERN conductor

Following steps 1 to 6 of the experimental procedure described in Chapter 5 Section 5.3, 45 series of results were obtained and stored in the Fluke Scope Meter, as depicted in the directory shown in Figure 13. The decision was made to include a large number of results in order to represent reasonable statistical data.

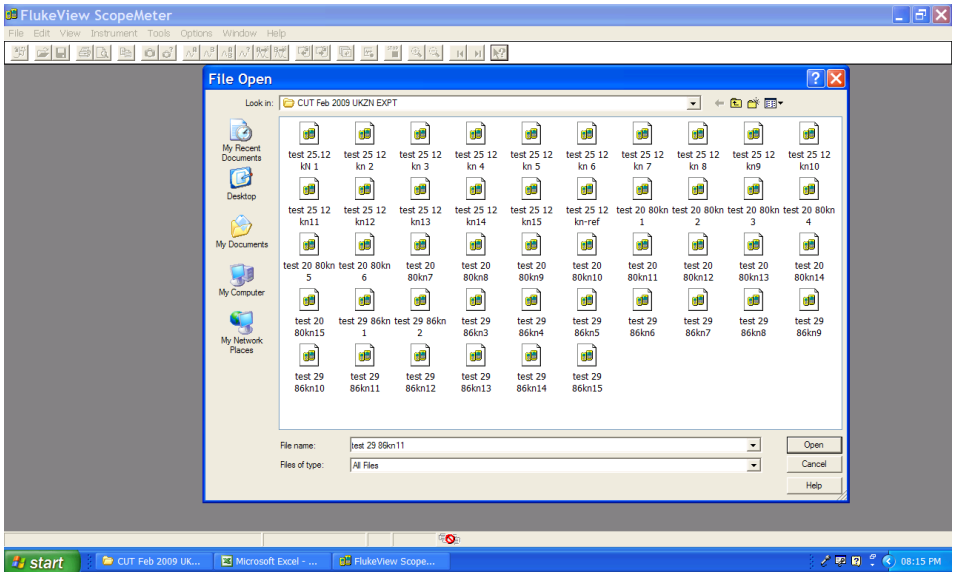

Figure 13: Directory containing 45 data series using Fluke Scope Meter

Figures 14 to 16 below show various results for the free vibration method; while Tables 6 to 9 depicts the corresponding analyses (see Chapter 7).

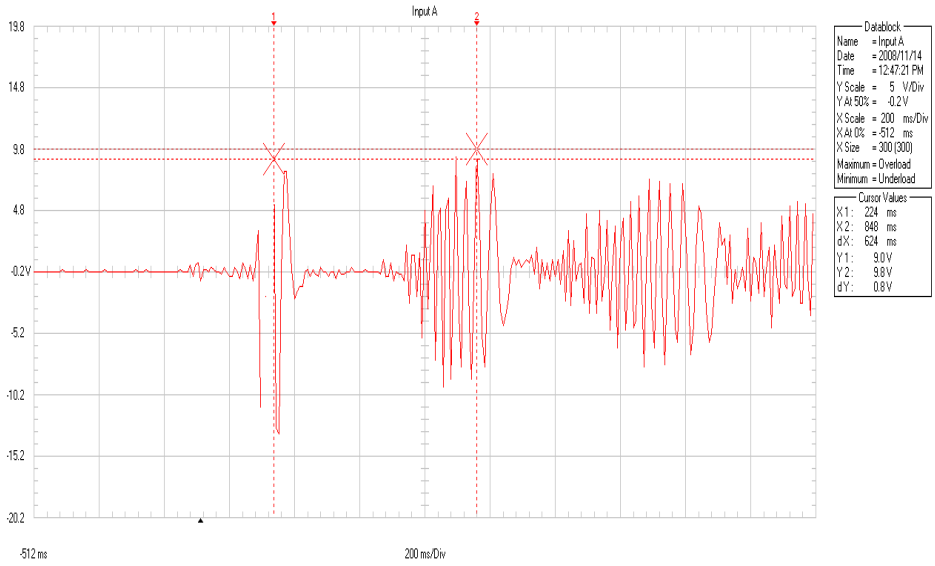

Figure 14: Excitation at $1.2\ m$ measured from load end, cable tension = 20.8kN

From Figure 14 the measurements of the peak amplitudes $(X_1, Y_1), (X_2, Y_2), \ldots, (X_6, Y_6)$ (where Y is in (mV-mill volts) and X is in (ms-mill seconds)) are obtained (using the legend under cursor values which correspond to the data block of input A) and analysed in Chapter 7 Table 6. The travelling wave forms are six in the first loop and also in the second lop see Figure 14 above. The time difference $(X_2 - X_1)$ or dX is used to obtain the frequency in (Hz) while the decaying portion of the travelling wave is used to obtain the log decrement, δ, damping coefficient, ζ, and frequency of decaying oscillations, ω, (see Chapter 7 Table 6 and Table 7).

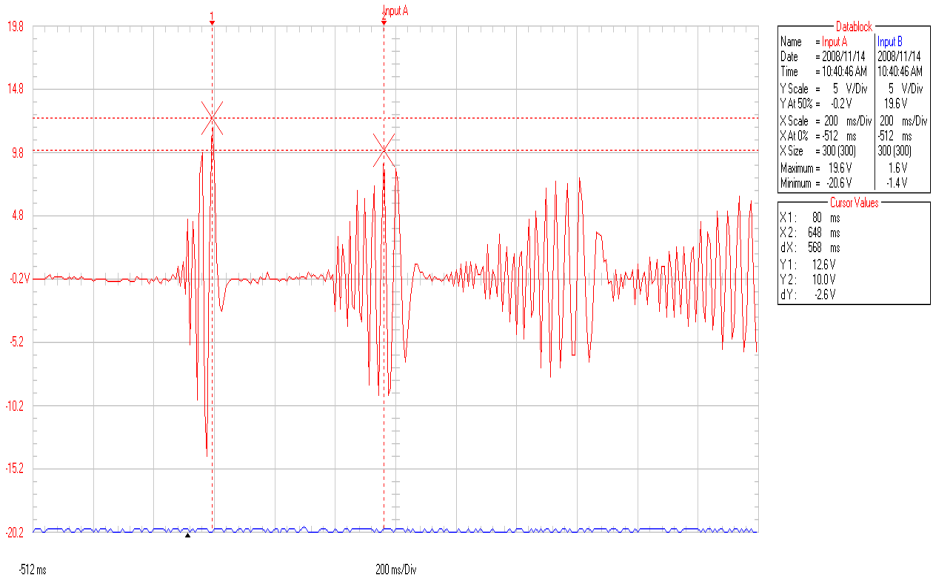

Figure 15: Excitation at $1.2\ m$ measured from load end, cable tension = 25.12 kN

From Figure 15 the measurements of the peak amplitudes $(X_1, Y_1), (X_2, Y_2), \ldots, (X_6, Y_6)$ (where Y is in (mV-mill volts) and X is in (ms-mill seconds)) are obtained (using the legend under cursor values which correspond to the data block of input A) and analysed in Chapter 7 Table 8. The travelling wave forms are three in the first loop and also in the second lop see Figure 15 above. The time difference $(X_2 - X_1)$ or dX is used to obtain the frequency in (Hz) while the decaying portion of the travelling wave is used to obtain the

log decrement, δ, damping coefficient, ζ, and frequency of decaying oscillations, ω, (see Chapter 7 Table 8).

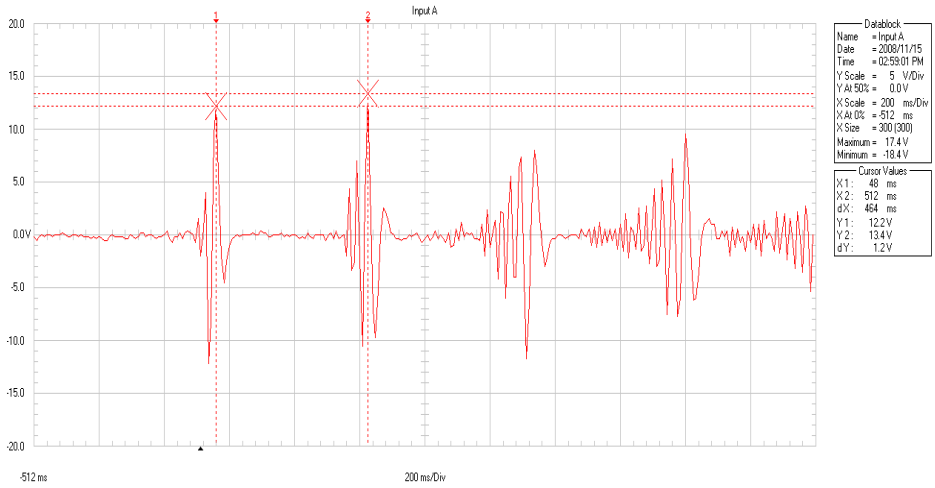

Figure 16: Excitation at $1.2\ m$ measured from load end, cable tension = 29.86 kN

From Figure 16 the measurements of the peak amplitudes $(X_1, Y_1), (X_2, Y_2), \ldots, (X_6, Y_6)$ (where Y is in (mV-mill volts) and X is in (ms-mill seconds)) are obtained (using the legend under cursor values which correspond to the data block of input A) and analysed in Chapter 7 Table 9. The travelling wave forms are two in the first loop, in the second lop and also in the third loop see Figure 16 above. The time difference $(X_2 - X_1)$ or dX is used to obtain the frequency in (Hz) while the decaying portion of the travelling wave is used to obtain the log decrement, δ, damping coefficient, ζ, and frequency of decaying oscillations, ω, (see Chapter 7 Table 9).

The tension of the transmission line was varied each time from 20.8 kN, then 25.12 kN, to 29.86 kN. This was done to show the effect of conductor tension on the characteristics of the conductor (frequency of decaying vibrations, log decrements and corresponding damping factors, and periodic time interval between travelling wave pulses and corresponding wavelength) which are analysed in Chapter 7 Section 7.2.

More results appear in Appendix I, including further magnified results stored in the Fluke ScopeMeter (Figures 66 to 89). Again, a large number of results were decided upon to represent reasonable statistical data.

6.2.2 Results of free vibration for the Aero-Z IEC62219-REV240609 conductor

Figures 17 to 25 below show various free vibration results of the Aero-Z IEC62219-REV240609 conductor, while Tables 10 to 15 depict the corresponding analyses (see Chapter 7).

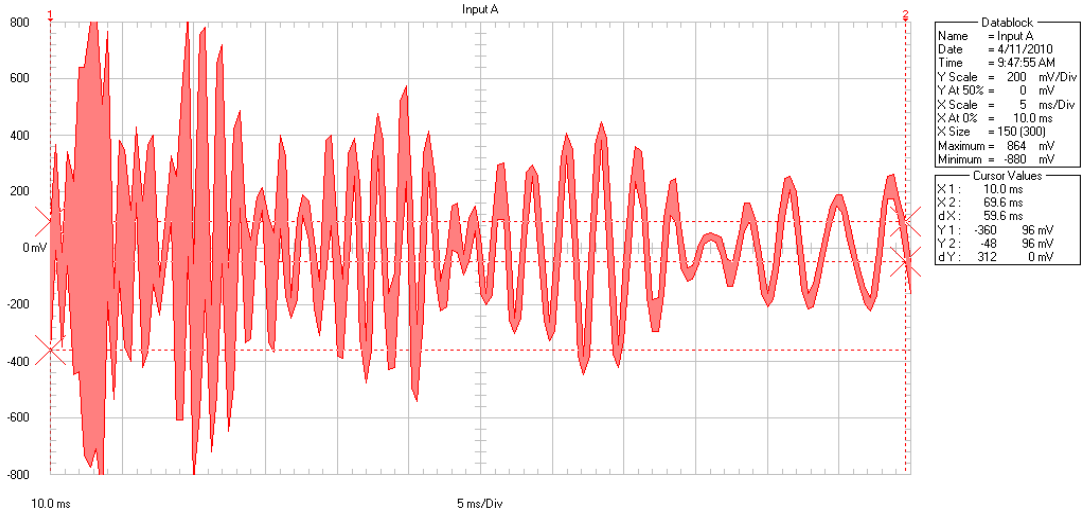

Figure 17: Excitation at $1.2\ m$ measured from load end, cable tension = 24.01 kN without mass absorber dampers.

From Figure 17 the measurements of the peak amplitudes $(X_1, Y_1), (X_2, Y_2), \ldots, (X_6, Y_6)$ (where Y is in (mV-mill volts) and X is in (ms-mill seconds)) are obtained (using the legend under cursor values which correspond to the data block of input A) and analysed in Chapter 7 Table 10. The travelling wave forms are four in the first loop and also in the second lop see Figure 17 above. The time difference $(X_2 - X_1)$ or dX is used to obtain the frequency in (Hz) while the decaying portion of the travelling wave is used to obtain the

log decrement, δ, damping coefficient, ζ, and frequency of decaying oscillations, ω, (see Chapter 7 Table 10).

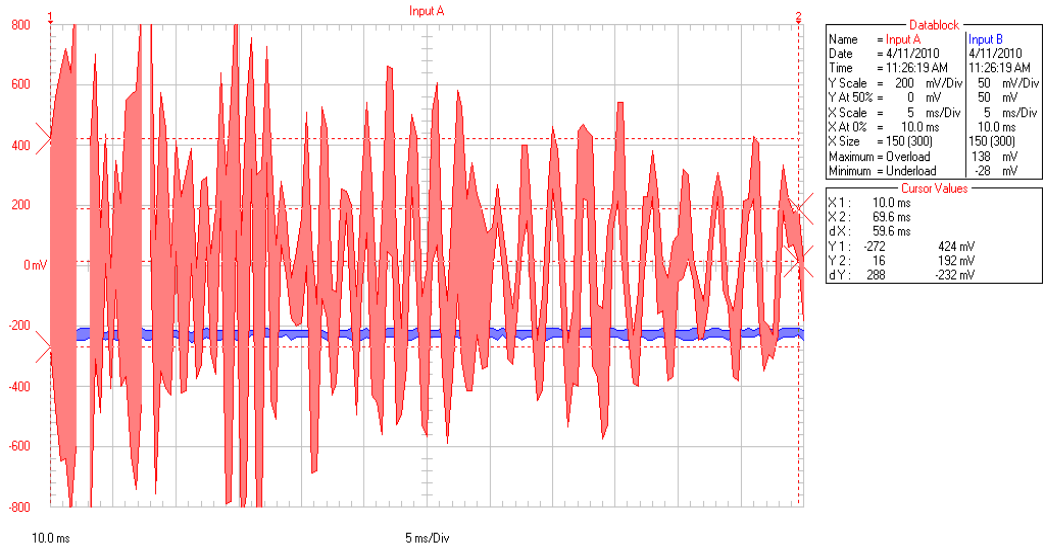

Figure 18: Excitation at $1.2\ m$ measured from load end, cable tension = 24.01 kN with one mass absorber damper.

From Figure 18 the measurements of the peak amplitudes $(X_1, Y_1), (X_2, Y_2), \ldots, (X_6, Y_6)$ (where Y is in (mV-mill volts) and X is in (ms-mill seconds)) are obtained (using the legend under cursor values which correspond to the data block of input A) and analysed in Chapter 7 Table 11. The travelling wave forms are six in the first loop and four in the second lop see Figure 18 above. The time difference $(X_2 - X_1)$ or dX is used to obtain the frequency in (Hz) while the decaying portion of the travelling wave is used to obtain the log decrement, δ, damping coefficient, ζ, and frequency of decaying oscillations, ω, (see Chapter 7 Table 11).

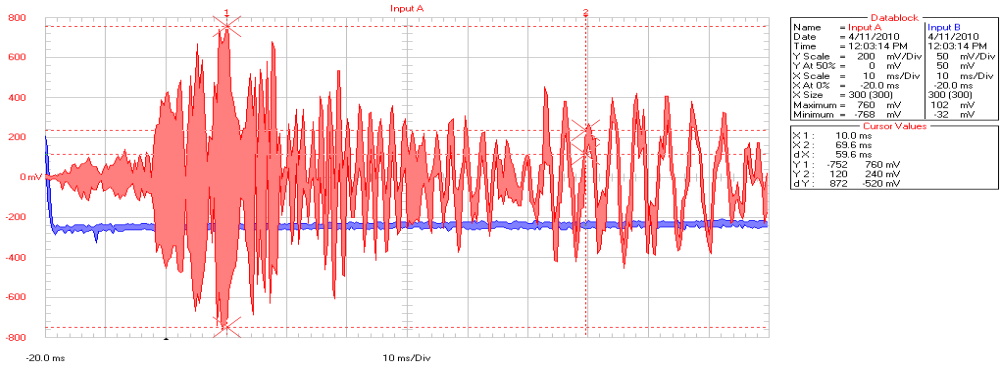

Figure 19: Excitation at $1.2\ m$ measured from load end, cable tension = 24.01 kN with two mass absorber dampers.

From Figure 19 the measurements of the peak amplitudes $(X_1, Y_1), (X_2, Y_2), \ldots, (X_6, Y_6)$ (where Y is (mV-mill volts) and X is (ms-mill seconds)) are obtained (using the legend under cursor values which correspond to the data block of input A) and analysed in Chapter 7 Table 12. The travelling wave forms are nine in the first loop and five in the second lop see Figure 19 above. The time difference $(X_2 - X_1)$ or dX is used to obtain the frequency in (Hz) while the decaying portion of the travelling wave is used to obtain the log decrement, δ, damping coefficient, ζ, and frequency of decaying oscillations, ω, (see Chapter 7 Table 12).

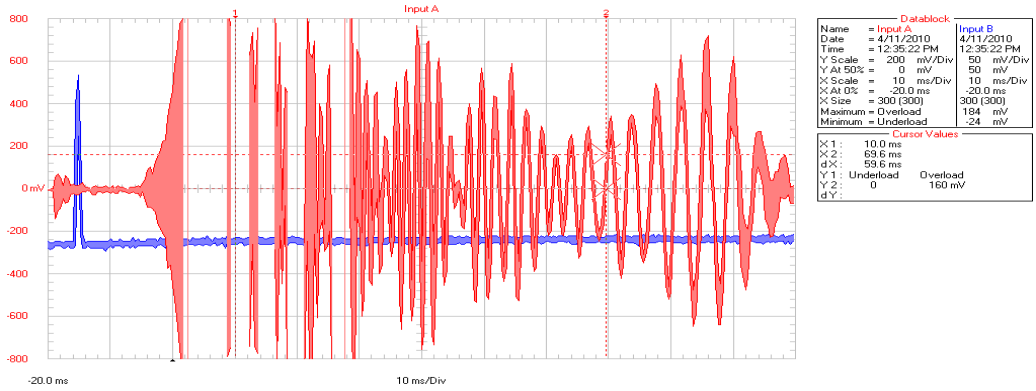

Figure 20: Excitation at $1.2\ m$ measured from load end, cable tension = 27.02 kN without mass absorber dampers.

From Figure 20 the measurements of the peak amplitudes $(X_1, Y_1), (X_2, Y_2), \ldots, (X_6, Y_6)$ (where Y is in (mV-mill volts) and X is in ms-mill seconds) are obtained (using the legend under cursor values which correspond to the data block of input A) and analysed in Chapter 7 Table 13. The travelling wave forms are five in the first loop and four in the second lop see Figure 20 above. The time difference $(X_2 - X_1)$or dX is used to obtain the frequency in (Hz) while the decaying portion of the travelling wave is used to obtain the log decrement, δ, damping coefficient, ζ, and frequency of decaying oscillations, ω, (see Chapter 7 Table 13).

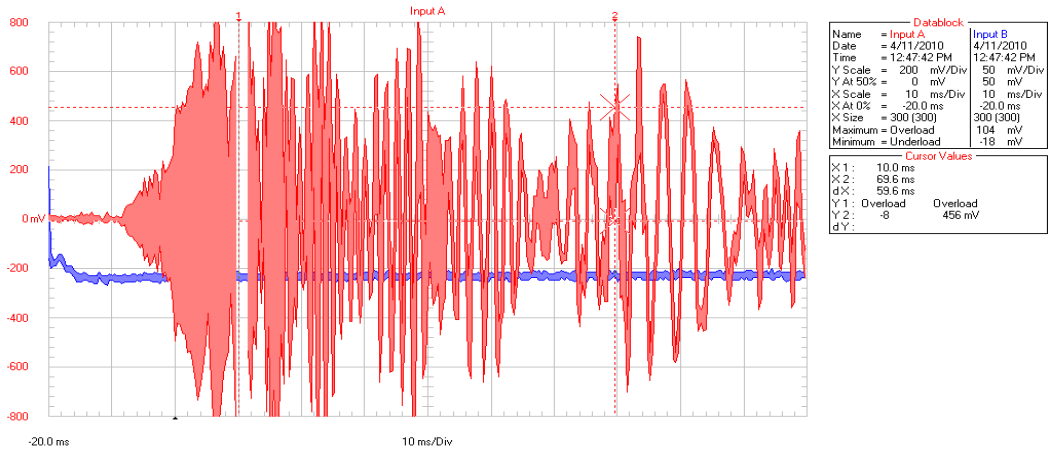

Figure 21: Excitation at $1.2\ m$ measured from load end, cable tension = 27.02 kN with one mass absorber damper.

From Figure 21 the measurements of the peak amplitudes $(X_1, Y_1), (X_2, Y_2), \ldots, (X_6, Y_6)$ (where Y is in (mV-mill volts) and X is in (ms-mill seconds)) are obtained (using the legend under cursor values which correspond to the data block of input A) and analysed in Chapter 7 Table 14. The travelling wave forms are six in the first loop and three in the second lop see Figure 21 above. The time difference $(X_2 - X_1)$or dX is used to obtain the frequency in (Hz) while the decaying portion of the travelling wave is used to obtain the

log decrement, δ, damping coefficient, ζ, and frequency of decaying oscillations, ω, (see Chapter 7 Table 14).

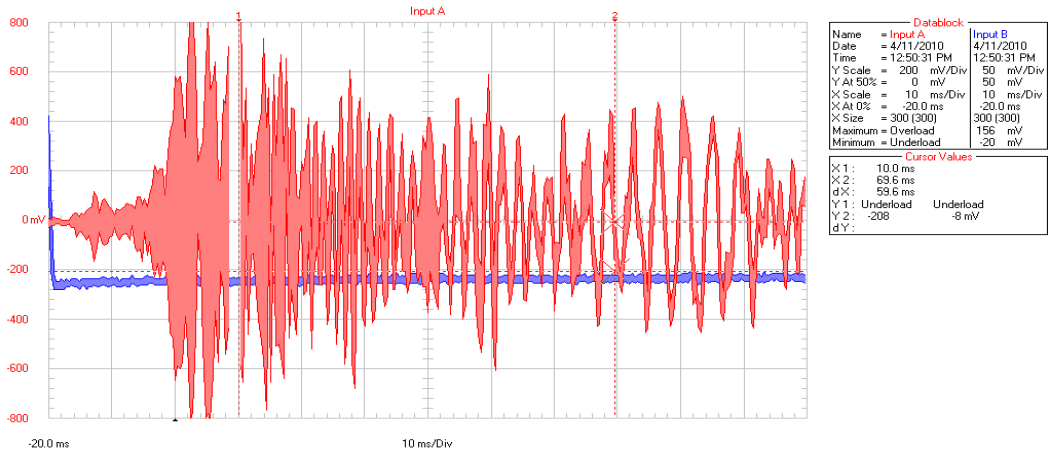

Figure 22: Excitation at $1.2\ m$ measured from load end, cable tension = 27.02 kN with two mass absorber dampers.

From Figure 22 the measurements of the peak amplitudes $(X_1, Y_1), (X_2, Y_2), \ldots, (X_6, Y_6)$ (where Y is in (mV) and X is in (ms)) are obtained (using the legend under cursor values which correspond to the data block of input A) and analysed in Chapter 7 Table 27. The travelling wave forms are seven in the first loop and five in the second lop see Figure 22 above. The time difference $(X_2 - X_1)$ or dX is used to obtain the frequency in (Hz) while the decaying portion of the travelling wave is used to obtain the log decrement, δ, damping coefficient, ζ, and frequency of decaying oscillations, ω, (see Chapter 7 Table 15).

The tension of the transmission line varied from 24.01 kN to 27.02 kN. This was done to show the effect of conductor tension on the characteristics of the conductor (frequency of decaying vibrations, log decrements and corresponding damping factors, and periodic time interval between travelling wave pulses and corresponding wavelength) which are analysed in Chapter 7 Section 7.3. Furthermore, tests were done on the cable without dampers, the cable with one mass absorber damper positioned 23.6 metres from one fixed end, and the

cable with two mass absorber dampers positioned 23.6 metres from each of the two fixed ends. Stockbridge dampers are mass absorbers used in these experiments.

More results appear in Appendix III, including further magnified results stored in the Fluke ScopeMeter (Figures 106 to 117). Again, a large number of results were decided upon to represent reasonable statistical data.

6.3 Results of forced vibration method

The results for the forced vibration method using the TERN conductor and also the Aero-Z IEC62219-REV240609 conductor are presented below. The PUMA system was used to capture and store the results from the accelerometers for both conductors.

6.3.1 Results of forced vibration for the TERN conductor

For steps 1 to 8 of the experimental procedure described in Chapter 5, the series of results shown in Figures 23 to 26 below were obtained. Figures 23 to 26 show the results for the sweep tests stored in the spectral dynamic viewer of the PUMA system. Results in the form of a spreadsheet were also extracted from the PUMA system and plotted in Microsoft Excel (see Figures 39, 41, 43, and 45 in Chapter 8) while Tables 16 to 19 depict the corresponding analyses (see Chapter 8). CH 15 represented data extracted from the accelerometer positioned at end-span while CH 10 represented data extracted from the accelerometer positioned at mid-span.

The results from the spreadsheet are easily amenable to analysis, as detailed in Chapter 8, because they are available as numbers. More results appear in Appendix II. In this case too, a large number of results were decided upon to represent reasonable statistical data.

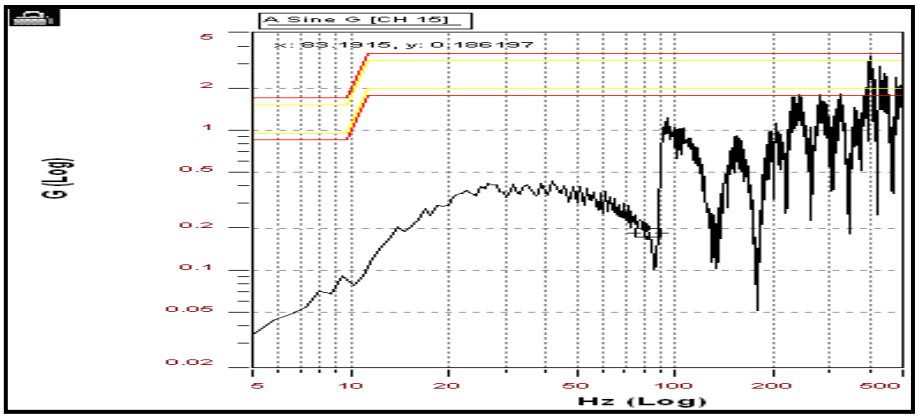

Figure 23: Sweep test from spectral dynamic viewer showing a graph of amplitude (G) versus frequency (Hz). "G" is force in Newton.
(Data extracted from the accelerometer positioned at end-span)

Figure 23 shows the results for the sweep test plotted by the spectral dynamic viewer of the PUMA system for a cable tension of 25.11kN. The results were captured from the accelerometer positioned at end-span of the TERN conductor cable. There are six most salient peaks in Figure 23 (for the frequency range of $5\,Hz$ to $300\,Hz$) and are clearer shown by the spreadsheet graph in Chapter 8, Figure 39. The data are analysed in Chapter 8, Figures 39 and 40 together with Table 16.

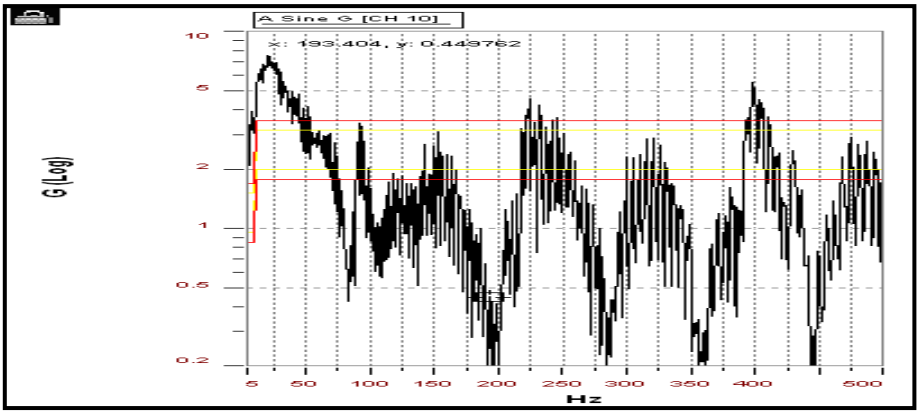

Figure 24: Sweep test from spectral dynamic viewer showing a graph of amplitude (G) versus frequency (Hz). "G" is force in Newton.
(Data extracted from the accelerometer positioned at mid-span)

Figure 24 shows the results for the sweep test plotted by the spectral dynamic viewer of the PUMA system for a cable tension of 25.11 kN. The results were captured from the accelerometer positioned at end-span of the TERN conductor cable. There are four most salient peaks in Figure 24 (for the frequency range of $5\,Hz$ to $300\,Hz$) and are clearer shown by the spreadsheet graph in Chapter 8, Figure 41. The data are analysed in Chapter 8, Figures 41 and 42 together with Table 17.

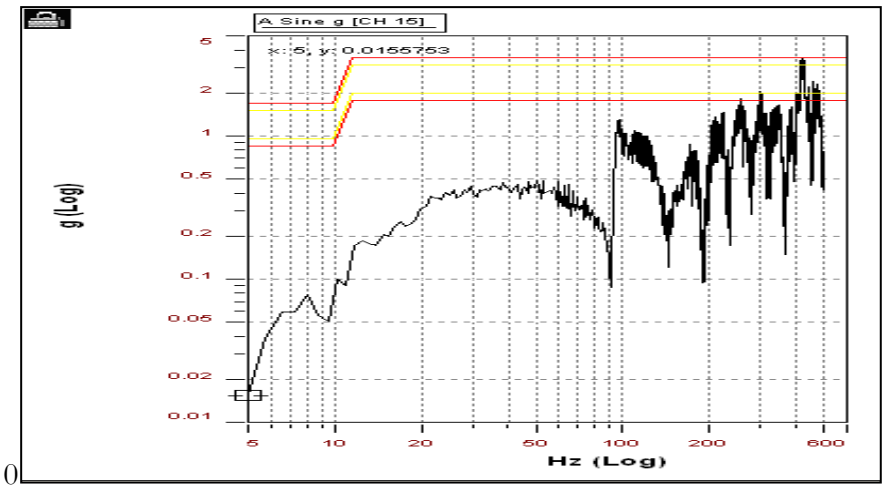

Figure 25: Sweep test from spectral dynamic viewer showing a graph of amplitude (G) versus frequency (Hz). "G" is force in Newton.
(Data extracted from the accelerometer positioned at end-span)

Figure 25 shows results from the sweep test plotted by the spectral dynamic viewer of the PUMA system for a cable tension of 29.56 kN. The results were captured from the accelerometer positioned at mid-span of the TERN conductor cable. There are five most salient peaks in Figure 25 (for the frequency range of $5\,Hz$ to $300\,Hz$) and are clearer shown by the spreadsheet graph in Chapter 8, Figure 43. The data are analysed in Chapter 8, Figures 43 and 44 together with Table 18.

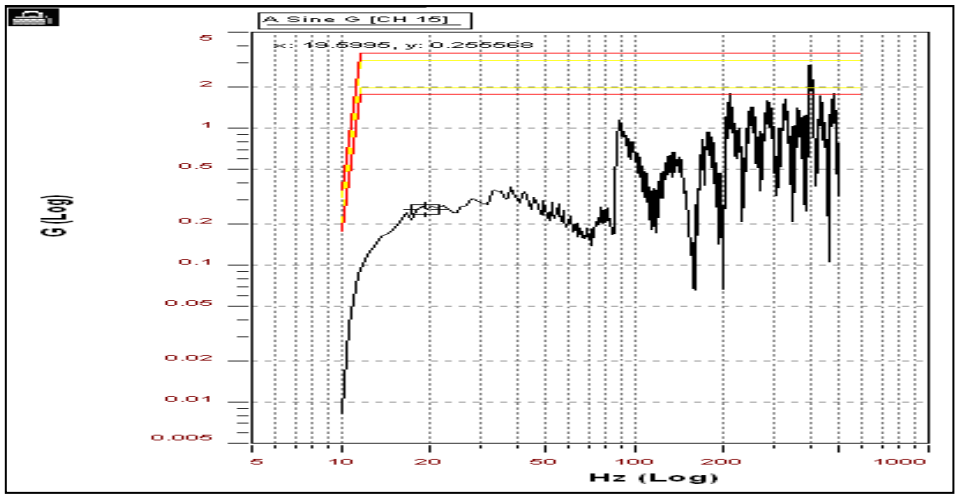

Figure 26: Sweep test from spectral dynamic viewer showing a graph of amplitude (G) versus frequency (Hz). "G" is force in Newton.
(Data extracted from the accelerometer positioned at end-span)

Figure 26 shows the results for the sweep test plotted by the spectral dynamic viewer of the PUMA system for a cable tension of 20.73 kN. The results were captured from the accelerometer positioned at end-span of the TERN conductor cable. There are seven most salient peaks in Figure 26 (for the frequency range of $5\,Hz$ to $300\,Hz$) and are clearer shown by the spreadsheet graph in Chapter 8, Figure 45. The data are analysed in Chapter 8, Figures 45 and 46 together with Table 19.

6.3.2 Results of forced vibration for the Aero-Z IEC62219-REV240609 conductor

For steps 1 to 8 of the experimental procedure described in Chapter 5, the series of results shown in Figures 26 to 37 below were obtained. Figures 26 to 37 show the results for the sweep tests stored in the spectral dynamic viewer of the PUMA system. Results in the form of a spreadsheet were also extracted from the PUMA system and plotted in Microsoft Excel as shown in Chapter 8, Figures 47, 49, 51, 53, 55, 57, 59, 61, 63, 65, 67 and 69, while Tables 20 to 31 depict the corresponding analyses (see Chapter 8).

These results from the spreadsheet are easily amenable to analysis, as detailed in Chapter 8, because they are available as numbers. More results appear in Appendix IV. In this case too, a large number of results were decided upon to represent reasonable statistical data.

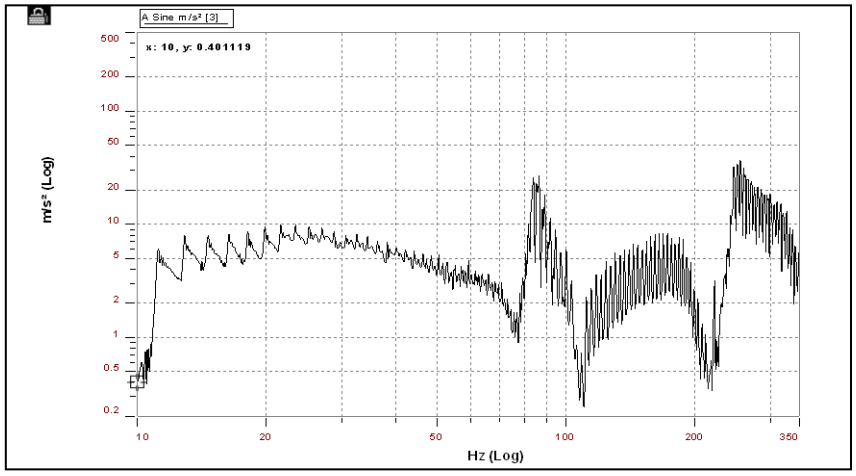

Figure 27: Sweep test from spectral dynamic viewer showing a graph of amplitude (G) versus frequency (Hz) without mass absorber dampers. "G" is force in Newton.
(Data extracted from the accelerometer positioned at mid-span)

Figure 27 shows the results for the sweep test plotted by the spectral dynamic viewer of the PUMA system for a cable tension of 24.01kN. The results were captured from the accelerometer positioned at mid-span of the Aero-Z IEC62219-REV240609 conductor cable. There are four most salient peaks in Figure 27 (for the frequency range of $10\ Hz$ to $350\ Hz$) and are clearer shown by the spreadsheet graph in Chapter 8, Figure 47. The data are analysed in Chapter 8, Figures 47 and 48 together with Table 20.

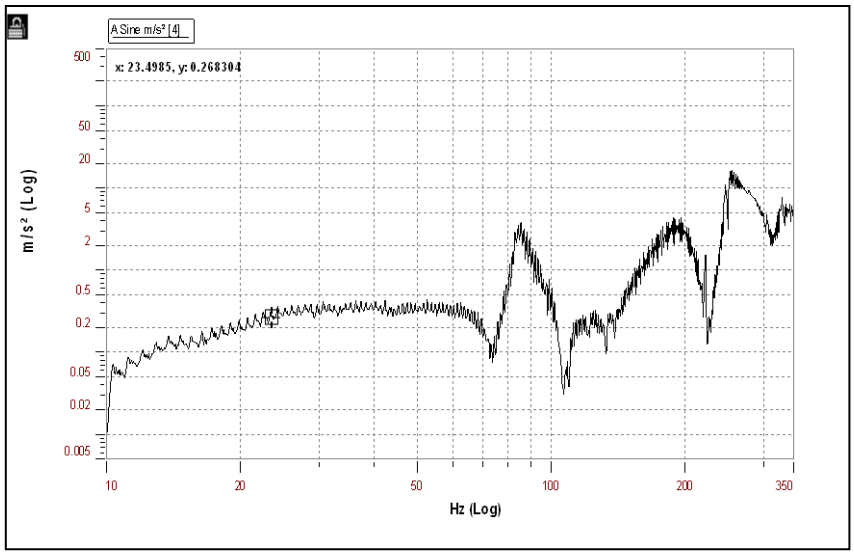

Figure 28: Sweep test from spectral dynamic viewer showing a graph of amplitude (G) versus frequency (Hz) without mass absorber dampers. "G" is force in Newton.
(Data extracted from the accelerometer positioned at end-span)

Figure 28 shows the results for the sweep test plotted by the spectral dynamic viewer of the PUMA system for a cable tension of 24.01kN. The results were captured from the accelerometer positioned at end-span of the Aero-Z IEC62219-REV240609 conductor. There are four most salient peaks in Figure 28 (for the frequency range of $10\,Hz$ to $350\,Hz$) and are clearer shown by the spreadsheet graph in Chapter 8, Figure 49. The data are analysed in Chapter 8, Figures 49 and 50 together with Table 21.

The mass absorber damper positioned at 23.6 metres.

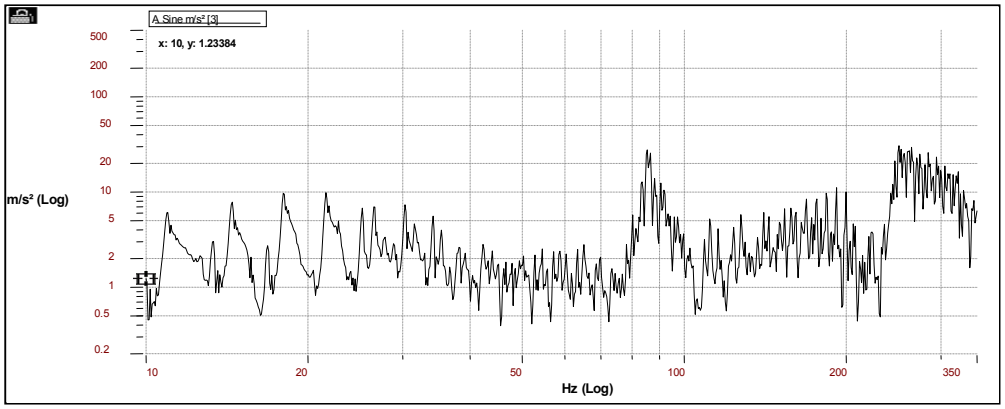

Figure 29: Sweep test from spectral dynamic viewer showing a graph of amplitude (G) versus frequency (Hz) with one mass absorber dampers. "G" is force in Newton.
(Data extracted from the accelerometer positioned at mid-span)

Figure 29 shows the results for the sweep test plotted by the spectral dynamic viewer of the PUMA system for a cable tension of 24.01kN. The results were captured from the accelerometer positioned at mid-span of the Aero-Z IEC62219-REV240609 conductor. There are four most salient peaks in Figure 29 (for the frequency range of $10\,Hz$ to $350\,Hz$) and are clearer shown by the spreadsheet graph in Chapter 8, Figure 51. The data are analysed in Chapter 8, Figures 51 and 52 together with Table 22.

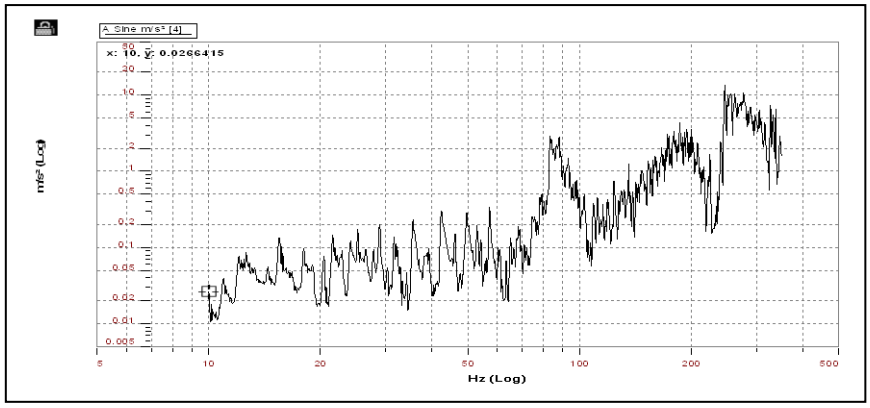

Figure 30: Sweep test from spectral dynamic viewer showing a graph of amplitude (G) versus frequency (Hz) with one mass absorber dampers. "G" is force in Newton.(Data extracted from the accelerometer positioned at end-span)

Figure 30 shows the results for the sweep test plotted by the spectral dynamic viewer of the PUMA system for a cable tension of 24.01kN. The results were captured from the accelerometer positioned at end-span of the Aero-Z IEC62219-REV240609 conductor. There are four most salient peaks in Figure 30 (for the frequency range of $10\ Hz$ to $350\ Hz$) and are clearer shown by the spreadsheet graph in Chapter 8, Figure 53. The data are analysed in Chapter 8, Figures 53and 54 together with Table 23.

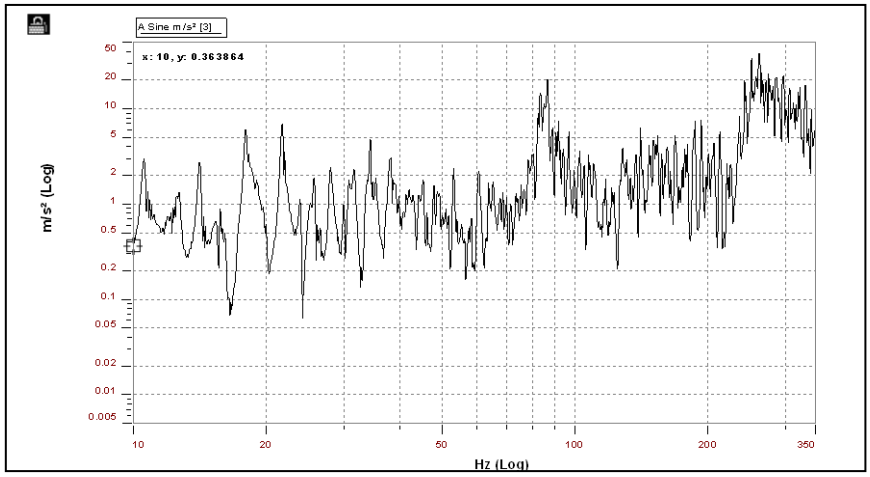

Figure 31: Sweep test from spectral dynamic viewer showing a graph of amplitude (G) versus frequency (Hz) with two mass absorber dampers. "G" is force in Newton.
(Data extracted from the accelerometer positioned at mid-span)

Figure 31 shows the results for the sweep test plotted by the spectral dynamic viewer of the sweep test plotted by the spectral dynamic viewer of the PUMA system for a cable tension of 24.01kN. The results were captured from the accelerometer positioned at mid-span of the Aero-Z IEC62219-REV240609 conductor. There are four most salient peaks in Figure 31 (for the frequency range of $10\ Hz\ to\ 350\ Hz$) and are clearer shown by the spreadsheet graph in Chapter 8, Figure 55. The data are analysed in Chapter 8, Figures 55 and 56 together with Table 24.

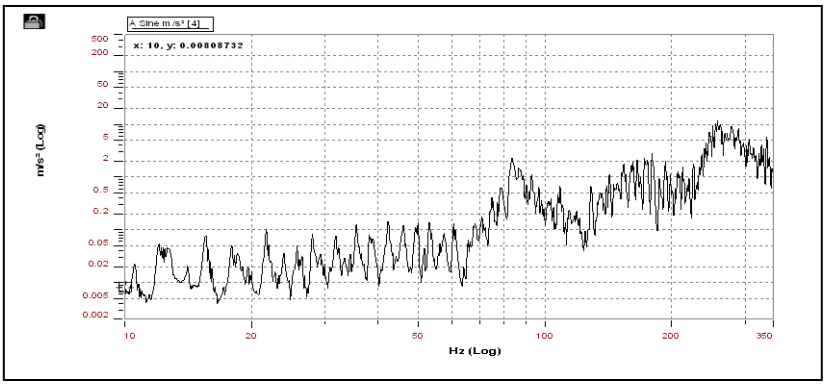

Figure 32: Sweep test from spectral dynamic viewer showing a graph of amplitude (G) versus frequency (Hz) with two mass absorber dampers. "G" is force in Newton.
(Data extracted from the accelerometer positioned at end-span)

Figure 32 shows the results for the sweep test plotted by the spectral dynamic viewer of the PUMA system for a cable tension of 24.01kN. The results were captured from the accelerometer positioned at end-span of the Aero-Z IEC62219-REV240609 conductor. There are four most salient peaks in Figure 32 (for the frequency range of $10\ Hz$ to $350\ Hz$) and are clearer shown by the spreadsheet graph in Chapter 8, Figure 57. The data are analysed in Chapter 8, Figures 57 and 58 together with Table 25.

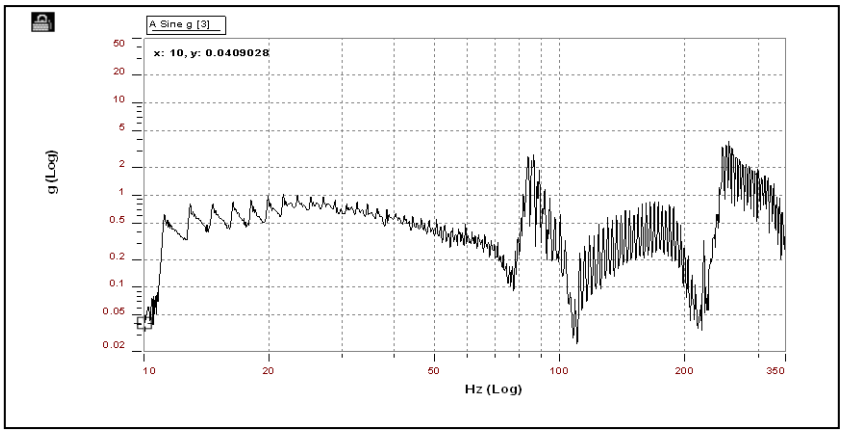

Figure 33: Sweep test from spectral dynamic viewer showing a graph of amplitude (G) versus frequency (Hz) without mass absorber dampers. "G" is force in Newton.
(Data extracted from the accelerometer positioned at mid-span)

Figure 33 shows the results for the sweep test plotted by the spectral dynamic viewer of the PUMA system for a cable tension of 27.02kN. The results were captured from the accelerometer positioned at mid-span of the Aero-Z IEC62219-REV240609 conductor. There are four most salient peaks in Figure 33 (for the frequency range of $10\ Hz$ to $350\ Hz$) and are clearer shown by the spreadsheet graph in Chapter 8, Figure 59. The data are analysed in Chapter 8, Figures 59 and 60 together with Table 26.

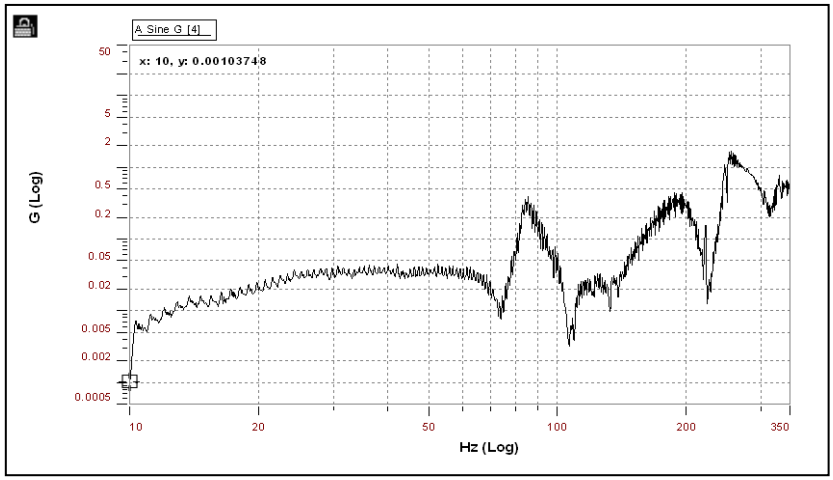

Figure 34: Sweep test from spectral dynamic viewer showing a graph of amplitude (G) versus frequency (Hz) without mass absorber dampers. "G" is force in Newton.
(Data extracted from the accelerometer positioned at mid-span)

Figure 34 shows the results for the sweep test plotted by the spectral dynamic viewer of the results for the sweep test plotted by the spectral dynamic viewer of the PUMA system for a cable tension of 27.02kN. The results were captured from the accelerometer positioned at mid-span of the Aero-Z IEC62219-REV240609 conductor. There are four most salient peaks in Figure 34 (for the frequency range of $10\ Hz$ to $350\ Hz$) and are clearer shown by the spreadsheet graph in Chapter 8, Figure 61. The data are analysed in Chapter 8, Figures 61 and 62 together with Table 27.

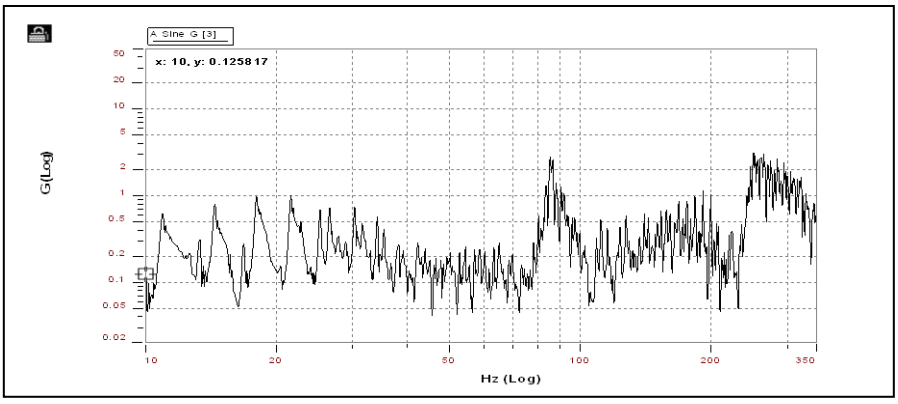

Figure 35: Sweep test from spectral dynamic viewer showing a graph of amplitude (G) versus frequency (Hz) with one mass absorber dampers. "G" is force in Newton.
(Data extracted from the accelerometer positioned at mid-span)

Figure 35 shows the results for the sweep test plotted by the spectral dynamic viewer of the PUMA system for a cable tension of 27.02kN. The results were captured from the accelerometer positioned at mid-span of the Aero-Z IEC62219-REV240609 conductor. There are four most salient peaks in Figure 35 (for the frequency range of $10\ Hz$ to $350\ Hz$) and are clearer shown by the spreadsheet graph in Chapter 8, Figure 63. The data are analysed in Chapter 8, Figures 63 and 64 together with Table 28.

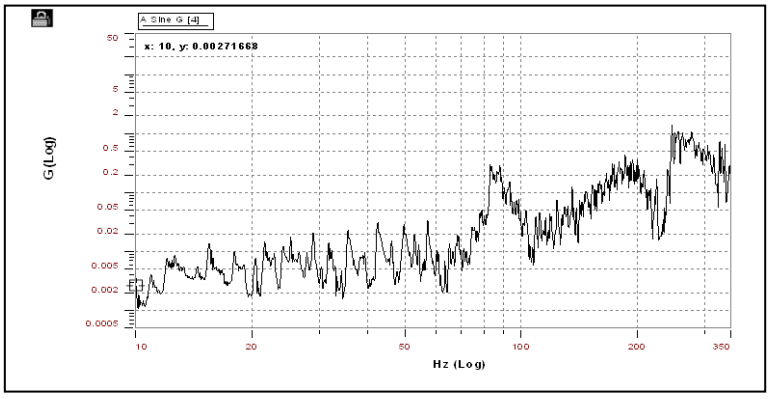

Figure 36: Sweep test from spectral dynamic viewer showing a graph of amplitude (G) versus frequency (Hz) with one mass absorber dampers. "G" is force in Newton.
(Data extracted from the accelerometer positioned at mid-span)

Figure 36 shows the results for the sweep test plotted by the spectral dynamic viewer of the PUMA system for a cable tension of 27.02kN. The results were captured from the accelerometer positioned at mid-span of the Aero-Z IEC62219-REV240609 conductor. There are four most salient peaks in Figure 36 (for the frequency range of $10\ Hz$ to $350\ Hz$) and are clearer shown by the spreadsheet graph in Chapter 8, Figure 65. The data are analysed in Chapter 8, Figures 65 and 66 together with Table 29.

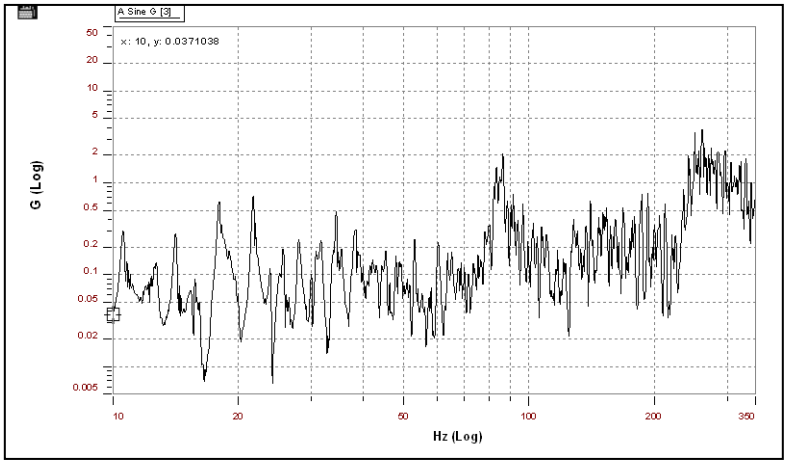

Figure 37: Sweep test from spectral dynamic viewer showing a graph of amplitude (G) versus frequency (Hz) with two mass absorber dampers. "G" is force in Newton.
(Data extracted from the accelerometer positioned at mid-span)

Figure 37 shows the results for the sweep test plotted by the spectral dynamic viewer of the PUMA system for a cable tension of 27.02kN. The results were captured from the accelerometer positioned at mid-span of the Aero-Z IEC62219-REV240609 conductor. There are four most salient peaks in Figure 37 (for the frequency range of $10\ Hz$ to $350\ Hz$) and are clearer shown by the spreadsheet graph in Chapter 8, Figure 67. The data are analysed in Chapter 8, Figures 67 and 68 together with Table 30.

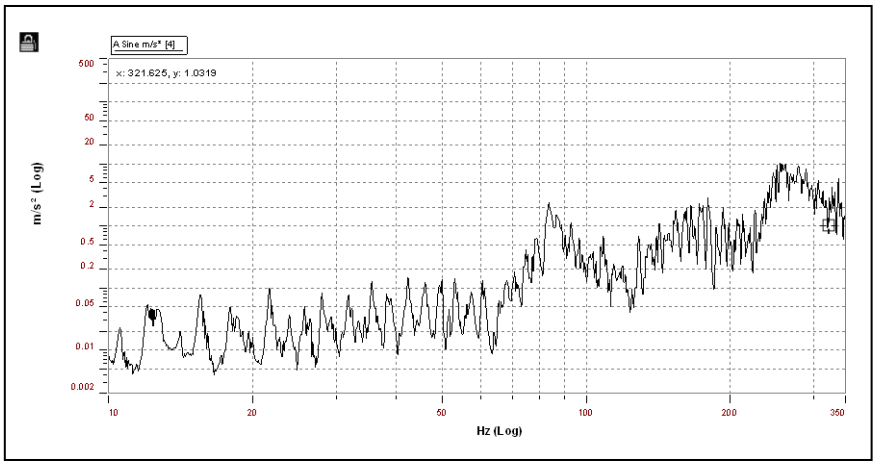

Figure 38: Sweep test from spectral dynamic viewer showing a graph of amplitude (G) versus frequency (Hz) with two mass absorber dampers. "G" is force in Newton.

(Data extracted from the accelerometer positioned at mid-span)

Figure 38 shows the results for the sweep test plotted by the spectral dynamic viewer of the PUMA system for a cable tension of 27.02 kN. The results were captured from the accelerometer positioned at end-span of the Aero-Z IEC62219-REV240609 conductor. There are four most salient peaks in Figure 38 (for the frequency range of $10\ Hz$ to $350\ Hz$) and are clearer shown by the spreadsheet graph in Chapter 8, Figure 69. The data are analysed in Chapter 8, Figures 69 and 70 together with Table 31.

The tension of the transmission line varied from 24.01 kN to 27.02 kN. This was done to show the effect of conductor tension on the characteristics of the conductor (frequency of decaying vibrations, log decrements and corresponding damping factors, and periodic time interval between travelling wave pulses and corresponding wavelength). Furthermore, the experiments were conducted on the cable without dampers, the cable with one mass absorber damper positioned 23.6 metres from one fixed end, and the cable with two mass absorber dampers positioned 23.6 metres from each of the two fixed ends. Stockbridge dampers were used for experiments. More results appear in Appendix IV, including further magnified results stored in the PUMA system and also stored as a spreadsheet (Figures 118 to 137). Again, a large number of results were decided upon to represent reasonable statistical data.

Chapter 7

ANALYSIS AND DISCUSSION OF RESULTS FOR THE FREE VIBRATION EXPERIMENTS

7.1 Introduction

In this Chapter, the results for the free vibration method (Chapter 6, Section 6.2) are analysed and discussed. The TERN conductor and the Aero-Z IEC62219-REV240609 conductor were used to find the differences in the self damping characteristics based on different conductors. Different tensions of range 20 kN to 30 kN were used to find the effects of tension in the self damping characteristics of the transmission line conductors. The effects of placing the accelerometers at mid-span and at the end-span of the conductor are discussed in this Chapter. Lastly, how to include the self damping in the mathematical model is discussed in this Chapter.

In this Chapter, Section 7.2 presents the analysis and discussion of free vibration method on the TERN conductor, Section 7.3 presents the analysis and discussion of free vibration method on the Aero-Z IEC62219-REV240609 conductor.

7.2 Analysis and discussion of free vibration method on the TERN conductor

The tension of the transmission line was varied each time from 20.8 kN, then 25.12 kN, to 29.86 kN. This was done to show the effect of conductor tension on the characteristics of the conductor (frequency of decaying vibrations, log decrements and corresponding damping factors, and periodic time interval between travelling wave pulses and corresponding wavelength). More results appear in Appendix I, including further magnified results stored in the Fluke ScopeMeter (Figures 71 to 94). Again, a large number of results were decided upon to represent reasonable statistical data.

7.2.1 Calculation of results for free vibration method

From the measurements of the peak amplitudes $(X_1, Y_1), (X_2, Y_2), \ldots, (X_6, Y_6)$ (where Y is in (mV) and X is in (ms)) obtained from Figure 14 of Chapter 6, the log decrement, δ, damping coefficient, ζ, and frequency of decaying oscillations, ω, are calculated using a Microsoft Excel spreadsheet as shown in Table 6 below.

Using the least squares approach based on equation (3.37) the results calculated in Table 6 show a corresponding viscous damping factor as detailed below

$$Zj = aYj + b \tag{7.1}$$

and z_j corresponding to $1n\,x_j, a\ to -\delta, y_j\ to\ j-1$ and $b\ to\ 1n\,x_1$ are noted. Hence the approach amounts to determining the constants a and b by minimising the sum of the square of the differences between the natural logarithm of the measured displacement and the straight line. The sum of the squares of the difference as the error is

$$\in = \sum_{j=1}^{6} (1nPj - aYj - b)^2 \tag{7.2}$$

To minimise the error, the two algebraic equations in the unknowns a and b to be written in the more explicit form are obtained.

$$\begin{gathered} \left(\sum_{j=1}^{6} Y^2 j\right) a + \left(\sum_{j=1}^{6} Yj\right) b = \sum_{j=1}^{6} (1nPY)Yj \\ \left(\sum_{j=1}^{6} Yj\right) a + 6b = \sum_{j=1}^{6} (1nPY) \end{gathered} \tag{7.3}$$

Inserting the values from Table 6 into equations (7.3) yields

$$\begin{gathered} 55a + 15b = 132.512 \\ 15a + 6b = 53.788 \end{gathered} \tag{7.4}$$

$$a = -0.1116, \quad b = 9.244 \tag{7.5}$$

Hence, inserting these values into equation (7.1), the straight line is given by

$$Zj = -0.116Yj + 0.944, \quad j = 1,2,\ldots 6 \tag{7.6}$$

The values of Zj are listed in Table 6.

The approximate viscous damping model yields the logarithmic decrement

$$\delta = -a = 0.1116 \tag{7.7}$$

and with the viscous damping factor

$$\zeta = \frac{\delta}{\sqrt{(2\pi)^2 + \delta^2}} = \frac{0.1116}{\sqrt{(2\pi)^2 + 0.1116}} = 0.0177 \tag{7.8}$$

Using equation (3.27) the period, wave speed and frequency are obtained as follows:

$$\tau = \frac{t_n - t_o}{n-1} = \frac{0.928 - 0.744}{6-1} = 0.0368 \text{ sec} \tag{7.9}$$

$$also \quad \omega = \frac{2\pi}{\tau} = \frac{2\pi}{0.0368} = 170.7 \ rad/s \tag{7.10}$$

$$f = \frac{1}{\tau} = \frac{1}{0.0368} = 27.2 \ Hz \tag{7.11}$$

These calculated results are shown below in the first row of Table 6.

Referring to Table 6 (from data of Figure 14 and the tension 20.8kN) the following were analysed: In the first loop; using least squares method, the log decrement was 0.112, damping factor was 0.018 and natural frequency was 170.8 rad/s. Further more in the second loop, the log decrement was 0.123, damping factor was 0.020 and natural frequency was 145.5 rad/s.

PX and PY shown in Tables 6, 8 and 9 are time (ms-milliseconds) and corresponding voltage peaks (mV-mill volts) extracted from corresponding Figures 14 to16. The rest are computed.

Table 6: Calculated results extracted from Figure 14

TERN j	PX (ms)	PY (mV)	FREQ (Hz)	ln PY	Yj	(lnPY)Yj	Yj^2	Zj	LogDec	Zeta	NatFreq (rad/s)	NatFreq (Hz)
1	744	9600.00		9.1695	0	0.0000	0	9.2442	0.112	0.018	170.8	27.2
2	768	9000.00	41.7	9.1050	1	9.1	1	9.1324				
3	800	8000.00	31.3	8.9872	2	17.9744	4	9.0205				
4	832	9000.00	31.3	9.1050	3	27.3149	9	8.9087				
5	872	8000.00	25.0	8.9872	4	35.9488	16	8.7969				
6	928	4600.00	17.9	8.4338	5	42.1691	25	8.6850				
SUM		48200.0		53.788	15	132.512	55					

Using least squares method, log-dec = 0.112, zeta = 0.018, frequency of decaying oscillation is 170.8 rad/s (27.2Hz)

TERN j	PX (ms)	PY (mV)	FREQ (Hz)	ln PY	Yj	(lnPY)Yj	Yj^2	Zj	LogDec	Zeta	NatFreq (rad/s)	NatFreq (Hz)
1	1376	7400.00		8.9092	0	0.0000	0	9.0240	0.123	0.020	145.5	23.2
2	1408	7200.00	31.3	8.8818	1	8.9	1	8.9009				
3	1440	7000.00	31.3	8.8537	2	17.7073	4	8.7778				
4	1480	7000.00	25.0	8.8537	3	26.5610	9	8.6547				
5	1528	5200.00	20.8	8.5564	4	34.2257	16	8.5316				
6	1592	3800.00	15.6	8.2428	5	41.2138	25	8.4085				
SUM		37600.0		52.298	15	128.590	55					

Using least squares method, log-dec = 0.123, zeta = 0.020, frequency of decaying oscillation is 145.5 rad/s (23.2 Hz)

Mode	Lamda (m)	Tau (s)	Freq (Hz)	Wave speed (rad/s)	Theoretical (rad/s)	Difference (rad/s)	Difference %
2	84.6	0.624	1.60	135.58	124.6	(10.99)	8.10
3	56.4	0.624	1.60	90.38		34.20	37.84
4	42.3	0.624	1.60	67.79		56.80	83.79
5	33.84	0.624	1.60	54.23		70.36	129.74

Mode	Lamda (m)	Tau (s)	Freq (Hz)	Wave speed (rad/s)	Theoretical (rad/s)	Difference (rad/s)	Difference %
2	84.6	0.528	1.89	160.23	124.6	(35.64)	22.24
3	56.4	0.528	1.89	106.82		17.77	16.64
4	42.3	0.528	1.89	80.11		44.48	55.52
5	33.84	0.528	1.89	64.09		60.50	94.39

Mode	Lamda (m)	Tau (s)	Freq (Hz)	Wave speed (rad/s)	Theoretical (rad/s)	Difference (rad/s)	Difference %
2	84.6	0.456	2.19	185.53	124.6	(60.94)	32.85
3	56.4	0.456	2.19	123.68		0.90	0.73
4	42.3	0.456	2.19	92.76		31.83	34.31
5	33.84	0.456	2.19	74.21		50.38	67.89

Conductor is excited in first mode but eventually vibrates in third mode

Experimental and theoretical wave number agree favourably at 124 rad/s within $0.73 \leq \varepsilon \leq 16.64$

Measurement of the wavelength, theoretical wave speed and experimental wave speed of a TERN conductor subjected to free vibration yielded the modes $r = 2, 3, 4 \text{ and } 5$ listed in Table 7 obtained from Figure 14 of Chapter 6.

The conductor was excited from the first mode where $r = 1$, that is, in the catenary position, but eventually vibrated in 2nd then followed by 3rd and again in 3rd modes. This was deduced from the least difference between theoretical and experimental wave speeds as shown by the calculation in Table 7 below. The experimental and theoretical wave speed agreed favourably at $124\ rad/s$ within $0.73 \leq error \leq 16.64$

Theoretical wave speed: Referring to equation (3.21) we obtain

$$c = \sqrt{\frac{T}{\rho}} = \sqrt{\frac{20730}{1.34}} = 124.38\ rad/s \tag{7.12}$$

Experimental wave speed: Referring to equation (3.26) we obtain

$$\begin{aligned} \omega &= c\frac{2\pi}{\lambda} \\ \therefore c &= \lambda f = 84.6 \times 1.6 = 135.36\ rad/s \end{aligned} \tag{7.13}$$

Other calculated results are shown in Table 18 below.

$$\begin{aligned} \%\ difference &= \frac{Calculated\ \ wave\ speed - Theoretical\ \ wave\ speed}{Calculated\ \ wave\ speed} \times 100\% \\ &= \frac{135.58 - 124.6}{135.58} \times 100\% \\ &= 8\% \end{aligned} \tag{7.14}$$

Using equations (3.29) and (3.25)

$$2kL = 2\frac{1}{\lambda}L = r, \quad r = 1, 2..., 4 \tag{7.15}$$

where r is mode, L is conductor length and λ is wavelength corresponding to a complete cycle with period τ.

r	1	2	3	4	5
mode	1 (Catenary)	2	3	4	5

At $r = 2$

$$2 \times \frac{1}{\lambda} \times 84.6 = 2, \text{ therefore } \lambda = 84.6\ m \tag{7.16}$$

At $r = 3$

TERN j	PX (ms)	PY (mV)	FREQ (Hz)	ln PY	Yj	(lnPY)Yj	Yj^2	Zj	LogDec	Zeta	NatFreq (rad/s)	(Hz)
1	744	9600.00		9.1695	0	0.0000	0	9.2442	0.112	0.018	170.8	27.2
2	768	9000.00	41.7	9.1050	1	9.1	1	9.1324				
3	800	8000.00	31.3	8.9872	2	17.9744	4	9.0205				
4	832	9000.00	31.3	9.1050	3	27.3149	9	8.9087				
5	872	8000.00	25.0	8.9872	4	35.9488	16	8.7969				
6	928	4600.00	17.9	8.4338	5	42.1691	25	8.6850				
SUM		48200.0		53.788	15	132.512	55					

$$2\times\frac{1}{\lambda}\times 84.6 = 3, \text{ therefore } \lambda = 56.4\ m \qquad (7.17)$$

Using least squares method, log-dec = 0.112, zeta = 0.018, frequency of decaying oscillation is 170.8 rad/s (27.2Hz)

At $r = 4$

$$2\times\frac{1}{\lambda}\times 84.6 = 4, \text{ therefore } \lambda = 42.3\ m \qquad (7.18)$$

At $r = 5$

$$2\times\frac{1}{\lambda}\times 84.6 = 5, \text{ therefore } \lambda = 33.84\ m \qquad (7.19)$$

Table 7: Experimental and theoretical wave numbers using results from Figure 14

Using least squares method, log-dec = 0.123, zeta = 0.020, frequency of decaying oscillation is 145.5 rad/s (23.2 Hz)

Mode	Lamda (m)	Tau (s)	Freq (Hz)	Wave speed (rad/s)	Theoretical (rad/s)	Difference (rad/s)	Difference %
2	84.6	0.624	1.60	135.58	124.6	(10.99)	8.10
3	56.4	0.624	1.60	90.38		34.20	37.84
4	42.3	0.624	1.60	67.79		56.80	83.79
5	33.84	0.624	1.60	54.23		70.36	129.74

Mode	Lamda (m)	Tau (s)	Freq (Hz)	Wave speed (rad/s)	Theoretical (rad/s)	Difference (rad/s)	Difference %
2	84.6	0.528	1.89	160.23	124.6	(35.64)	22.24
3	56.4	0.528	1.89	106.82		17.77	16.64
4	42.3	0.528	1.89	80.11		44.48	55.52
5	33.84	0.528	1.89	64.09		60.50	94.39

Mode	Lamda (m)	Tau (s)	Freq (Hz)	Wave speed (rad/s)	Theoretical (rad/s)	Difference (rad/s)	Difference %
2	84.6	0.456	2.19	185.53	124.6	(60.94)	32.85
3	56.4	0.456	2.19	123.68		0.90	0.73
4	42.3	0.456	2.19	92.76		31.83	34.31
5	33.84	0.456	2.19	74.21		50.38	67.89

Conductor is excited in first mode but eventually vibrates in third mode

Experimental and theoretical wave number agree favourably at 124 rad/s within $0.73 \le \varepsilon \le 16.64$

7.2.2 Tabulation of calculated results for free vibration method on TERN conductor

The following tabulated results for the TERN conductor were found by following the steps shown in Section 7.2.1 above. The important calculated results were the log decrement, δ, damping factor, ζ, and frequency of decaying oscillations, ω, Other results appear in Appendix I.

Referring to Table 8 (from data of Figure 15 and the tension 25.12 kN) the following were analysed: In the first loop; using least squares method, the log decrement was 0.162, damping factor was 0.026 and natural frequency was 143 rad/s. Further more in the second loop, the log decrement was 0.127, damping factor was 0.020 and natural frequency was 175 rad/s.

Measurement of the wavelength, theoretical wave speed and experimental wave speed of a TERN conductor subjected to free vibration yielded the modes $r = 2, 3, 4\ and\ 5$ listed in Table 8 obtained from Figure15 of Chapter 5. The conductor was excited from the first mode where r=1, that is, in the catenary position, but eventually vibrated in 2nd, then followed 2nd and again 2nd modes. This was deduced from the least difference between theoretical and experimental wave speeds as shown by the calculations in Table 8 below. The experimental and theoretical wave speed agreed favourably at $137\,rad/s$ within $4.87 \le error \le 14.55$.

Table 8: Calculated results from data of Figure 15

TERN	PX	PY	FREQ	ln PY	Yj	(lnPY)Yj	Yj^2	Zj	LogDec	Zeta	NatFreq
j	(ms)	(mV)	(Hz)								(rad/s)
1	632	9400.0		9.15	0	0.00	0	9.20	0.162	0.026	143
2	664	9400.0	31.3	9.15	1	9.15	1	9.04			
3	720	6800.0	17.9	8.82	2	17.65	4	8.88			
SUM		25600.0		27.12	3	26.80	5				
Using least squares method, log-dec = 0.162, zeta = 0.026, frequency of decaying oscillation is 143 rad/s (22.7											
TERN	PX	PY	FREQ	ln PY	Yj	(lnPY)Yj	Yj^2	Zj	LogDec	Zeta	NatFreq
j	(ms)	(mV)	(Hz)								(rad/s)
1	1200	8000.0		8.99	0	0.00	0	8.99	0.127	0.020	175
2	1232	7200.0	31.3	8.88	1	8.88	1	8.87			
3	1272	6200.0	25.0	8.73	2	17.46	4	8.74			
SUM		21400.0		26.60	3	26.35	5				
Using least squares method, log-dec = 0.127, zeta = 0.020, frequency of decaying oscillation is 175 rad/s (27.8											
Mode	Lamda	Tau	Freq	Wave speed	Theoretical	Difference	Difference %				
	(m)	(s)	(Hz)	(rad/s)	(rad/s)	(rad/s)					
2	84.6	0.568	1.76	148.94	136.9	(12.03)	8.07				
3	56.4	0.568	1.76	99.30		37.62	37.89				
4	42.3	0.568	1.76	74.47		62.45	83.85				
Mode	Lamda	Tau	Freq	Wave speed	Theoretical	Difference	Difference %				
	(m)	(s)	(Hz)	(rad/s)	(rad/s)	(rad/s)					
2	84.6	0.648	1.54	130.56	136.9	6.36	4.87				
3	56.4	0.648	1.54	87.04		49.88	57.31				
4	42.3	0.648	1.54	65.28		71.64	109.75				
5	33.84	0.648	1.54	52.22		84.69	162.18				
Mode	Lamda	Tau	Freq	Wave speed	Theoretical	Difference	Difference %				
	(m)	(s)	(Hz)	(rad/s)	(rad/s)	(rad/s)					
2	84.6	0.528	1.89	160.23	136.9	(23.31)	14.55				
3	56.4	0.528	1.89	106.82		30.10	28.18				
4	42.3	0.528	1.89	80.11		56.80	70.90				
5	33.84	0.528	1.89	64.09		72.83	113.63				
Conductor is excited in first mode and continues vibrating in second mode											
Experimental and theoritical wave number agree favourably at 137 rad/s within 4.87 ≤ ε ≤ 14.55											

Referring to Table 9 (from data of Figure 16 and the tension 29.86 kN) the following were analysed: In the first loop; using least squares method, the log decrement was 0.078, damping factor was 0.012 and natural frequency was 157 rad/s. Further more in the second loop, the log decrement was 1.369, damping factor was 0.213 and natural frequency was 115 rad/s. Lastly, in the third loop, the log decrement was 0.262, damping factor was 0.042 and natural frequency was 112 rad/s.

Measurement of the wavelength, theoretical wave speed and experimental wave speed of a TERN conductor subjected to free vibration yielded the modes $r = 2, 3, 4\ and\ 5$ listed in Table 9 obtained from Figure16 of Chapter 6. The conductor was excited from the first

mode where r=1, that is, in the catenary position, but eventually vibrated in 2nd, then followed 2nd and again 2nd modes. This was deduced from the least difference between theoretical and experimental wave speeds as shown by the calculations in Table 9 below. The experimental and theoretical wave speed agreed favourably at $149\,rad/s$ within $9.66 \le error \le 18.13$.

Table 9: Calculated results from data of Figure 16

TERN j	PX (ms)	PY (mV)	FREQ (Hz)	ln PY	Yj	(lnPY)Yj	Yj^2	Zj	LogDec	Zeta	NatFreq (rad/s)	NatFreq (Hz)
1	496	10600.00		9.269	0	0.0000	0	9.269	0.078	0.012	157	25.0
2	536	9800.00	25.0	9.190	1	9.2	1	9.190				
SUM		20400.0		18.459	1	9.190	1					

Using least squares method, log-dec = 0.078, zeta = 0.012, frequency of decaying oscillation is 157 rad/s (25.0 Hz)

TERN j	PX (ms)	PY (mV)	FREQ (Hz)	ln PY	Yj	(lnPY)Yj	Yj^2	Zj	LogDec	Zeta	NatFreq (rad/s)	
1	1000	11800.00		9.376	0	0.0000	0	9.376	1.369	0.213	115	18.3
2	1056	3000.00	17.9	8.006	1	8.0	1	8.006				
SUM		14800.0		17.382	1	8.006	1					

Using least squares method, log-dec = 1.369, zeta = 0.213, frequency of decaying oscillation is 115 rad/s (18.3 Hz)

TERN j	PX (ms)	PY (mV)	FREQ (Hz)	ln PY	Yj	(lnPY)Yj	Yj^2	Zj	LogDec	Zeta	NatFreq (rad/s)	
1	1464	7800.00		8.962	0	0.0000	0	8.962	0.262	0.042	112	17.9
2	1520	6000.00	17.9	8.700	1	8.7	1	8.700				
SUM		13800.0		17.661	1	8.700	1					

Using least squares method, log-dec = 0.262, zeta = 0.042, frequency of decaying oscillation is 112 rad/s (17.9 Hz)

Mode	Lamda (m)	Tau (s)	Freq (Hz)	Wave speed (rad/s)	Theoretical (rad/s)	Difference (rad/s)	Difference %
2	84.6	0.464	2.16	182.33	149.3	(33.05)	18.13
3	56.4	0.464	2.16	121.55		27.73	22.81
4	42.3	0.464	2.16	91.16		58.11	63.75
5	33.84	0.464	2.16	72.93		76.35	104.68

Mode	Lamda (m)	Tau (s)	Freq (Hz)	Wave speed (rad/s)	Theoretical (rad/s)	Difference (rad/s)	Difference %
2	84.6	0.512	1.95	165.23	149.3	(15.96)	9.66
3	56.4	0.512	1.95	110.16		39.12	35.51
4	42.3	0.512	1.95	82.62		66.66	80.68
5	33.84	0.512	1.95	66.09		83.18	125.86

Mode	Lamda (m)	Tau (s)	Freq (Hz)	Wave speed (rad/s)	Theoretical (rad/s)	Difference (rad/s)	Difference %
2	84.6	0.464	2.16	182.33	149.3	(33.05)	18.13
3	56.4	0.464	2.16	121.55		27.73	22.81
4	42.3	0.464	2.16	91.16		58.11	63.75
5	33.84	0.464	2.16	72.93		76.35	104.68

Conductor is excited in first mode and continues vibrating in second mode
Experimental and theoretical wave number agree favourably at 149 rad/s within 9.66 ≤ ε ≤ 18.13

7.2.3 Discussion of results for free vibration method on TERN conductor

1. A damping factor of $0.01 \le \varsigma \le 0.2$ was determined from 45 tests. The most dominant damping factor was $\varsigma = 0.02.$ See for example Figures 14 to 16 together with corresponding Tables 21 to 24.
2. For the free vibration method, decaying of oscillations for the TERN conductor was observed for a frequency range of $18 \le f_n \le 28\,(Hz)$. This is an indication of how fast the energy is dissipated (Also observed as 1st dominant resonance frequency). See Figures 14 to 16 together with corresponding Tables 21 to 24.
3. Travelling wave numbers were obtained. Theoretical and experimental wave numbers agreed favourably. For a tension range of $20-29\,kN,$ a wave number range of $124-149\,rad/s$ was obtained. This is also known as the c-value given by equation (3.21). See Figures 14 to 16 together with corresponding Tables 21 to 24.
4. The travelling wave numbers obtained are directly proportional to tension used. For $T = 20\,kN, c = 124\,rad/s$ and was increasing until at $T = 29\,kN, c = 149\,rad/s$.
5. From different tensions used (tension range of $20-29\,kN$) there is no effect of tension in self damping characteristics of the TERN conductor as the damping factor is within the same range of $0.01 \le \varsigma \le 0.2$.
6. Impulsive forces were introduced at position $1.2\,m,$ as well as at $1/4$ and $1/2$ span positions measured from the load-end fixed block. The damping factor was not affected by the position of impulsive forces (as damping factor is $0.01 \le \varsigma \le 0.2$ for positions $1.2\,m, 1/4$ and $1/2$) these had an effect on the mode of vibration of the conductor (the conductor excited in the mode can vibrate in second mode or vibrate in third mode) as shown in Figures 14 to 16 together with corresponding Tables 6 to 9.

7.3 Analysis and discussion of results for free vibration method on the Aero-Z IEC62219-REV240609 conductor

The tension of the transmission line varied from 24.01 kN to 27.02 kN to show the effect of conductor tension on the characteristics of the conductor (frequency of decaying vibrations, log decrements and corresponding damping factors).

The results on the cable without dampers, the cable with one mass absorber damper, and the cable with two mass absorber dampers were also analysed. This was done to check if it was necessary for external damping mechanisms to be used together with transmission conductors.

More results appear in Appendix III, including further magnified results stored in the Fluke ScopeMeter (Figures 106 to 117). Again, a large number of results were decided upon to represent reasonable statistical data.

7.3.1 Tabulation of calculated results for free vibration method on Aero-Z IEC62219-REV240609 conductor

The following tabulated results for the Aero-Z IEC62219-REV240609 conductor were found by following the steps shown in Section 7.2.1 above. The calculated results are the log decrement, δ, damping coefficient, ζ, and frequency of decaying oscillations, ω.

Referring to Table 10 (from data of Figure 17 and the tension 24.01 kN) the following were analysed: In the first loop; using least squares method, the log decrement was 0.50, damping factor was 0.079 and natural frequency was 3927 rad/s. Further more in the second loop, the log decrement was 0.66, damping factor was 0.105 and natural frequency was 2480 rad/s.

Table 10: Calculated results of tension 24.01 kN without mass absorber damper from data of Figure 17

Aero-Z I	PX	PY	FREQ	ln PY	Yj	(lnPY)Yj	Yj^2	b	a	Zj	LogDec	Zeta	Period	NatFre	NatFreq
j	(ms)	(mV)	(Hz)											(rad/s)	(Hz)
1	34.8	576		6.4	0	0.0	0	6.36	-0.5	6.36	0.50	0.079	0.0016	3927	625
2	36.4	416	625	6.0	1	6.0	1			5.87					
3	38.4	160	500	5.1	2	10.2	4			5.37					
4	39.6	152	833	5.0	3	15.1	9			4.88					
SUM		1304		22.5	6	31.3	14								
Using least squares method, log-dec = 0.495, zeta = 0.079, frequency of decaying oscillation = 3927 rad/s (625 Hz)															
Aero-Z I	PX	PY	FREQ	ln PY	Yj	(lnPY)Yj	Yj^2			Zj	LogDec	Zeta		NatFre	NatFreq
j	(ms)	(mV)	(Hz)											(rad/s)	(Hz)
1	48.4	448		6.1	0	0.0	0	6.37	-0.66	6.37	0.66	0.105	0.0025	2480	394.7
2	50.8	360	417	5.9	1	5.9	1			5.71					
3	53.6	248	357	5.5	2	11.0	4			5.05					
4	56	56	417	4.0	3	12.1	9			4.39					
SUM		1112		21.5	6	29.0	14								
Using least squares method, log-dec = 0.661, zeta = 0.105, frequency of decaying oscillation = 2480.2rad/s (394.7Hz)															

Referring to Table 11 (from data of Figure 18 and the tension 24.01 kN) the following were analysed: In the first loop; using least squares method, the log decrement was 0.16, damping factor was 0.026 and natural frequency was 3272 rad/s. Further more in the second loop, the log decrement was 0.19, damping factor was 0.029 and natural frequency was 2356 rad/s.

Table 11: Calculated results of tension 24.01 kN with one mass absorber damper from data of Figure 18

Aero-Z IE j	PX (ms)	PY (mV)	FREQ (Hz)	ln PY	Yj	(lnPY)Yj	Yj^2	b	a	Zj	LogDec	Zeta	Period	NatFreq (rad/s)	NatFreq (Hz)
1	36	664		6.50	0	0.0	0	6.6	-0.161	6.56	0.16	0.026	0.002	3272	520.8
2	38.8	504	357	6.22	1	6.2	1			6.40					
3	40.8	608	500	6.41	2	12.8	4			6.24					
4	42.4	584	625.0	6.37	3	19.1	9			6.08					
5	43.6	344	833.3	5.84	4	23.4	16			5.92					
6	45.6	272	500.0	5.61	5	28.0	25			5.75					
SUM		2976		36.9	15	89.5	55								

Using least squares method, log-dec = 0.166, zeta = 0.026, frequency of decaying oscillation = 3272.5 rad/s (520.8 Hz)

Aero-Z IE j	PX (ms)	PY (mV)	FREQ (Hz)	ln PY	Yj	(lnPY)Yj	Yj^2			Zj	LogDec	Zeta		NatFreq (rad/s)	NatFreq (Hz)
1	55.2	544		6.30	0	0.0	0	6.2	-0.185	6.22	0.19	0.029	0.003	2356	375.0
2	58	384	357.1	5.95	1	6.0	1			6.03					
3	60.4	320	416.7	5.77	2	11.5	4			5.85					
4	63.2	312	357.1	5.74	3	17.2	9			5.66					
SUM		1560		23.8	6	34.7	14								

Using least squares method, log-dec = 0.661, zeta = 0.105, frequency of decaying oscillation = 2480.2rad/s (394.7Hz)

Referring to Table 12 (from data of Figure 19 and the tension 24.01 kN) the following were analysed: In the first loop; using least squares method, the log decrement was 0.074, damping factor was 0.012 and natural frequency was 3491 rad/s. Further more in the second loop, the log decrement was 0.210, damping factor was 0.033 and natural frequency was 2285 rad/s.

Table 12: Calculated results of tension 24.01 kN with two mass absorber dampers from data of Figure 19

Aero-Z I j	PX (ms)	PY (mV)	FREQ (Hz)	ln PY	Yj	(lnPY)Yj	Yj^2	b	a	Zj	LogDec	Zeta	Period	NatFreq (rad/s)	NatFreq (Hz)
1	28.4	536		6.28	0	0.0	0	6.06	-0.074	6.06	0.074	0.012	0.002	3491	555.6
2	30	296	625	5.69	1	5.7	1			5.98					
3	32	368	500	5.91	2	11.8	4			5.91					
4	34	328	500.0	5.79	3	17.4	9			5.83					
5	35.6	296	625.0	5.69	4	22.8	16			5.76					
6	37.6	360	500.0	5.89	5	29.4	25			5.69					
7	39.6	296		5.69	6	34.1	36								
8	40.8	240		5.48	7	38.4	49								
9	42.8	224		5.41	8	43.3	64								
SUM		2944		51.835	36	202.9	204								

Using least squares method, log-dec = 0.074, zeta = 0.012, frequency of decaying oscillation = 3491 rad/s (555.6 Hz)

Aero-Z I j	PX (ms)	PY (mV)	FREQ (Hz)	ln PY	Yj	(lnPY)Yj	Yj^2			Zj	LogDec	Zeta		NatFreq (rad/s)	NatFreq (Hz)
1	49	312		5.74	0	0.0	0	5.72	-0.210	5.72	0.210	0.033	0.003	2285	363.6
2	52.8	232	263.2	5.45	1	5.4	1			5.51					
3	54.8	192	500.0	5.26	2	10.5	4			5.30					
4	56.4	192	625.0	5.26	3	15.8	9			5.09					
5	60	120	277.8	4.79	4	19.1	16			4.88					
SUM		1048		26.492	10	50.9	30								

Using least squares method, log-dec = 0.210, zeta = 0.033, frequency of decaying oscillation = 2285 rad/s (363.6 Hz)

Referring to Table 13 (from data of Figure 20 and the tension 27.02 kN) the following were analysed: In the first loop; using least squares method, the log decrement was 0.694, damping factor was 0.110 and natural frequency was 3696 rad/s. Further more in the second loop, the log decrement was 0.416, damping factor was 0.066 and natural frequency was 2618 rad/s.

Table 13: Calculated results of tension 27.02 kN without mass absorber damper from data of Figure 20

Aero-Z I j	PX (ms)	PY (mV)	FREQ (Hz)	ln PY	Yj	(lnPY)Y	Yj^2	b	a	Zj	LogDec	Zeta	period	NatFreq (rad/s)	NatFreq (Hz)
1	39.2	768		6.64	0	0.00	0	7.15	-0.69	7.15	0.694	0.110	0.0017	3696.0	588.2
2	41.2	696	500	6.55	1	6.55	1			6.46					
3	42.8	616	625	6.42	2	12.85	4			5.76					
4	44.8	248	500	5.51	3	16.54	9			5.07					
5	46	40	833	3.69	4	14.76	16			4.37					
SUM		2368		28.81	10	50.69	30								

Using least squares method, log-dec = 0.694, zeta = 0.110, frequency of decaying oscillation = 3696 rad/s (588.2 Hz)

Aero-Z I j	PX (ms)	PY (mV)	FREQ (Hz)	ln PY	Yj	(lnPY)Y	Yj^2			Zj	LogDec	Zeta		NatFreq (rad/s)	NatFreq (Hz)
1	54.4	592		6.38	0	0.00	0	6.39	-0.42	6.39	0.416	0.066	0.002	2618.0	416.7
2	56.8	376	417	5.93	1	5.93	1			5.98					
3	59.2	296	417	5.69	2	11.38	4			5.56					
4	61.6	160	417	5.08	3	15.23	9			5.15					
SUM		1424		23.08	6	32.54	14								

Using least squares method, log-dec = 0.416, zeta = 0.066, frequency of decaying oscillation = 2618.0rad/s (416.7Hz)

Referring to Table 14 (from data of Figure 21 and the tension 27.02 kN) the following were analysed: In the first loop; using least squares method, the log decrement was 0.216, damping factor was 0.034 and natural frequency was 4620 rad/s. Further more in the second loop, the log decrement was 0.168, damping factor was 0.027 and natural frequency was 2417 rad/s.

Table 14: Calculated results of tension 27.02 kN with one mass absorber damper from data of Figure 21

Aero-Z	PX	PY	FREQ	ln PY	Yj	(lnPY)Yj	Yj^2	b	a	Zj	LogDec	Zeta	Period	NatFreq	NatFreq
j	(ms)	(mV)	(Hz)											(rad/s)	(Hz)
1	23.2	904		6.81	0	0.00	0	6.81	-0.216	6.81	0.216	0.034	0.0014	4620	735
2	24.4	848	833	6.74	1	6.74	1			6.60					
3	25.6	592	833	6.38	2	12.77	4			6.38					
4	23.2	336	-416.7	5.82	3	17.45	9			6.17					
5	28.4	448	192.3	6.10	4	24.42	16			5.95					
6	30	328	625.0	5.79	5	28.97	25			5.74					
SUM		3456		37.648	15	90.35	55								
Using least squares method, log-dec = 0.216, zeta = 0.034, frequency of decaying oscillation = 4620 rad/s (735 Hz)															
Aero-Z	PX	PY	FREQ	ln PY	Yj	(lnPY)Yj	Yj^2	b	a	Zj	LogDec	Zeta	Period	NatFreq	NatFreq
j	(ms)	(mV)	(Hz)											(rad/s)	(Hz)
1	38.4	828		6.72	0	0.00	0	2.63	-0.168	2.63	0.168	0.027	0.0026	2417	385
2	40	440	625	6.09	1	6.09	1			2.46					
3	43.6	592	278	6.38	2	12.77	4			2.29					
SUM		1860		19.189	3	18.85	5								
Using least squares method, log-dec = 0.168, zeta = 0.027, frequency of decaying oscillation =2417 rad/s (385 Hz)															

Referring to Table 15 (from data of Figure 22 and the tension 27.02 kN) the following were analysed: In the first loop; using least squares method, the log decrement was 1.38, damping factor was 0.21 and natural frequency was 3740 rad/s. Further more in the second loop, the log decrement was 0.30, damping factor was 0.047 and natural frequency was 2732 rad/s.

Table 15: Calculated results of tension 27.02 kN with two mass absorber dampers from data of Figure 22

Aero-Z j	PX (ms)	PY (mV)	FREQ (Hz)	ln PY	Yj	(lnPY)Yj	Yj^2	b	a	Zj	LogDec	Zeta	Period	NatFreq (rad/s)	NatFreq (Hz)
1	27.6	608		6.41	0	0.00	0	11.87	-1.38	11.87	1.38	0.21	0.0017	3740	595.24
2	29.2	496	625	6.21	1	6.21	1			10.49					
3	30.8	440	625	6.09	2	12.17	4			9.11					
4	32.4	392	625	5.97	3	17.91	9			7.73					
5	34	432	625	6.07	4	24.27	16			6.35					
6	36	352	500	5.86	5	29.32	25			4.97					
7	37.6	280		5.63	6	33.81	36								
SUM		3000		42.24	21	123.69	91								

Using least squares method, log-dec = 1.380, zeta = 0.21, frequency of decaying oscillation = 3740 rad/s (595.2 Hz)

Aero-Z j	PX (ms)	PY (mV)	FREQ (Hz)	ln PY	Yj	(lnPY)Yj	Yj^2			Zj	LogDec	Zeta		NatFreq (rad/s)	NatFreq (Hz)
1	49.6	592		6.38	0	0.00	0	6.3444	-0.30	6.34	0.30	0.047	0.0023	2732	435
2	51.6	384	500	5.95	1	5.95	1			6.05					
3	54.4	344	357	5.84	2	11.68	4			5.75					
4	56.8	224	417	5.41	3	16.23	9			5.45					
5	58.8	176	500	5.17	4	20.68	16			5.16					
SUM		1720		28.76	10	54.55	30								

Using least squares method, log-dec = 0.297, zeta = 0.047, frequency of decaying oscillation = 2731.8 rad/s (434.8 Hz)

7.3.2 Analysis and discussion of results for free vibration method on Aero-Z IEC62219-REV240609 conductor

The use of no damper, one damper or two dampers did not affect the internal damping factor of the Aero-Z IEC62219-REV240609 conductor as the damping factor was within the same range of $0.01 \leq \varsigma \leq 0.2$. (Refer to Figures 17 to 22 together with corresponding

Tables 10 to 15 and also in Appendix III). There was no tension effect in self damping characteristics of transmission line conductor as the damping factor was within the same range of $0.01 \leq \varsigma \leq 0.2$ for the different tensions of 24.01 kN and 27.02 kN.

1. A damping factor of $0.01 \leq \varsigma \leq 0.2$ was determined. See for example Figures 12 to 17 together with corresponding Tables 25 to 30. Other results appear in Appendix III.
2. For the free vibration method, decaying of oscillations for the Aero-Z IEC62219-REV240609 conductor was observed for a frequency range of $363 \leq f_n \leq 962\ (Hz)$. This is an indication of how fast the energy is dissipated (Also observed as 1st dominant resonance frequency). See Figures 17 to 22 together with corresponding Tables 10 to 15.
3. Impulsive forces were introduced at position $1.2\ m$ span measured from the load-end fixed block.

Chapter 8

ANALYSIS OF RESULTS FOR THE FORCED VIBRATION EXPERIMENT

8.1 Introduction

In this Chapter, the results for the forced vibration (Chapter 6, Section 6.4) for both TERN and Aero-Z IEC62219-REV240609 conductors are analysed and discussed. Forced vibrations of the TERN conductor and the Aero-Z IEC62219-REV240609 conductor were induced to find the differences in the self damping characteristics of different conductors. Different tensions (20 to 30 kN) were investigated to determine their effect on the self damping characteristics of the conductors. The effects of placing the accelerometer at mid-span and at the end span of the Aero-Z IEC62219-REV240609 conductor are analysed as well. Lastly, the inclusion of mathematical model that incorporates self damping is also discussed in this Chapter.

In this Chapter, Section 8.2 presents analysis of forced vibration results for the TERN conductor and discussion of forced vibration results for the TERN conductor are also presented in Section 8.3. Section 8.4 presents analysis of forced vibration results for the Aero-Z IEC62219-REV240609 conductor while Section 8.5 presents the discussion of forced vibration results for the Aero-Z IEC62219-REV240609 conductor.

8.2 Analysis of forced vibration results for the TERN conductor

The tension of the transmission line varied from 20.73 kN, then 25.11 kN, to 29.56 kN. This was done to show the effect of conductor tension on the characteristics of the conductor (the most dominant resonance frequencies, f_n, bandwidth, Δf, quality factor, Q, and the damping factor, ζ). Channel 15 represented results captured when

accelerometer was placed at end-span. Channel 10 also represented results captured when the accelerometer was placed at mid-span.

The results for the forced vibration of the TERN conductor under the tensions of 25.11 kN and 29.56 kN were analysed and discussed as shown in Appendix II. More results for all tension with corresponding channels appeared in Appendix II. Again, a large number of results were decided upon to represent reasonable statistical data. The analysed results are within the frequency range of 5 *Hz* to 300 *Hz*.

8.2.1 Calculation of results for forced vibration

Figure 39 is a graph of acceleration versus frequency obtained from the results of the spreadsheet data extracted from the PUMA system for a cable tension of 25.11 kN. The same graph appears in the spectral dynamic viewer as shown in Figure 23. This spreadsheet graph is more amenable to analysis. Furthermore, the frequency peaks are extracted to form Table 16 below.

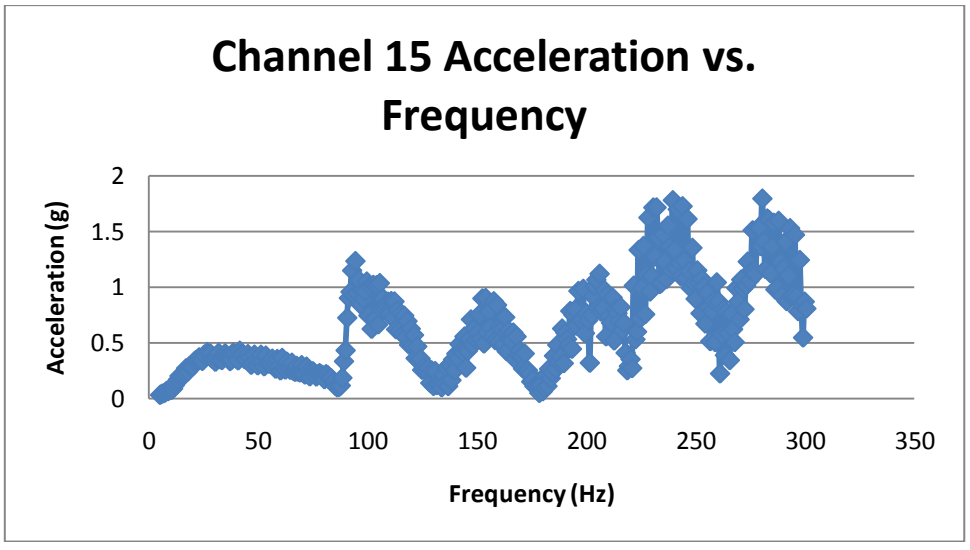

Figure 39: Graph showing acceleration (G) versus frequency (Hz)
Channel 15 represents data from the accelerometer at end-span)

Using results given in Figure 39: The results were calculated as follows:

Given $f_n = 41.489$ from Figure 39 (also recorded in the first column of Table 16 below), with the excitation frequencies f_1 and f_2 that correspond to a magnification factor of $0.707/2\zeta$ (as shown in Figure 11), then $f_1 = 18.4\ Hz$ and $f_2 = 67.6\ Hz$. From the theory developed in Chapter 4, it follows that

$$Q = \frac{f_n}{f_2 - f_1} = \frac{41.489}{67.6 - 18.4} = 0.843$$

Therefore

$$Q = 0.0843 = \frac{1}{2\zeta} \text{ and } \zeta = 0.592.$$

8.2.2 Tabulation of forced vibration calculated results for the TERN conductor

Referring to Table 16 and Figure 40, at frequencies higher than $100\ Hz$, the values of the damping factors were $0.023 \le \zeta \le 0.039.$ The maximum damping factor (0.592) is observed at $41.49\ Hz.$ These results presented were for the tension of 25.11 kN and the accelerometer was placed at end-span. Moreover the conductor was without Stockbridge dampers.

Table 16: Data collected from Figure 39

resonance frequency f_n	acceleration **a**	half-power f_1	half-power f_2	bandwidth Δf	quality factor **Q**	damping factor **ζ**
41.490	0.433	18.4	67.6	49.15	0.8	0.592
94.361	1.238	91.4	104.0	12.66	7.5	0.067
153.936	0.907	148.7	160.6	11.92	12.9	0.039
206.064	1.124	203.1	213.5	10.43	19.8	0.025
239.574	1.785	235.9	247.0	11.17	21.4	0.023
280.532	1.800	278.3	295.4	17.13	16.4	0.031

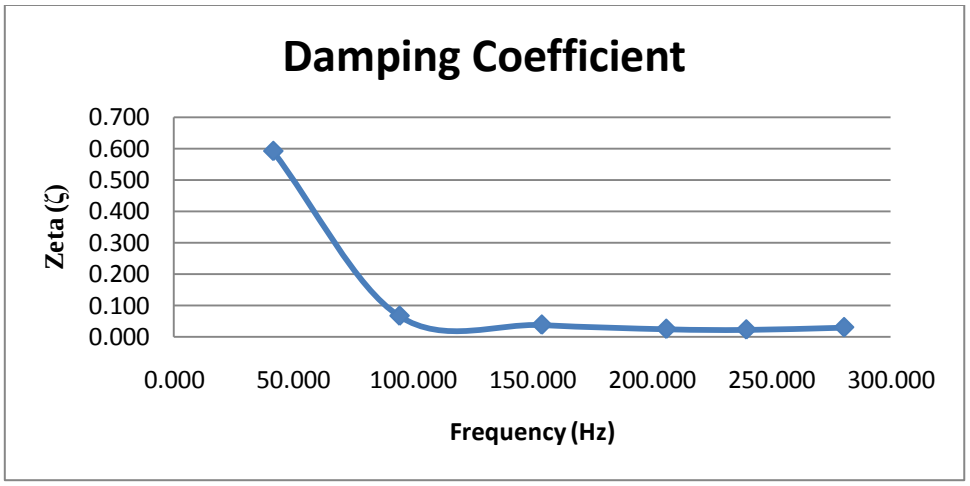

Figure 40: Graph showing damping factor (ς) versus frequency f_n (Hz)

Figure 41 is a graph of acceleration versus frequency obtained from the results of the spreadsheet data extracted from the PUMA system for a cable tension of 25.11 kN. The same graph appears in the spectral dynamic viewer as shown in Figure 24. This spreadsheet graph is more amenable to analysis. Furthermore, the frequency peaks are extracted to form Table 17 below.

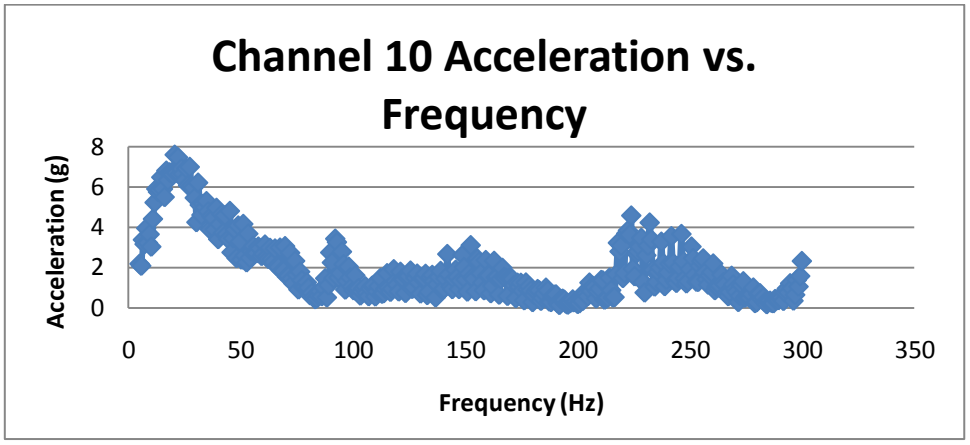

Figure 41: Graph showing acceleration (G) versus frequency (Hz)
Channel 10 represents data from the accelerometer at mid-span)

Referring to Table 17 and Figure 42, at frequencies higher than $100\,Hz$, the values of the damping factors were $0.025 \le \zeta \le 0.032$. The maximum damping factor (0.451) is observed at $20.638\,Hz$.

These results presented were for the tension of 25.11 kN and the accelerometer was placed at mid-span. During the experiment, the conductor was without Stockbridge dampers.

Table 17: Data for Figure 41

Resonance frequency	Acceleration	Half-power	Half-power	Band-width	Quality factor	Damping factor
f_n	a	f_1	f_2	Δf	Q	ζ
20.638	7.587	12.4	31.1	18.62	1.1	0.451
92.128	3.425	90.0	95.9	5.87	15.7	0.032
152.447	3.103	148.7	157.2	8.45	18.0	0.028
223.936	4.573	218.0	229.1	11.17	20.0	0.025

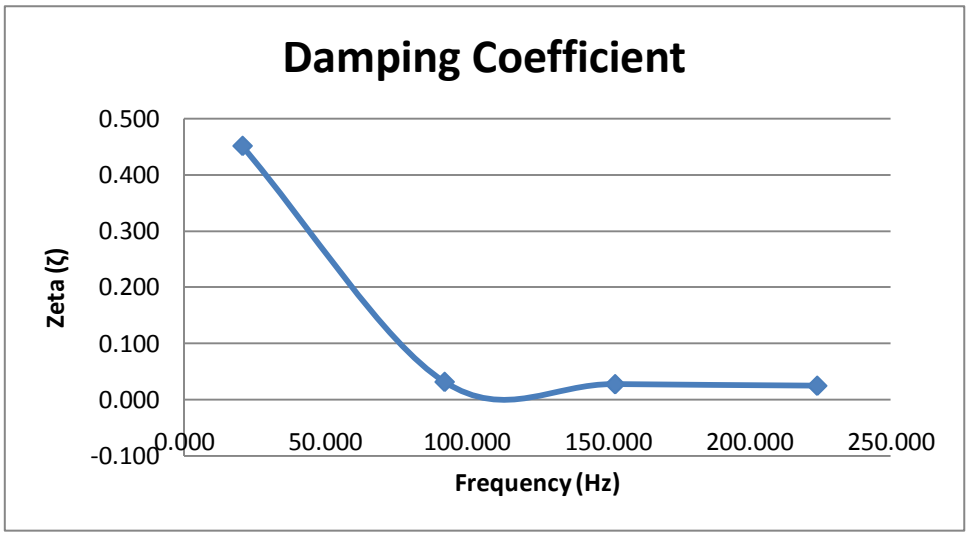

Figure 42: Graph showing damping factor (ζ) versus frequency f_n (Hz)

Figure 43 is a graph of acceleration versus frequency obtained from the results of the spreadsheet data extracted from the PUMA system for a cable tension of 29.56 kN. The

same graph appears in the spectral dynamic viewer as shown in Figure 25. This spreadsheet graph is more amenable to analysis. Furthermore, the frequency peaks are extracted to form Table 18 below.

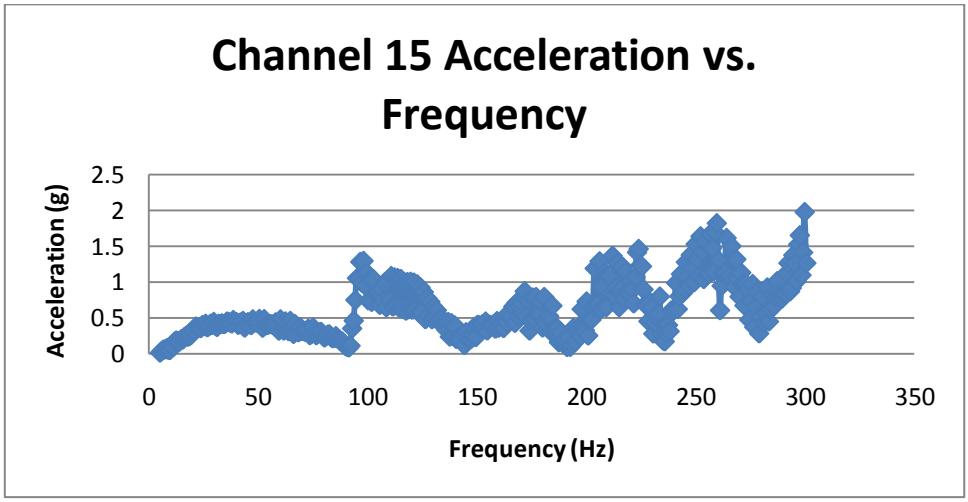

Figure 43: Graph showing acceleration (G) versus frequency (Hz)
Channel 15 represents data from the accelerometer at end-span)

Referring to Table 18 and Figure 44, at frequencies higher than $100\ Hz$, the values of the damping factors were $0.044 \le \zeta \le 0.052$. The maximum damping factor (0.532) is observed at $50.426\ Hz$. These results presented were for the tension of 29.56 kN and the accelerometer was placed at end-span. Moreover the conductor was without Stockbridge dampers.

Table 18: Data for Figure 43

Resonance frequency	Acceleration	Half-power	Half-power	Band-width	Quality factor	Exciting force	Damping factor
$f_{n\,(Hz)}$	a (G)	f_1	f_2	Δf	Q	$F_{o\,(N)}$	ζ
50.426	0.489	21.4	75.0	53.62	0.9	577.6	0.532
98.085	1.301	95.1	124.1	29.04	3.4	428.2	0.148
171.809	0.876	166.6	184.5	17.89	9.6	101.4	0.052
223.936	1.468	203.8	226.2	22.34	10.0	162.9	0.050
259.681	1.827	245.5	268.6	23.09	11.2	180.6	0.044

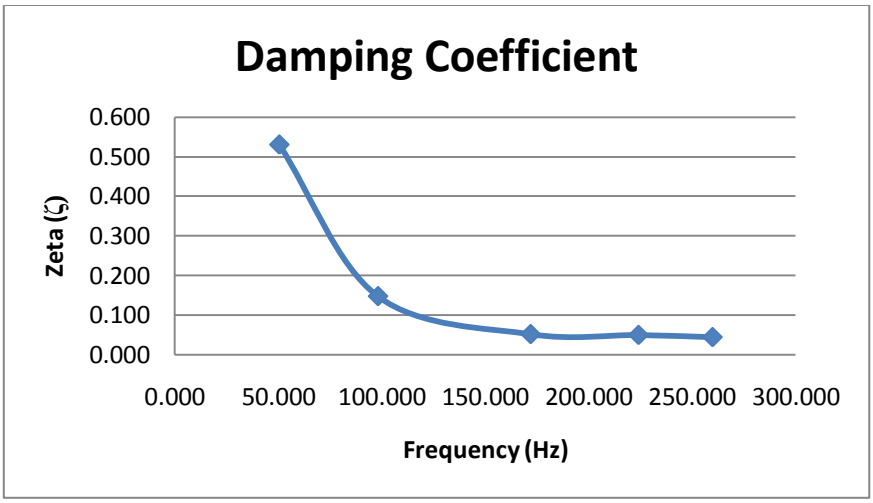

Figure 44: Graph showing damping factor (ς) versus frequency f_n (Hz)

Figure 45 is a graph of acceleration versus frequency obtained from the results of the spreadsheet data extracted from the PUMA system for a cable tension of 20.73 kN. The same graph appears in the spectral dynamic viewer as shown in Figure 26. This spreadsheet graph is more amenable to analysis. Furthermore, the frequency peaks are extracted to form Table 19 below.

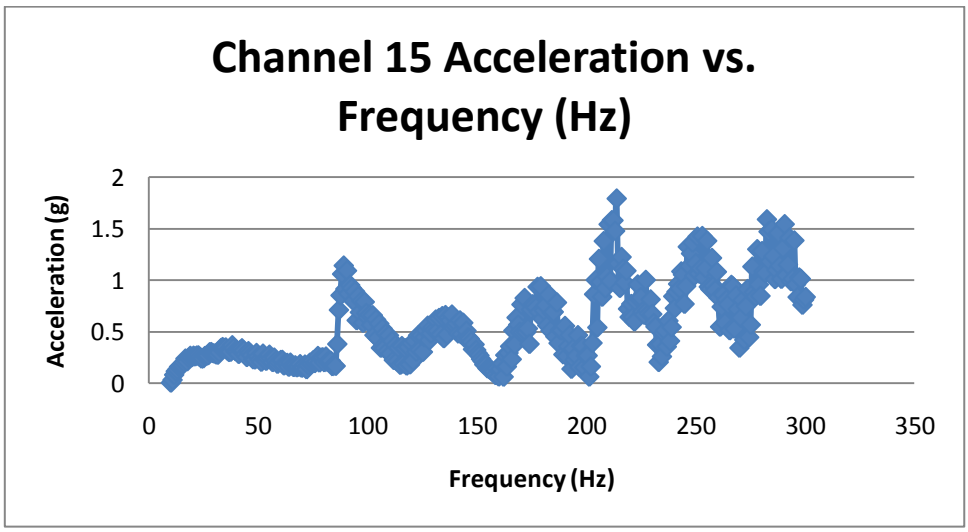

Figure 45: Graph showing acceleration (G) versus frequency (Hz)
Channel 15 represents data from the accelerometer at end-span)

Referring to Table 19 and Figure 46, at frequencies higher than $100\ Hz$, the values of the damping factors were $0.016 \le \zeta \le 0.048$. The maximum damping factor (0.495) is observed at $38.06\ Hz$. These results presented were for the tension of 20.73 kN and the accelerometer was placed at end-span. Moreover the conductor was without Stockbridge dampers.

Table 19: Data for Figure 45

Resonance frequency	Acceleration	Half-power	Half-power	Band-width	Quality factor	Exciting force	Damping factor
f_n	a	f_1	f_2	Δf	Q	F_o	ζ
38.060	0.371	19.6	57.3	37.66	1.0	408.3	0.495
89.011	1.144	87.5	97.1	9.60	9.3	137.2	0.054
138.486	0.669	166.5	192.4	25.84	5.4	138.8	0.093
177.622	0.937	167.3	184.3	16.98	10.5	99.7	0.048
213.805	1.793	207.9	214.5	6.65	32.2	62.0	0.016
252.941	1.430	243.3	260.3	16.98	14.9	106.8	0.034
282.478	1.592	275.8	295.0	19.20	14.7	120.3	0.034

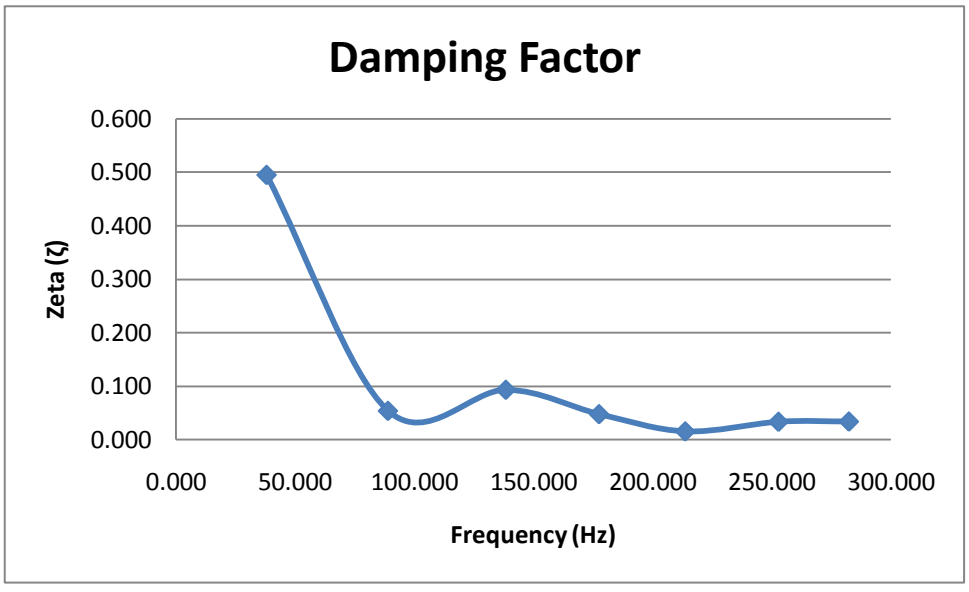

Figure 46: Graph showing acceleration (G) versus frequency (Hz)
Channel 15 represents data from the accelerometer at end-span)

8.3 Discussion of forced vibration results for the TERN transmission line conductor

Using the forced vibration method, the values of the damping factors obtained using the free vibration method described in Chapter 7 were confirmed.

1. At frequencies lower than $100\ Hz$, the damping factors were high, and the graph of damping factor versus frequency was plotted for one set of data as shown in Figures 40, 42, 44 and 46.
2. At frequencies higher than $100\ Hz$, the damping factors levelled to constant values of $\zeta \leq 0.05$, which compared favourably with those obtained using the free vibration method. Refer to Figures 40, 42, 44 and 46.
3. For the forced vibration method, the first dominant resonance frequency was observed, using the sweep tests, to be between $12 \leq f_n \leq 51\,(Hz)$. This is in close agreement with that obtained for the free vibration method as shown in Figures 14 to 16 together with corresponding Tables 6 to 9.
4. At frequencies higher than $100\ Hz$, the damping factors levelled to constant values for both accelerometers at mid-span and end-span. Also the dominant frequency peaks levels were approximately the same. Refer to Figures 40, 42, 44 and 46.
5. At frequencies lower than $100\ Hz$, the damping factors were different for accelerometers placed at mid-span and end-span. Also the dominant frequency peaks levels were not the same as shown in Figures 40, 42, 44 and 46.

8.4 Analysis of forced vibration results for the Aero-Z iec62219-REV240609 transmission line conductor

The tension of the transmission line varied from 24.01 kN to 27.02 kN in order to show the effect of conductor tension on the characteristics of the conductor. The results on the cable without Stockbridge dampers, the cable with one Stockbridge damper or mass

absorber damper, and the cable with two Stockbridge damper or mass absorber dampers are also analysed in order to check if it was necessary for external damping mechanisms to be used with transmission conductors. The difference when placing the accelerometer at mid-span and at the end of the conductor was also observed.

8.4.1 Tabulation of forced vibration calculated results for the Aero-Z iec62219-REV240609 conductor

The following tabulated results for the Aero-Z IEC62219-REV240609 conductor were found by following the steps shown in Section 8.2.1 above. Attention was focused on the most dominant (resonance) frequency peaks with corresponding accelerations and the damping factor, ζ.

More results appear in Appendix V. Again, a large number of results were decided upon to represent reasonable statistical data.

Figure 47 is a graph of acceleration versus frequency obtained from the results of the spreadsheet data extracted from the PUMA system for a cable tension of 24.01 kN. The same graph appears in the spectral dynamic viewer as shown in Figure 26. This spreadsheet graph is more amenable to analysis. Furthermore, the frequency peaks are extracted to form Table 20 below.

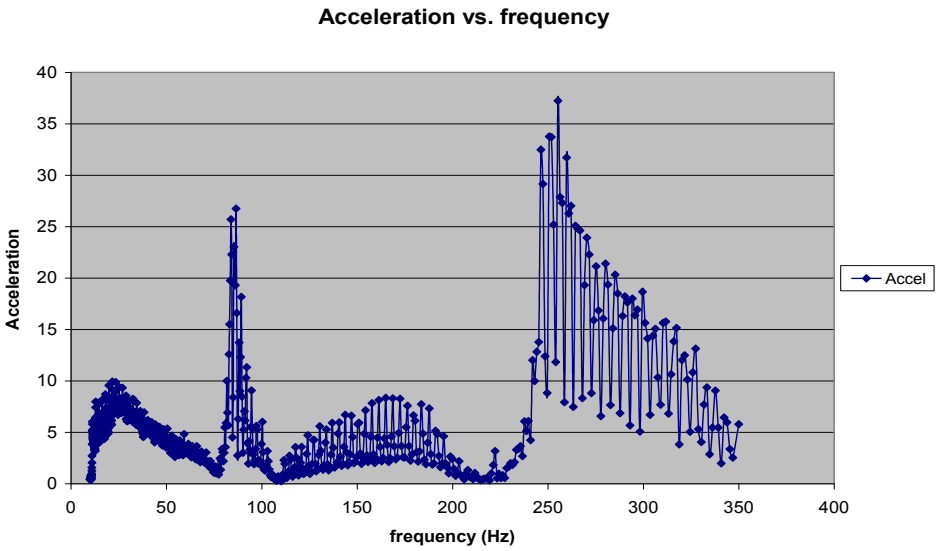

Figure 47 Sweep test extracted from Microsoft Excel data
(Channel 15 represents data from the accelerometer at mid-span)

Referring to Table 20 and Figure 48, at frequencies higher than $50\,Hz$, the values of the damping factors were $0.020 \le \zeta \le 0.157$. The maximum damping factor (0.626) is observed at $21.593\,Hz$.

The results presented were for the tension of 24.01 kN and the accelerometer was placed at mid-span and the conductor was without Stockbridge dampers.

Table 20: Data at mid-span for tension 24.01 without dampers, collected from Figure 47

resonance frequency	acceleration	half-power	half-power	bandwidth	quality factor	damping factor
f_n	**a**	f_1	f_2	Δf	**Q**	**ζ**
21.593477	9.93031	14.0	40.982899	27.021223	0.799	0.626
86.549149	26.7413	84.644798	88.103424	3.458626	25.024	0.0200
164.99675	8.34953	137.48105	189.40128	51.920227	3.178	0.1573
255.18811	37.2414	246.26372	263.26184	16.998123	15.013	0.0333

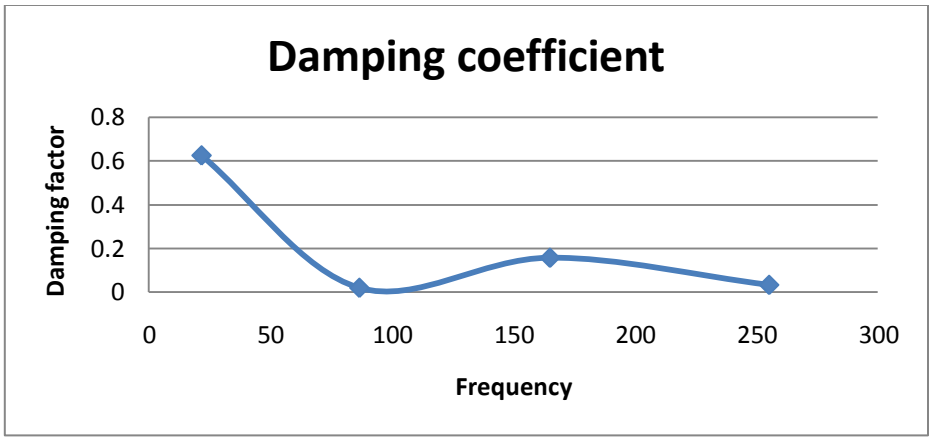

Figure 48: Graph showing damping factor vs. Frequency

Figure 49 shows the results for the sweep test plotted by the spreadsheet of the PUMA system for a cable tension of 24.01kN. The same graph appears in the spectral dynamic viewer as shown in Figure 27. The results were captured from the accelerometer positioned at end-span of the Aero-Z IEC62219-REV240609 conductor. This spreadsheet graph is more amenable to analysis. Furthermore, the frequency peaks are extracted to form Table 21 below.

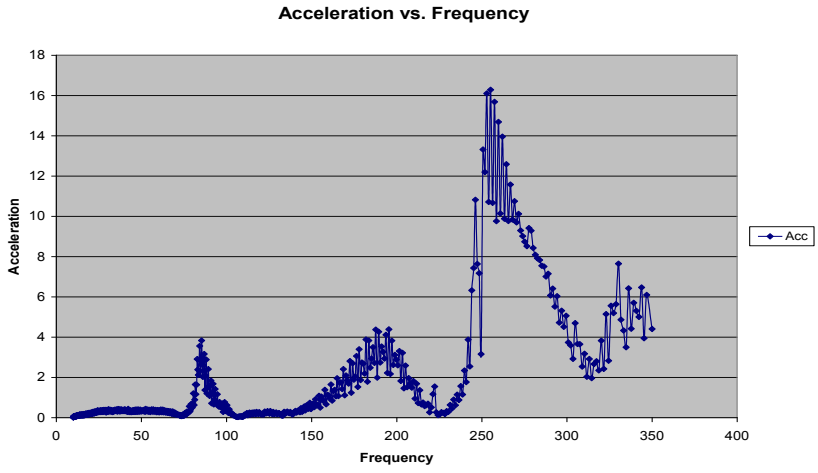

Figure 49: Sweep test extracted from Microsoft Excel data
(Channel 15 represents data from the accelerometer at end-span)

Referring to Table 21 and Figure 50, at frequencies higher than $50\,Hz$, the values of the damping factors were $0.032 \le \zeta \le 0.069,$ and at the frequencies below $50\,Hz$

The results presented were for the tension of 24.01 kN and the accelerometer was placed at the end-span position and the conductor was without Stockbridge dampers.

Table 21: Data at end-span for tension 24.01 without dampers, collected from Figure 49

resonance frequency	acceleration	half-power	half-power	bandwidth	quality factor	damping factor
f_n	a	f_1	f_2	Δf	Q	ζ
85.401459	3.82825	84.3	89.685615	5.416625	15.767	0.032
195.393631	4.38334	177.17212	204.2845	27.112381	7.207	0.0694
255.18811	16.285	250.6862	267.98959	17.303391	14.748	0.0339

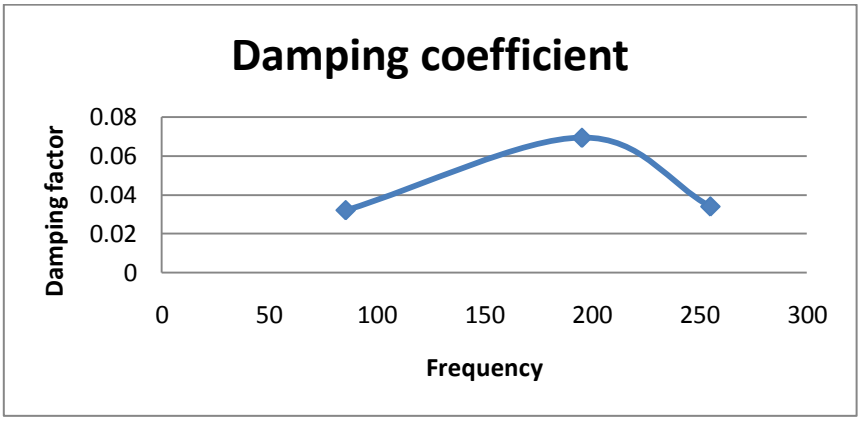

Figure 50: Graph showing damping factor vs. Frequency

Figure 51 is a graph of acceleration versus frequency obtained from the results of the spreadsheet data extracted from the PUMA system for a cable tension of 24.01 kN. The same graph appears in the spectral dynamic viewer as shown in Figure 28. This spreadsheet graph is more amenable to analysis. Furthermore, the frequency peaks are extracted to form Table 22 below.

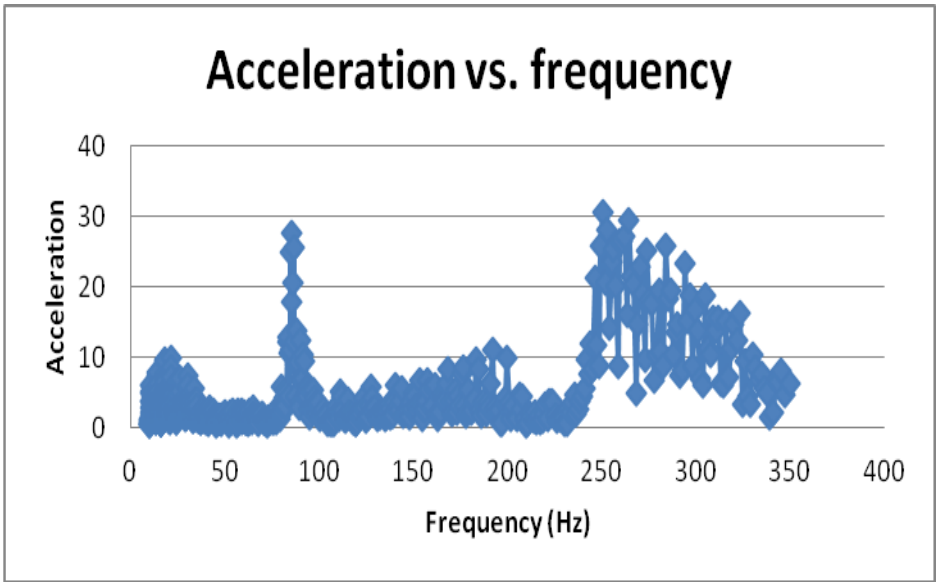

Figure 51 Sweep test extracted from Microsoft Excel data
(Channel 15 represents data from accelerometer at mid-span)

Referring to Table 22 and Figure 52, at frequencies higher than $50\,Hz$, the values of the damping factors were $0.011 \le \zeta \le 0.089$. The maximum damping factor (0.626) is observed at $21.593\,Hz$.

These results presented were for the tension of 24.01 kN and the accelerometer was placed at mid-span and conductor was with one Stockbridge damper.

Table 22: Data at mid-span for tension 24.01 with one damper, collected from Figure 51

resonance frequency	acceleration	half-power	half-power	bandwidth	quality factor	damping factor
f_n	a	f_1	f_2	Δf	Q	ζ
21.593477	9.84096	14.7	30.689524	15.962075	1.353	0.370
85.401459	27.7198	85.401459	87.322823	1.921364	44.448	0.0112
191.946594	11.0894	168.70885	200.6806	31.971756	6.004	0.0833
250.686203	30.628	249.5732	294.23914	44.66594	5.612	0.0891

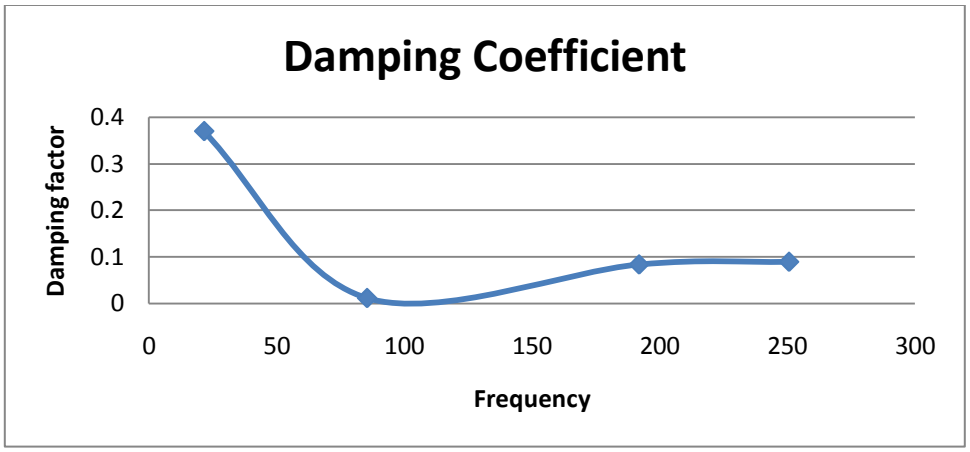

Figure 52: Graph showing damping factor vs. Frequency

Figure 53 is a graph of acceleration versus frequency obtained from the results of the spreadsheet data extracted from the PUMA system for a cable tension of 24.01 kN. The same graph appears in the spectral dynamic viewer as shown in Figure 29. This spreadsheet graph is more amenable to analysis. Furthermore, the frequency peaks are extracted to form Table 23 below.

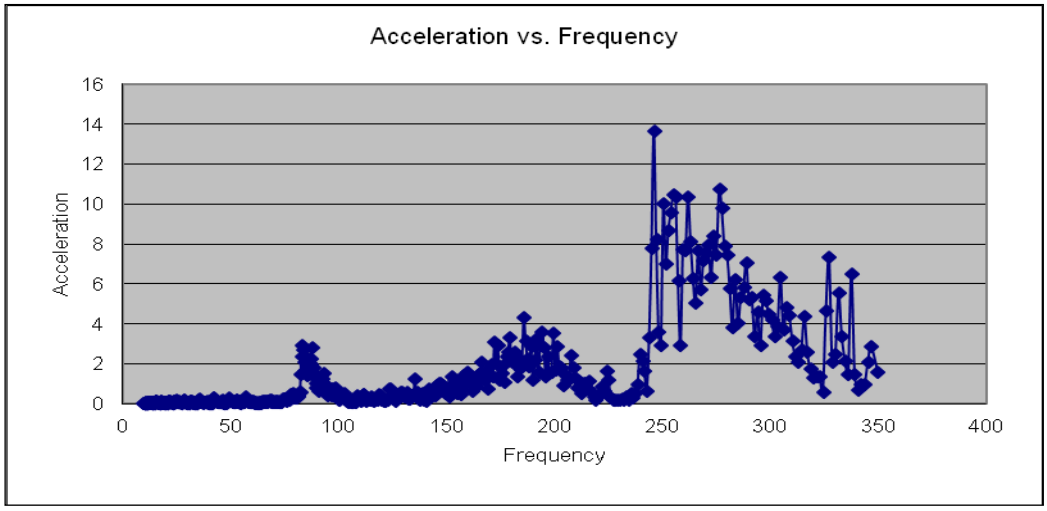

Figure 53: Sweep test extracted from Microsoft Excel data
(Channel 15 represents data from the accelerometer at end-span)

Referring to Table 23 and Figure 54, at frequencies higher than $50\,Hz$, the values of the damping factors were $0.032 \le \zeta \le 0.073$.

The results presented were for the tension of 24.01 kN and the accelerometer was placed at end-span. and conductor was with Stockbridge one damper.

Table 23: Data at end-span for tension 24.01 with one damper, collected from Figure 53

resonance frequency	acceleration	half-power	half-power	bandwidth	quality factor	damping factor
f_n	a	f_1	f_2	Δf	Q	ζ
83.151535	2.90829	83.2	88.496338	5.344803	15.557	0.032
186.059952	4.3049	172.50449	199.78961	27.285126	6.819	0.0733
246.263718	13.6564	245.17035	277.70132	32.530975	7.570	0.0660

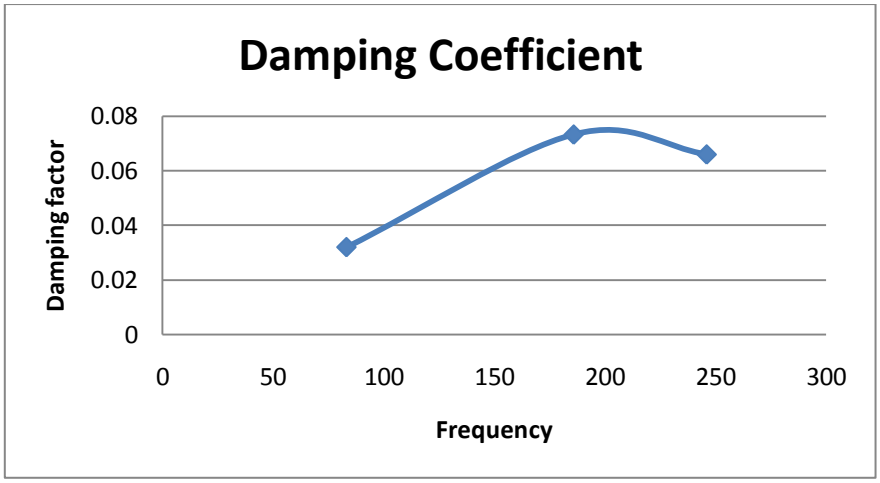

Figure 54: Graph showing damping factor vs. Frequency

Figure 55 is a graph of acceleration versus frequency obtained from the results of the spreadsheet data extracted from the PUMA system for a cable tension of 24.01 kN. The same graph appears in the spectral dynamic viewer as shown in Figure 30. This spreadsheet graph is more amenable to analysis. Furthermore, the frequency peaks are extracted to form Table 24 below.

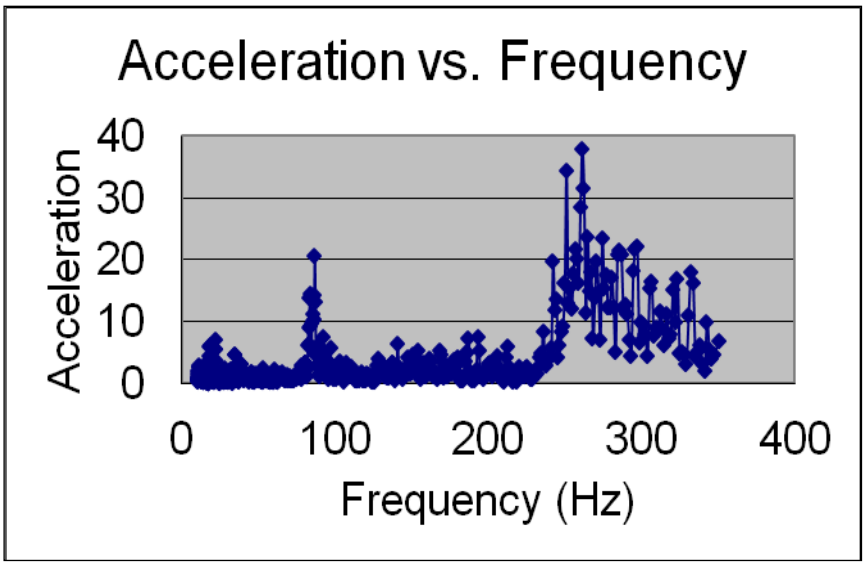

Figure 55: Sweep test extracted from Microsoft Excel data
(Channel 15 represents data from the accelerometer at mid-span)

Referring to Table 24 and Figure 56, at frequencies higher than $50\,Hz$, the values of the damping factors were $0.022 \le \zeta \le 0.184$. The maximum damping factor (0.368) is observed at $21.688\,Hz$.

The results presented were for the tension of 24.01 kN and the accelerometer was placed at mid-span.and the conductor was with two Stockbridge dampers.

Table 24: Data at mid-span for tension 24.01 with two dampers, collected from Figure 55

resonance frequency	acceleration	half-power	half-power	bandwidth	quality factor	damping factor
f_n	a	f_1	f_2	Δf	Q	ζ
21.68777	7.00361	19.6	35.543701	15.963932	1.359	0.368
86.549149	20.508	85.022285	88.890999	3.868714	22.372	0.0223
192.802597	7.55625	142.46326	213.57991	71.116653	2.711	0.1844
260.929352	37.9182	250.6862	264.43591	13.74971	18.977	0.0263

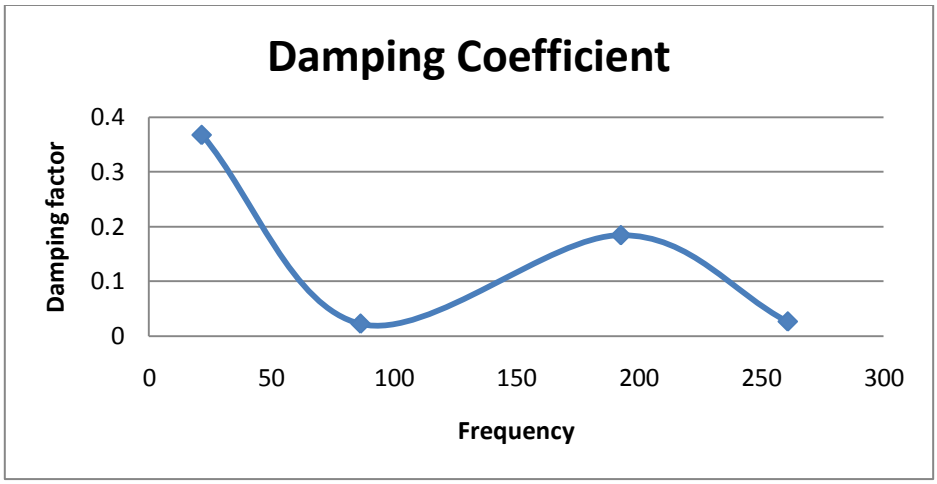

Figure 56: Graph showing damping factor vs. Frequency

Figure 57 is a graph of acceleration versus frequency obtained from the results of the spreadsheet data extracted from the PUMA system for a cable tension of 24.01 kN. The same graph appears in the spectral dynamic viewer as shown in Figure 31. This spreadsheet graph is more amenable to analysis. Furthermore, the frequency peaks are extracted to form Table 25 below.

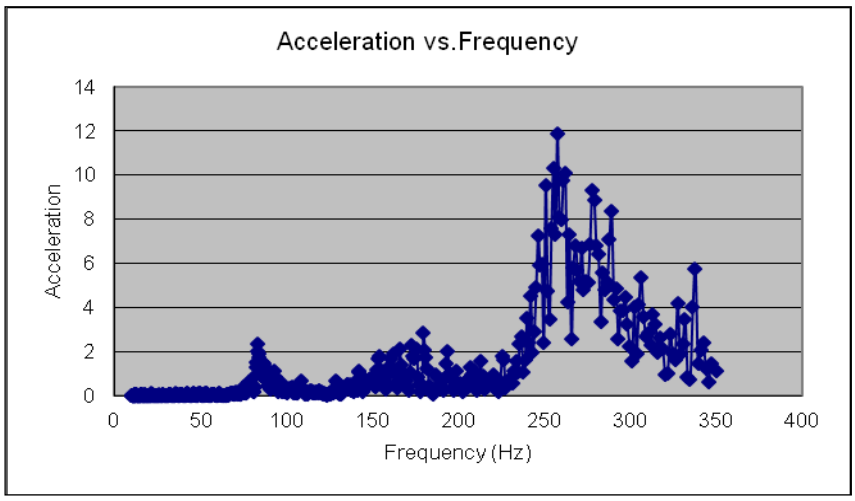

Figure 57: Sweep test extracted from Microsoft Excel data
(Channel 15 represents data from the accelerometer at end-span)

Referring to Table 25 and Figure 58, at frequencies higher than $50\,Hz$, the values of the damping factors were $0.011 \leq \zeta \leq 0.080.$

The results presented were for the tension of 24.01 kN and the accelerometer was placed at end-span and the conductor was with two Stockbridge dampers.

Table 25: Data at end-span for tension 24.01 with two dampers, collected from Figure 57

resonance frequency	acceleration	half-power	half-power	bandwidth	quality factor	damping factor
f_n	a	f_1	f_2	Δf	Q	ζ
83.522362	2.34719	83.5	85.401459	1.879097	44.448	0.011
179.553085	2.8266	165.73257	194.52611	28.793534	6.236	0.0802
257.469299	11.8604	250.6862	289.04831	38.362106	6.712	0.0745

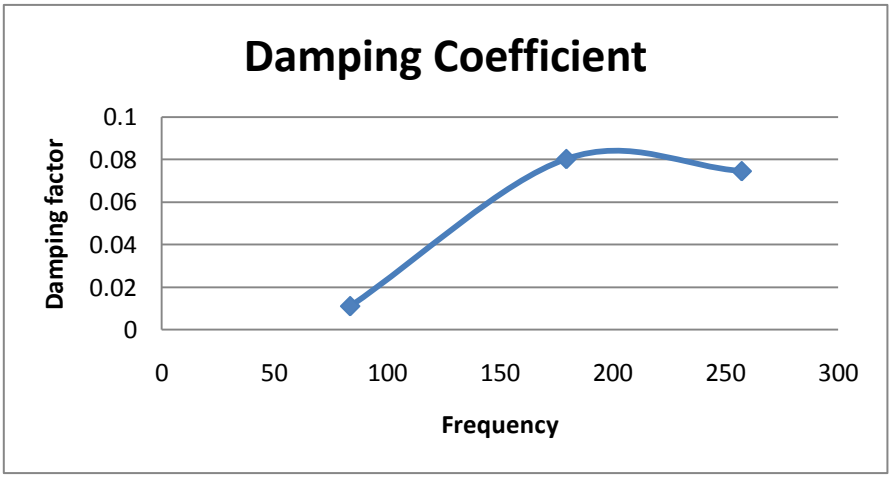

Figure 58: Graph showing damping factor vs. Frequency

Figure 59 is a graph of acceleration versus frequency obtained from the results of the spreadsheet data extracted from the PUMA system for a cable tension of 27.02 kN. The same graph appears in the spectral dynamic viewer as shown in Figure 32. This spreadsheet graph is more amenable to analysis. Furthermore, the frequency peaks are extracted to form Table 26 below.

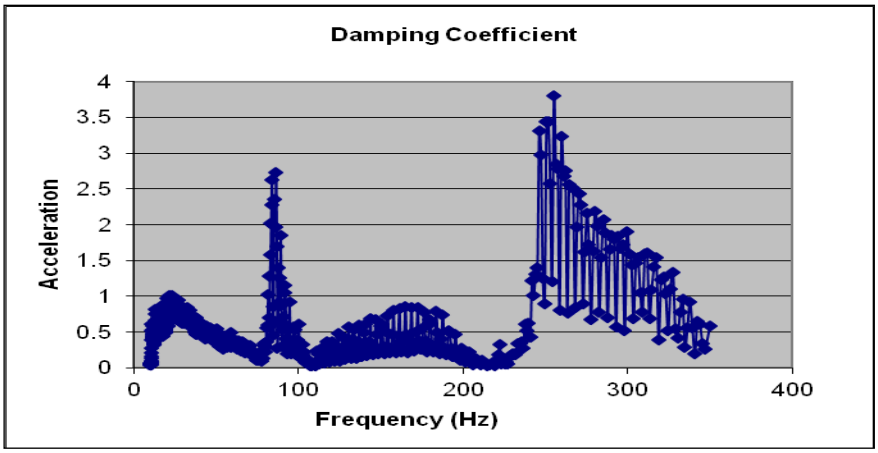

Figure 59: Sweep test extracted from Microsoft Excel data
(Channel 15 represents data from the accelerometer at mid-span)

Referring to Table 26 and Figure 60, at frequencies higher than $50\,Hz$, the values of the damping factors were $0.020 \le \zeta \le 0.157$. The maximum damping factor (0.544) is observed at $23.394\ Hz$.

The results presented were for the tension of 27.02 kN and the accelerometer was placed at mid-span and the conductor was without Stockbridge dampers.

Table 26: Data at mid-span for tension 27.02 without dampers, collected from Figure 59

resonance frequency	acceleration	half-power	half-power	bandwidth	quality factor	damping factor
f_n	**a**	f_1	f_2	Δf	**Q**	**ζ**
23.394167	1.00811	13.1	38.50771	25.447505	0.919	0.544
86.549149	2.72685	83.522362	86.935127	3.412765	25.360	0.0197
164.99675	0.851415	136.87065	188.56036	51.689713	3.192	0.1566
255.18811	3.79756	246.26372	262.09302	15.8293	16.121	0.0310

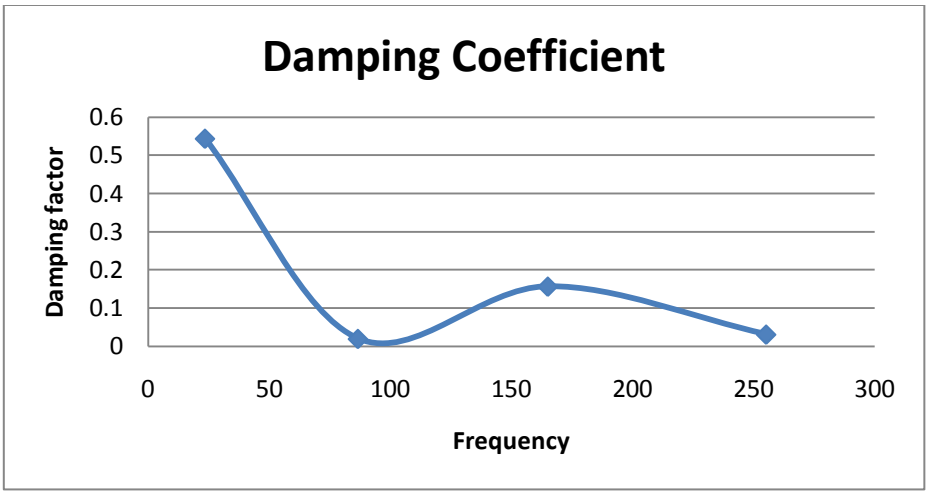

Figure 60: Graph showing damping factor vs. Frequency

Figure 61 is a graph of acceleration versus frequency obtained from the results of the spreadsheet data extracted from the PUMA system for a cable tension of 27.02 kN. The same graph appears in the spectral dynamic viewer as shown in Figure 33. This spreadsheet graph is more amenable to analysis. Furthermore, the frequency peaks are extracted to form Table 27 below.

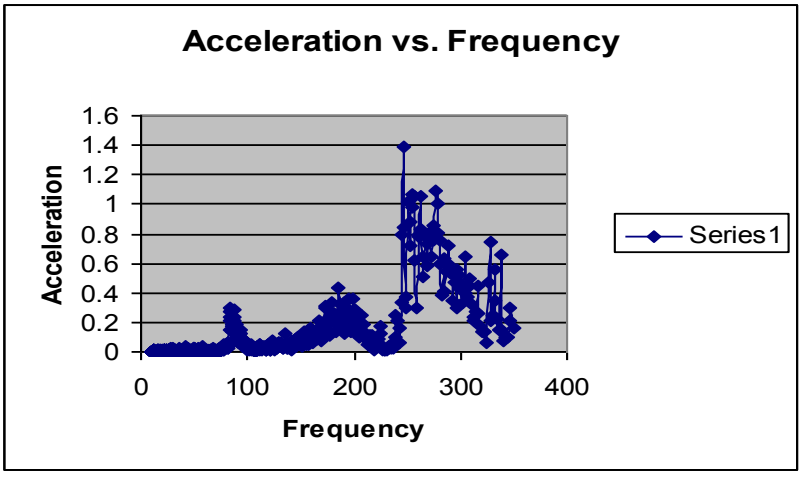

Figure 61: Sweep test from spectral dynamic viewer
(Data extracted from the accelerometer positioned at end-span)

Referring to Table 27 and Figure 62, at frequencies higher than $50\,Hz$, the values of the damping factors were $0.011 \leq \zeta \leq 0.0895$.

The results presented were for the tension of 27.02 kN and the accelerometer was placed at end-span and the conductor was without Stockbridge dampers.

Table 27: Data at end-span for tension 27.02 without dampers, collected from Figure 61

resonance frequency	acceleration	half-power	half-power	bandwidth	quality factor	damping factor
f_n	a	f_1	f_2	Δf	Q	ζ
83.151535	0.296563	83.2	85.022285	1.87075	44.448	0.011
186.059952	0.438977	165.73257	193.66245	27.929871	6.662	0.0751
246.263718	1.39256	246.26372	290.33737	44.073654	5.588	0.0895

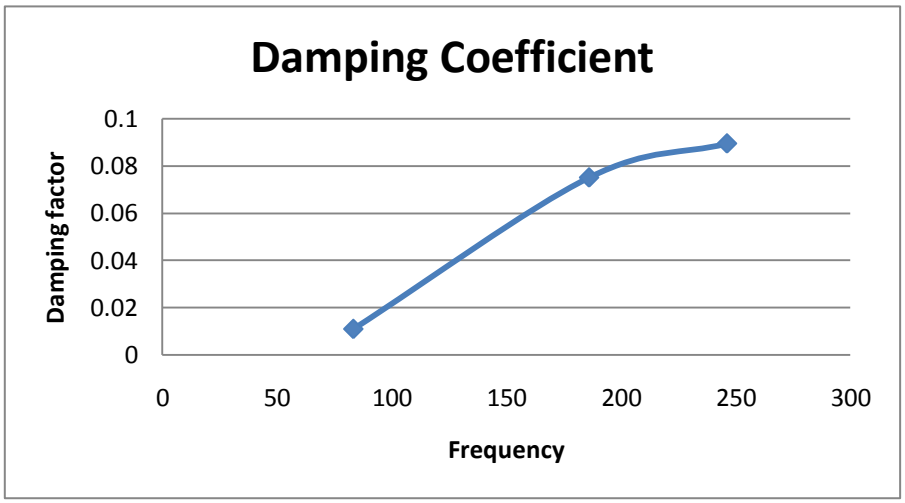

Figure 62: Graph showing damping factor vs. Frequency

Figure 63 is a graph of acceleration versus frequency obtained from the results of the spreadsheet data extracted from the PUMA system for a cable tension of 27.02 kN. The same graph appears in the spectral dynamic viewer as shown in Figure 34. This spreadsheet graph is more amenable to analysis. Furthermore, the frequency peaks are extracted to form Table 28 below.

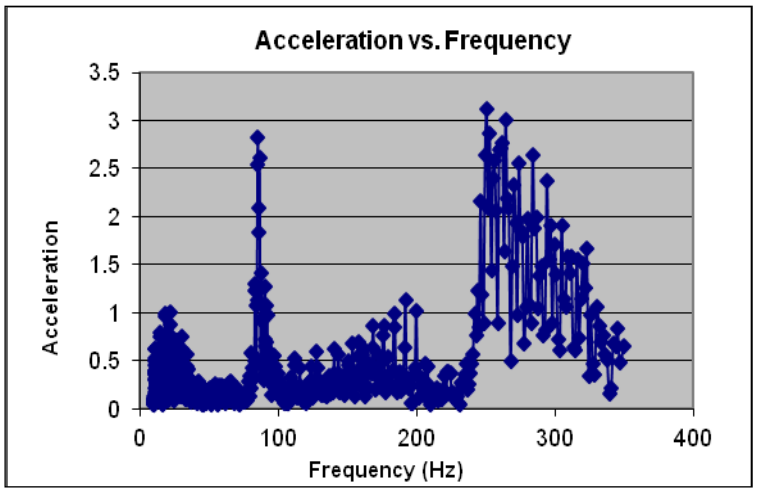

Figure 63: Sweep test extracted from Microsoft Excel data
(Channel 15 represents data from the accelerometer at mid-span)

Referring to Table 28 and Figure 64, at frequencies higher than $50\,Hz$, the values of the damping factors were $0.009 \le \zeta \le 0.089$. The maximum damping factor (0.365) is observed at $21.593\,Hz$.

The results presented were for the tension of 27.02 kN and the accelerometer was placed at mid-span and the conductor was with one Stockbridge damper.

Table 28: Data at mid-span for tension 27.02 with one damper, collected from Figure 63

resonance frequency	acceleration	half-power	half-power	bandwidth	quality factor	damping factor
f_n	**a**	f_1	f_2	Δf	**Q**	**ζ**
21.593477	1.0035	14.9	30.689524	15.764156	1.370	0.365
85.401459	2.82663	85.401459	86.935127	1.533668	55.684	0.0090
191.946594	1.1308	168.70885	199.78961	31.080765	6.176	0.0810
250.686203	3.12319	249.5732	294.23914	44.66594	5.612	0.0891

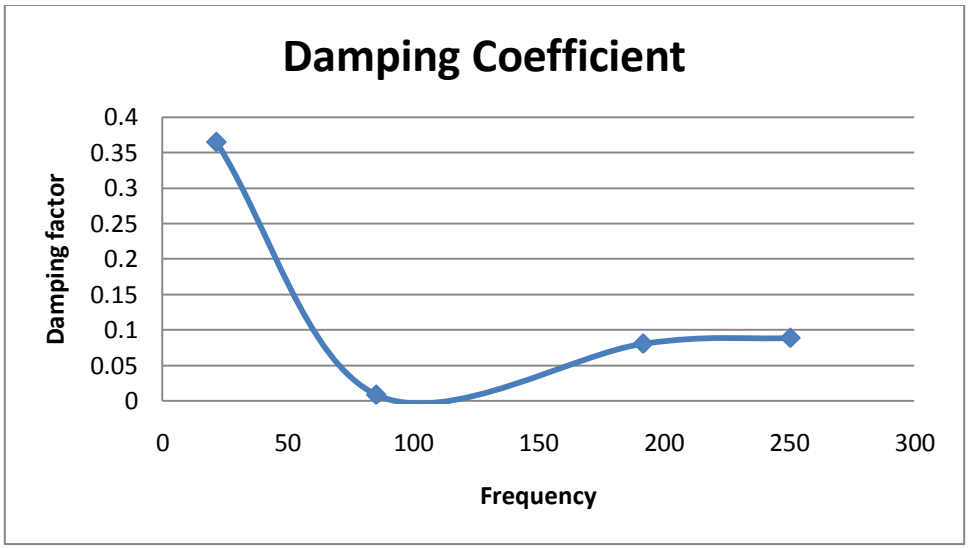

Figure 64: Graph showing damping factor vs. Frequency

Figure 65 is a graph of acceleration versus frequency obtained from the results of the spreadsheet data extracted from the PUMA system for a cable tension of 27.02 kN. The same graph appears in the spectral dynamic viewer as shown in Figure 35. This spreadsheet graph is more amenable to analysis. Furthermore, the frequency peaks are extracted to form Table 29 below.

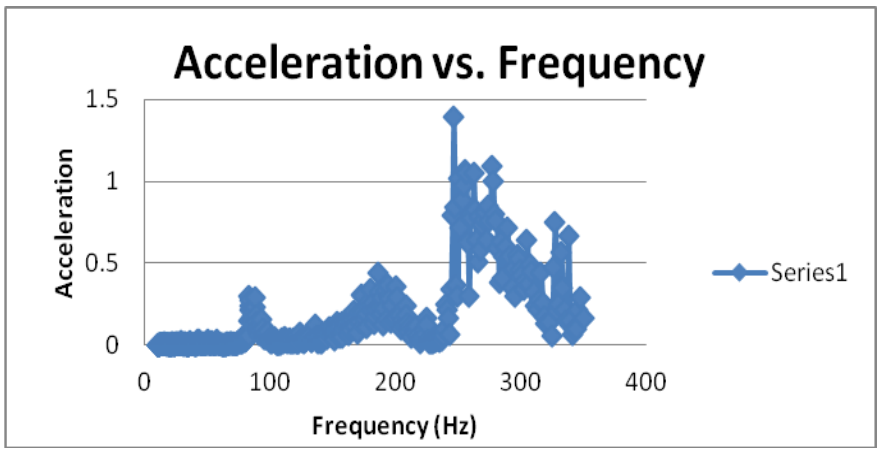

Figure 65: Sweep test extracted from Microsoft Excel data
(Channel 15 represents data from the accelerometer at end-span)

Referring to Table 29 and Figure 66, at frequencies higher than $50\,Hz$, the values of the damping factors were $0.032 \le \zeta \le 0.074$.

The results presented were for the tension of 27.02 kN and the accelerometer was placed at end-span and the conductor was with one Stockbridge damper.

Table 29: Data at end-span for tension 27.02 with one damper, collected from Figure 65

resonance frequency	acceleration	half-power	half-power	bandwidth	quality factor	damping factor
f_n	a	f_1	f_2	Δf	Q	ζ
83.1515235	0.296563	83.151535	88.496338	5.344803	15.557	0.032
186.059952	0.438977	173.27379	200.6806	27.406815	6.789	0.0737
246.263718	1.39256	245.17035	277.70132	32.530975	7.570	0.0660

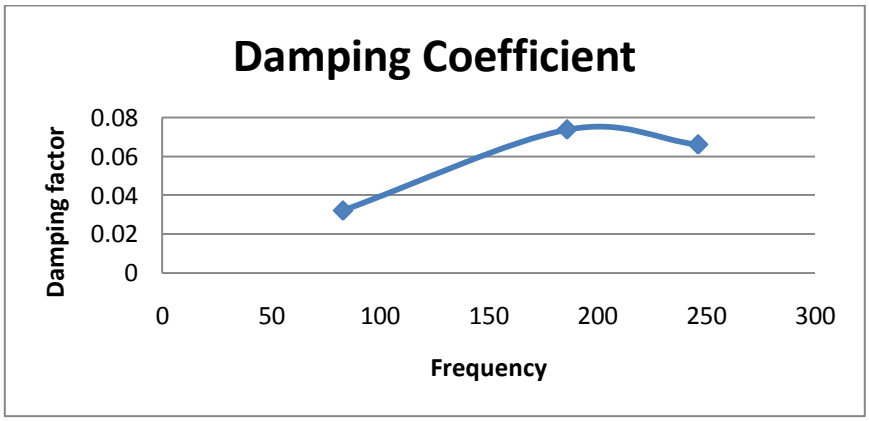

Figure 66: Graph showing damping factor vs. Frequency

Figure 67 is a graph of acceleration versus frequency obtained from the results of the spreadsheet data extracted from the PUMA system for a cable tension of 27.02 kN. The same graph appears in the spectral dynamic viewer as shown in Figure 36. This spreadsheet graph is more amenable to analysis. Furthermore, the frequency peaks are extracted to form Table 30 below.

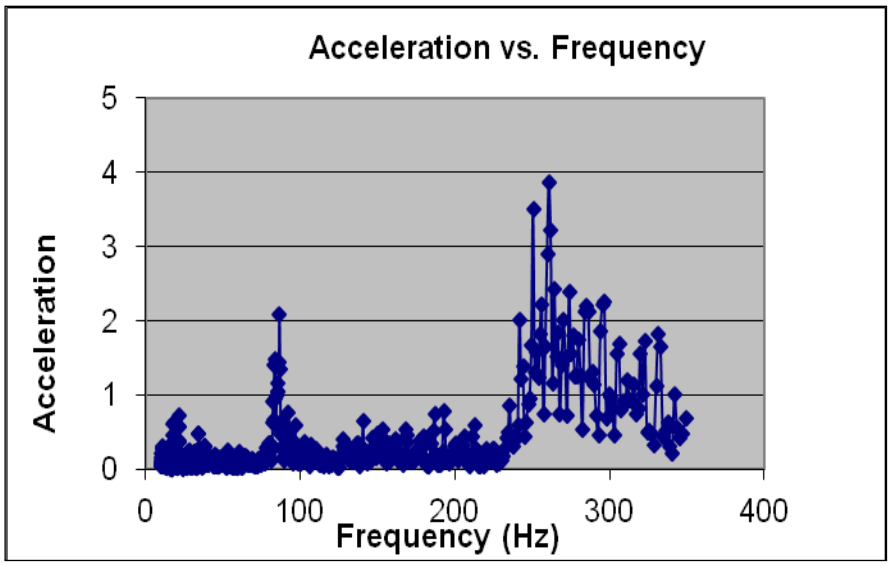

Figure 67: Sweep test extracted from Microsoft Excel data
(Channel 15 represents data from the accelerometer at mid-span)

Referring to Table 30 and Figure 68, at frequencies higher than $50\,Hz$, the values of the damping factors were $0.020 \le \zeta \le 0.187$. The maximum damping factor (0.381) is observed at $21.593\,Hz$.

The results presented were for the tension of 27.02 kN and the accelerometer was placed at mid-span and the conductor was with two Stockbridge dampers.

Table 30: Data at mid-span for tension 27.02 with two dampers, collected from Figure 67

resonance frequency	acceleration	half-power	half-power	bandwidth	quality factor	damping factor
f_n	**a**	f_1	f_2	Δf	**Q**	**ζ**
21.593477	0.71417	18.3	34.761631	16.446077	1.313	0.381
85.401459	2.09123	83.894844	87.322823	3.427979	24.913	0.0201
191.946594	0.770523	140.97411	212.63165	71.657541	2.679	0.1867
250.686203	3.86658	249.5732	262.09302	12.519822	20.023	0.0250

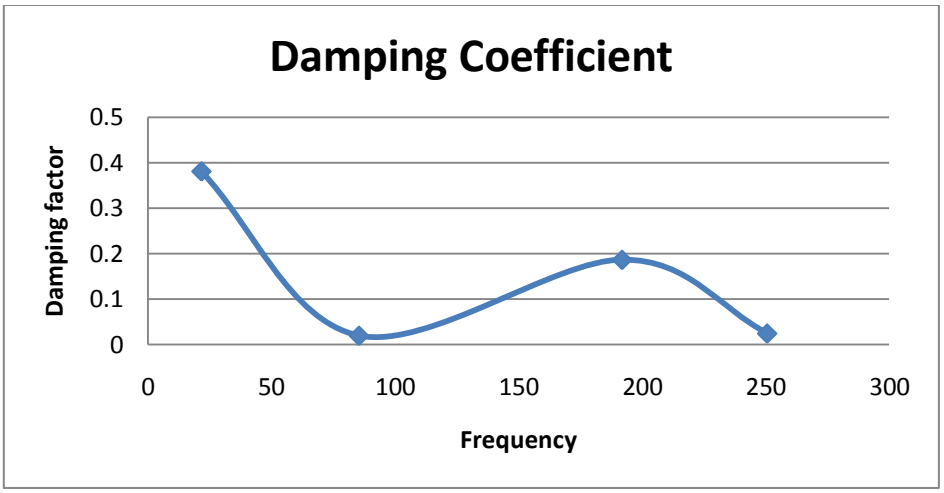

Figure 68: Graph showing damping factor vs. Frequency

Figure 69 is a graph of acceleration versus frequency obtained from the results of the spreadsheet data extracted from the PUMA system for a cable tension of 27.02 kN. The same graph appears in the spectral dynamic viewer as shown in Figure 37. This spreadsheet graph is more amenable to analysis. Furthermore, the frequency peaks are extracted to form Table 31 below.

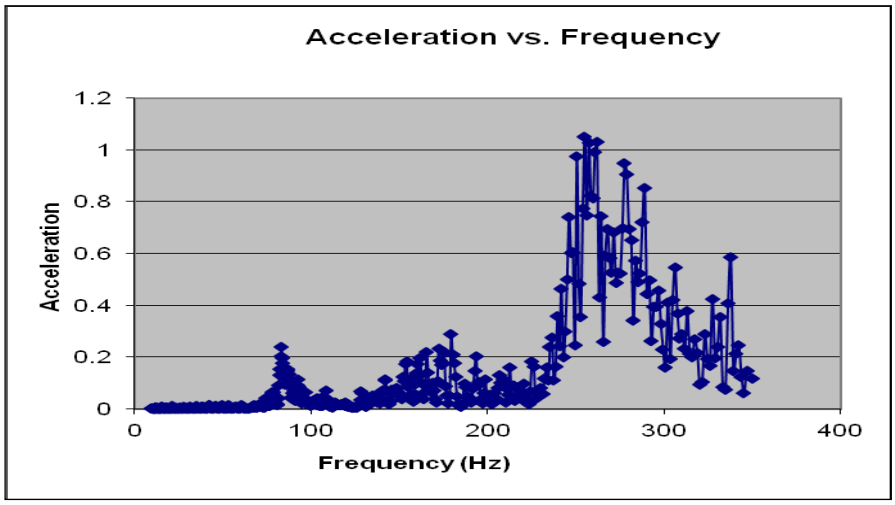

Figure 69: Sweep test extracted from Microsoft Excel data
(Channel 15 represents data from the accelerometer at end-span)

Referring to Table 31 and Figure 70, at frequencies higher than $50\,Hz$, the values of the damping factors were $0.011 \le \zeta \le 0.0864.$

The results presented were for the tension of 27.02 kN and the accelerometer was placed at end-span and the conductor was with two Stockbridge dampers.

Table 31: Data at end-span for tension 27.02 with two dampers, collected from Figure 69

resonance frequency f_n	acceleration a	half-power f_1	half-power f_2	bandwidth Δf	quality factor Q	damping factor ζ
83.522362	0.239347	83.2	85.022285	1.87075	44.646	0.011
179.553085	0.288236	165.73257	193.66245	27.929871	6.429	0.0778
255.18811	1.04982	246.26372	290.33737	44.073654	5.790	0.0864

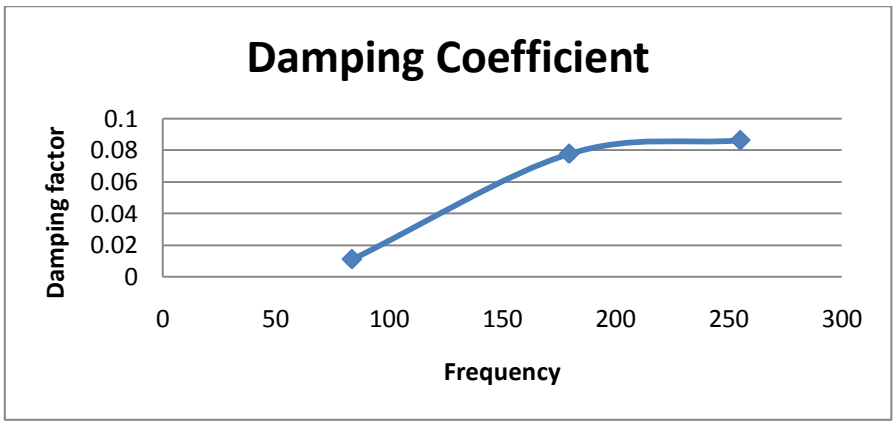

Figure 70: Graph showing damping factor vs. Frequency

8.5 Discussion of forced vibration results for the Aero-ZIEC62219-REV240609 transmission line conductor cable

For transmission lines with no dampers, one damper or two dampers, the damping coefficient $\zeta < 1.0$. Whether the Stockbridge damper is present or not, the self-damping coefficient is roughly the same. Damping of transmission lines is therefore confirmed not

to depend on the tuned absorbers but rather on the *viscous* or *friction* damping mechanism. The term "mass absorber damper" as used by the Stockbridge manufacturing firm is mere jargon. The actual external damping mechanism is called a "tuned absorber" in vibration theory. This mechanism tunes to certain dominant frequencies in order to cancel the resonance modes of vibration.

Using the forced vibration method, the values of the damping factors obtained using the free vibration method were confirmed as shown in Figures 47 to 70 together with corresponding Tables 20 to 31.

At frequencies lower than $50\ Hz$, the damping factors were high (for examples, see Figures 48, 52, 56, 60, 64 and 68, which show graphs of damping factor versus frequency, for corresponding data sets extracted from Figures 47, 51, 55, 59 63 and 67, respectively). A possible reason for the high damping factors in this frequency range $12 \le f_n \le 51(Hz)$, is that it coincides with the dominant resonance frequency for the transmission line and also coincides with the region where the shaker control system ramps up, before reaching steady state conditions and affects results. This is evident in Figures 23 to 26, shown by orange and yellow lines. The sensitivity of the control system is not good in this region.

1. At frequencies higher than $50\ Hz$, the damping factors levelled to constant values of $\zeta \le 0.2$, which compared favourably with those obtained using the free vibration method.
2. For the forced vibration method, the first dominant resonance frequency was observed, using the sweep tests, to be $12 \le f_n \le 51(Hz)$. This is in close agreement with that found using the free vibration method.
3. At frequencies higher than $50\ Hz$, the damping factors levelled to constant values for both accelerometers at mid-span and end-span. Also the dominant frequency

peaks levels were the same. Refer to Figures 48,50,52,54,56,58,60,62,64,66,68 and 70.

4. At frequencies lower than $50\ Hz$ for the accelerometer placed at end-span, the damping factors were not analysed, the most dominant frequency were not easy to pick. Also for the accelerometer placed at mid-end span; at frequencies lower than $50\ Hz$ the damping factors were high $(0.3 \leq \zeta \leq 0.7)$.

Chapter 9

DISCUSSIONS OF RESULTS

9.1 Introduction

In this Chapter, a concise summary is provided with an emphasis based on the important findings from the experimental analysis and discussion of results from both the TERN and Aero-Z IEC62219-REV240609 conductors due to free and forced vibration methods.

In this Chapter, Section 9.2 will be the discussions of results for free and forced vibration methods on the TERN conductor. Section 9.3 will be the summary and discussion of results for both free and forced vibration methods of the Aero-Z IEC62219-REV240609 conductor. Lastly, Section 9.4 will be the mathematical model for both free and forced vibration methods.

9.2 Discussion of results for free and forced vibration methods on the TERN conductor

A procedure for self-damping characteristics has been developed, with the characteristic curves for the damping factor versus frequency for the TERN conductor in good agreement with similar results obtained by other researchers. For both the free and forced vibration methods, the following results were found (see Table 32 and Table 33 which gives out the summary of calculated results for both free and forced vibration methods).

1. A damping factor of $\varsigma = 0.02$ was determined using the free vibration method from 45 tests. Refer also to Table 32 shown below.
2. For the free vibration method, decaying of oscillations for the TERN conductor was observed for a frequency range of $18 \le f_n \le 28\,(Hz)$. This is an indication of

how fast the energy is dissipated (Also observed as 1st dominant resonance frequency). See also the summary shown in Table32 below.

3. Travelling wave numbers were obtained. Theoretical and experimental wave numbers agreed favourably. For a tension range of $20-29\,kN$, a wave number range of $124-149\,rad/s$ was obtained. This is also known as the c value given by equation (3.21). See Figures 14 to 16 together with corresponding Tables.
4. Using the forced vibration method, the results were able to confirm the values of the damping factors obtained using the free vibration method. Refer to the results by comparing Table 32 and Table 33 below.
5. At frequencies lower than $100\,Hz$, the damping factors were high, and the graph of damping factor versus frequency was plotted for one set of data as shown in Figure 17. See also Table 33 below.
6. At frequencies higher than $100\,Hz$, the damping factors levelled to constant values of $\zeta \le 0.05$, which compared favourably with those obtained using the free vibration method. Refer also to the summary of the results in Table 33.
7. For the forced vibration method, the first dominant resonance frequency was observed, using the sweep tests, to be $12 \le f_n \le 51\,(Hz)$. This is in close agreement with that found for the free vibration method. See also Table 33 for the confirmation of the results.

Table 32: summary of results for free vibration of the TERN conductor

Tension (kN)	Damping coefficient	Frequency (Hz)
20.73	0.018 (see Table 6)	27.2 (see Table 6)
	0.020 (see Table 6)	23.2 (see Table 6)
25.11	0.026 (see Table 8	22.7 (see Table 8)
	0.020 (see Table 8)	27.8 (see Table 8)
29.56	0.012 (see Table 9)	25.0 (see Table 9)
	0.213 (see Table 9)	18.3 (see Table 9)
	0.042 (see Table 9)	17.9 (see Table 9)

Table 33: summary of results for forced vibration of the TERN conductor

Tension of 20.73 kN (see Table 19)		Tension of 25.11 kN (see Table 16)		Tension of 29.56 kN (see Table 18)	
Damping coefficient	Frequency (Hz)	Damping coefficient	Frequency (Hz)	Damping coefficient	Frequency (Hz)
0.495	38.06	0.592	41.49	0.532	50.426
0.054	89.011	0.067	94.361	0.148	98.085
0.093	138.486	0.039	153.936	0.052	171.809
0.048	177.622	0.025	206.064	0.05	223.936
0.016	213.805	0.023	239.574	0.044	259.681
0.034	252.941	0.031	280.532		
0.034	282.478				

9.3 Discussion of results for free and forced vibration methods on the Aero-Z IEC62219-REV240609 conductor

A procedure for self-damping characteristics has been developed, with the The characteristic curves for the damping factor versus frequency for the Aero-Z IEC62219-REV240609 conductor in good agreement with similar results found by other researchers. For both the free and forced vibration methods, the following results were found:

For transmission lines with no dampers, one damper or two dampers, the damping coefficient $\zeta < 1.0$. Whether the damper is present or not, the self-damping coefficient is roughly the same. Damping of the transmission lines is therefore confirmed not to depend on the tuned absorbers but rather on *viscous* or *friction* damping mechanism. The name "mass absorber damper" used by Stockbridge is mere jargon. The actual external damping mechanism is termed a "tuned absorber" in vibration theory. This mechanism tunes to certain dominant frequencies in order to cancel the resonance modes of vibration.

For both the free and forced vibrations methods, the following was determined:

1. The damping factors (damping coefficients) of $0.012 \le \varsigma \le 0.2$ were determined. See Figures 17 to 22 together with corresponding Tables 25 to 30. Other results appear in Appendix III. Refer also to the summary of results shown in Table 34 below.
2. For the free vibration method, decaying of oscillations for the Aero-Z IEC62219-REV240609 conductor was observed for a frequency range of $50 \le f_n \le 100\,(Hz)$. This is an indication of how fast the energy is dissipated. (Also observed as 1st dominant resonance frequency.) See Figures 17 to 22 together with corresponding Tables 25 to 30.

Impulsive forces were introduced at position $1.2\,m$ span measured from the load-end fixed block. While the damping coefficient was not affected by the position of impulsive forces, these had an effect on the mode of vibration of the conductor as shown in Figures 17 to 22 together with corresponding Tables 25 to 30. Also the summary shown in Table 34 and Table 35 showed the effects of damping coefficient at different impulse forces.

3. At frequencies lower than $50\,Hz$, the damping factors were high, and the graph of damping factor versus frequency was plotted for one set of data as shown in Figure 18 above Refer also to Table 35 below.
4. At frequencies higher than $50\,Hz$, the damping factors levelled to constant values of $0.011 \le \zeta \le 0.2$, which compared favourably with those obtained using the free vibration method. At frequency below $50\,Hz$ the damping coefficient are high but less than 1 ($\zeta < 1.0$). See Figures 48, 52, 56, 60, 64 and 68 with corresponding Tables. See also Table 35 below.
5. For the forced vibration method, the first dominant resonance frequency was observed, using the sweep tests, to be $12 \le f_n \le 51\,(Hz)$. This is in close agreement with that found for the free vibration method. The results are compared in Tables 34 and 35 below.

The summary of results for the Aero-Z IEC62219-REV240609 conductor is shown in Tables 34 and 35 below.

Table 34: summary of results for free vibration of the Aero-Z IEC62219-REV240609 conductor

	Tension of 24.01 kN		Tension 27.02 kN	
	damping coefficient	Frequency (Hz)	damping coefficient	Frequency (Hz)
no mass abssorber	0.079 (see Table 10)	625	0.11 (see Table 13)	588
	0.105 (see Table 10)	395	0.066 (see Table 13)	417
	0.039 (see Table 72	962	0.102 (see Table 78)	625
	0.046 (see Table 72)	714	0.057 (see Table 78)	435
one mass absober	0.026 (see Table 11)	521	0.21 (see Table 79)	658
	0.029 (see Table 11)	375	0.04 (see Table 79)	400
	0.062 (see Table 74)	465	0.034 (see Table 14)	735
	0.023 (see Table 74)	385	0.027 (see Table 14)	385
two mass absober	0.012 (see Table 12)	556	0.21 (see Table 15)	595
	0.033 (see Table 12)	364	0.047 (see Table 15)	435
	0.012 (see Table 76)	583	0.22 (see Table 82)	625
	0.042 (see Table 76)	417	0.074 (see Table 82)	417

Table 35: summary of results for forced vibration of the Aero-Z IEC62219-REV240609 conductor

	Tension of 24.01 kN				Tension 27.02 kN			
	damping coefficient		Frequency (Hz)		damping coefficient		Frequency (Hz)	
	mid-span	end-span	mic-spna	end-span	mid-span	end-span	mid-span	end-span
no mass abssorber	0.626	0.032	22	85	0.544	0.011	23	83
	0.020	0.069	87	195	0.020	0.075	87	186
	0.157	0.034	165	255	0.157	0.090	165	246
	0.033		255		0.031		255	
	see Table 20	see Table 21	see Table 20	see Table 21	see Table 26	see Table 27	see Table 26	see Table 27
one mass absober	0.370	0.032	22	83	0.365	0.032	22	83
	0.011	0.073	85	186	0.009	0.074	85	186
	0.083	0.066	192	246	0.081	0.066	192	246
	0.089		251		0.089		251	
	see Table 22	see Table 23	see Table 22	see Table 23	see Table 28	see Table 29	see Table 28	see Table 29
two mass absober	0.368	0.011	22	84	0.381	0.011	22	84
	0.022	0.080	87	180	0.020	0.078	85	180
	0.184	0.075	193	257	0.187	0.086	192	255
	0.026		261		0.025		251	
	see Table 24	see Table 25	see Table 24	see Table 25	see Table 30	see Table 31	see Table 30	see Table 31

9.4 Mathematical model

The equation of motion for a system possessing a combination of friction and viscous damping is complex. Structural or hysteretic damping can be summarised in the following equation taken from Beard (1995).

$$m\ddot{x} + \left(\frac{c_H}{\omega}\right)\dot{x} + kx = 0$$

Under harmonic excitation, the response is given by

$$x = Xe^{j\omega t},\ \dot{x} = j\omega Xe^{j\omega t} = j\omega x \text{ and it follows that } \left(\frac{c_H}{\omega}\right)\dot{x} = jc_H x$$

The equation of motion reduces to

$$m\ddot{x} + (jc_H + k)x = 0 \text{ or } m\ddot{x} + k^* x = 0$$

$$k^* = k\left(1 + j\frac{c_H}{k}\right) = k(1 + j\eta)$$

Some definitions according to Beard (1995) and Meirovitch (2001).

$$\Delta E_{cyc} = \alpha X^2 = c\pi\omega X^2$$
$$\alpha = c\pi\omega$$

$\Delta E_{cyc} \equiv$ Energy dissipated per cycle
$k^* \equiv$ complex stiffness
$c \equiv$ viscous damping coefficient
$k \equiv$ elastic constant
$m \equiv$ mass
$\Delta E_{cyc} = \alpha X^2 = c\pi\omega X^2$
$c_H = \dfrac{\alpha}{\pi\omega} \equiv$ hysteretic or structural damping coefficient
$\eta \equiv$ hysteretic or structural damping loss factor (Beard)
$\gamma \equiv$ hysteretic or structural damping loss factor (Meirovitch)

How do we define viscous damping coefficient, c *in light of mass,* m*, elastic constant,* k *and damping factor or ratio,* ζ *?*

$c_c^2 = 4mk$ where $\zeta = \frac{c}{c_c}$ (i.e. $c = \zeta c_c$) and $c_c \equiv$ viscous critical damping coefficient, the damping ratio, $0 < \zeta < 0.2$ is obtained from experiments using the log decrement, δ (free vibration) method or quality factor, Q (forced vibration) method.

The self damping characteristics of transmission lines, usually not supplied by manufacturers, were therefore successfully determined using simple approaches developed in the dissertation. In the transmission lines investigated, the damping ratio $0 < \zeta < 0.2$ is considered to summarize the self damping characteristics. This damping factor or ratio is used to define $c = \zeta c_c$, then $\alpha = c\pi\omega$ and then $c_H = \frac{\alpha}{\pi\omega}$, the circular frequency $\omega = 2\pi f$ is any excitation frequency of vibration. The hysteretic or structural damping coefficient is then included in the mathematical model or equation of motion.

Chapter 10

CONCLUSION

A simple procedure for determining the self-damping characteristics of the TERN and Aero-Z IEC62219-REV240609 conductors was developed, with the damping factor found to be $\zeta \leq 0.2$ for both conductors. The damping factor of the TERN conductor was confirmed to be $\zeta \leq 0.05$, whereas the damping factor of the Aero-Z IEC62219-REV240609 was confirmed to be $\zeta \leq 0.2$ from both the free and forced vibration methods.

The self-damping of the transmission lines is confirmed not to depend on tuned absorbers such as Stockbridge dampers, but on the *viscous* or *friction* damping mechanism. The self-damping of the transmission lines is weak and not adequate to suppress Aeolian vibration.

The mathematical model was developed based on the books by Beard (1995) and Meirovitch (2001).

Chapter 11

RECOMMENDATIONS

An experimental procedure for determining the self-damping characteristics of transmission line conductors subjected to free and forced vibration has been developed in this research. However, a number of issues require further investigation:

The optimal position of external damping mechanisms on a general transmission line; and

The most suitable size for external damping mechanisms on a general transmission line.

Chapter 12

REFERENCES

Adhikari, S. 2006. Damping modelling using generalized proportional damping. *Journal of Sound and Vibration*, 293: 156-170.

Adhikari, S.; Friswell, M.; Lonkar, K. & Sarkar, A. 2009. Experimental case studies for uncertainty quantification in structural dynamics. *Probabilistic Engineering Mechanics*, 24: 473-492.

Adhikari, S. & Woodhouse, J. 2001. Identification of damping: Viscous damping. *Journal of Sound and Vibration*, 243: 43-88.

Barbieri, N.; Junior, H. & Barbieri, R. 2004. Experimental identification of damping: Dynamical analysis of transmission line cables: Linear theory. *Mechanical Systems and Signal Processing,* 18: 659-1007.

Barbieri, N.; Novak, P. & Barbieri, R. 2004. Experimental identification of damping. *International Journal of Solids and Structures,* 41: 3585-3594.

Beards, C.F. 1995. Engineering vibration analysis with application to control systems. London: Edward Arnold.

Boltezar, M. & Otrin, M. 2007. Damped lateral vibrations of straight and curved cables with no axial pre-load. *Journal of Sound and Vibration*, 300: 676-694.

Boltezar, M. & Otrin, M. 2009. On the modelling of vibration transmission over a spatially curved cable with casing. *Journal of Sound and Vibration*, 325: 798-815.

Boltezar, M.; Slavic, J. & Simonovski, I. Damping identification using a continuous wavelet transform: Application to real data. *Journal of Sound and Vibration*, 262: 291-307.

Brennan, M.J.; Carrella, A.; Waters, T.P. & Lopes, V. Jr. 2008. On the dynamic behaviour of a mass supported by a parallel combination of a spring and an elastically connected damper. *Journal of Sound and Vibration,* 309: 823-837.

Ceballos, M.A. & Prato, C.A. 2008.Determination of the axial force on stay cables accounting for their bending stiffness and rotational end restraints by free vibration tests. *Journal of Sound and Vibration,* 317: 127-141.

Chucheepsakul, S.; Srinil, N. & Rega, G. 2004. Three-dimensional non-linear coupling and dynamic tension in large-amplitude free vibrations of arbitrarily sagged cables. *Journal of Sound and Vibration,* 269: 823-852.

Cooper, D. & Nuckles, K. 1996. *Self-damping tests of various "Drake" conductors.* Carrollton, GA: Southwire Company.

Cornila, M.; Capolungoa, L, Qua J and Jairazbhoy V. Free vibration of a beam subjected to large static deflection, *Journal of Sound and Vibration* 303 (2007) 723–740.

Diana, G.; Bruni, S.; Cheli, F.; Fossati, F. & Manenti, A. 1998. Dynamic analysis of the transmission line crossing "Lago de Maracaibo". *Journal of Wind Engineering and Industrial Aerodynamics,* 7476: 977-986.

Diana, G.; Falco, M.; Cigada, A. & Manenti, A. 2000. On the measurement of overhead transmission lines conductor self-damping. *IEEE Transactions on Power Delivery,* 15(1): 285-292.

EPRI (Electric Power Research Institute). 1979. *Transmission line reference book: Wind-induced conductor motion*. Palo Alto, CA: EPRI.

Fang, J. & Lyons, G. 1996. Structural damping of tensioned pipes with reference to cables. *Journal of Sound and Vibration,* 193(4): 891-907.

Fekr, M.R. & McClure, G. 1998. Numerical modelling of the dynamic response of ice-shedding on electrical transmission lines. *Atmospheric Research,* 46: 1-11.

Hagedorn, P.; Mitra, N. & Hadulla, T. 2002. Vortex–excited vibrations in bundled conductors: A mathematical model. *Journal of Fluids and Structures,* 16(7): 843-854.

Hardy, C. & Leblond, A. 1993. Comparison of conductor self-damping measurements. Paris: CIGRE.

Inman, D.J. 2001. *Engineering vibrations*. 2nd Edition. Upper Saddle River, NJ: Prentice Hall.

Inman, D. J. 2008. *Engineering vibrations*. 3rd Edition. New York, NY: Pearson Education.

James, M.L.; Smith, G.M.; Wolford, J.C. & Whaley, P.W. 1989. Vibration of mechanical and structural systems: With microcomputer applications. New York, NY: Harper and Row.

Kahla, N.B. 1995. Dynamics of a single guy cable. *Computers and Structures,* 54(6): 1197-1211.

Koh, C.G. & Rong, Y. 2004. Dynamic analysis of large displacement cable motion with experimental verification. *Journal of Sound and Vibration,* 272: 187-206.

McClure, G. & Lapointe, M. 2003. Modelling the structural dynamic response of overhead transmission lines. *Computers and Structures,* 81: 825-834.

Meirovitch, L. 2001. *Fundamentals of vibrations*. New York, NY: McGraw-Hill.

Meriam, J.L. 2008. *Engineering mechanics: Statics and dynamics – SI version.* New York, NY: John Wiley & Sons, Inc.

Ni, Y.Q.; Ko, J.M. & Zheng, G. 2002. Dynamic analysis of large-diameter sagged cables taking into account flexural rigidity. *Journal of Sound and Vibration,* 257(2): 301-319.

Noiseux, D.U. 1992. Similarity laws of the internal damping of stranded cables in transverse vibrations. *IEEE Transactions on Power Delivery,* 7(3): 1574-1581.

Oliveira, R.E. & Preire, G. 1994. Dynamical modelling and analysis of Aeolian vibrations of single conductors. *IEEE Transactions on Power Delivery*, 9(3): 1685-1693.

Park, S.K.; Lyu, K.W. & Lee, H.S. 2008. Estimation of damping characteristics for cable using system identification scheme. In: H.M. Koh. *Bridge Maintenance, Safety Management, Health Monitoring and Informatics*. New York, NY: CRC/Taylor & Francis.

PLP (Preformed Line Products). 2008. *Aeolian vibration basics*. Cleveland, Ohio: PLP.

Pon, C. 2009. IEEE guide on conductor self-damping measurements and IEEE guide for laboratory measurement of the power dissipation characteristics of Aeolian vibration dampers for single conductors: An overview. Presentation at the Conductors and Accessories WG Meeting. Calgary, Canada. 27 July 2009.

Rawlins, C.B. 2000. The long-span problem in the analysis of conductor vibration damping. *IEEE Transactions on Power Delivery*, 15(2): 770-776.

Rawlins, C.B. 2009. Flexural self-damping in overhead electrical transmission conductors. *Journal of Sound and Vibration*, 323: 232-256.

Sorokin, S.V. & Rega, G. 2007. On modelling and linear vibrations of arbitrarily sagged inclined cables in a quiescent viscous fluid. *Journal of Fluids and Structures*, 23(1): 1077-1092.

Thomson, W.T. & Dahleh, M.D. 1998. *Theory of vibrations with applications*. 5th Edition. Upper Saddle River, NJ: Prentice Hall.

Vecchiarelli J.; Currie, I.G. & Havard, D.G. 1995. *Modelling of single conductor and damper vibrations*. Paper presented at the Electricity '95 Conference of the Canadian Electrical Association. Vancouver, Canada. 28 March 1995.

Vecchiarelli, J.; Currie, I.G. & Havard, D.G. 2000. Computational analysis of Aeolian vibration with a Stockbridge-type damper. *Journal of Fluids and Structures,* 14: 489-509.

Yamaguchi, H. & Adhikari, R. 1995. Energy-based evaluation of modal damping in structural cables with and without damping treatment. *Journal of Sound and Vibration*, 181: 71-83.

Yamaguchi, H.; Alauddin, M.D. & Poovarodom, N. 2001. Dynamic characteristics and vibration control of a cable system with sub-structural interactions. *Engineering Structure*, 23: 1348-1358.

APPENDIX I

RESULTS FOR FREE VIBRATION METHOD ON TERN CONDUCTOR

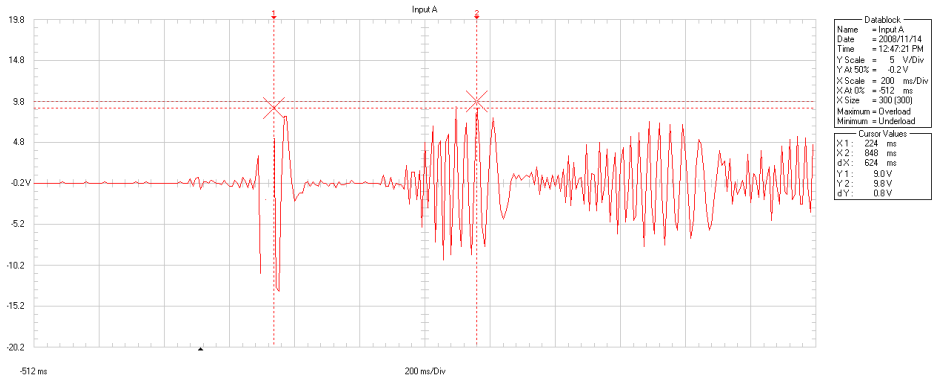

Figure 71: Excitation at $1.2\ m$ measured from load end, cable tension = 20.8 kN

Table 36: Calculated results from data of Figure 71

TERN j	PX (ms)	PY (mV)	FREQ (Hz)	ln PY	Yj	(lnPY)Yj	Yj^2	Zj	LogDec	Zeta	NatFreq (rad/s)	NatFreq (Hz)
1	744	9600.00		9.1695	0	0.0000	0	9.2442	0.112	0.018	170.8	27.2
2	768	9000.00	41.7	9.1050	1	9.1	1	9.1324				
3	800	8000.00	31.3	8.9872	2	17.9744	4	9.0205				
4	832	9000.00	31.3	9.1050	3	27.3149	9	8.9087				
5	872	8000.00	25.0	8.9872	4	35.9488	16	8.7969				
6	928	4600.00	17.9	8.4338	5	42.1691	25	8.6850				
SUM		48200.0		53.788	15	132.512	55					

Using least squares method, log-dec = 0.112, zeta = 0.018, frequency of decaying oscillation is 170.8 rad/s (27.2Hz)

TERN j	PX (ms)	PY (mV)	FREQ (Hz)	ln PY	Yj	(lnPY)Yj	Yj^2	Zj	LogDec	Zeta	NatFreq (rad/s)	
1	1376	7400.00		8.9092	0	0.0000	0	9.0240	0.123	0.020	145.5	23.2
2	1408	7200.00	31.3	8.8818	1	8.9	1	8.9009				
3	1440	7000.00	31.3	8.8537	2	17.7073	4	8.7778				
4	1480	7000.00	25.0	8.8537	3	26.5610	9	8.6547				
5	1528	5200.00	20.8	8.5564	4	34.2257	16	8.5316				
6	1592	3800.00	15.6	8.2428	5	41.2138	25	8.4085				
SUM		37600.0		52.298	15	128.590	55					

Using least squares method, log-dec = 0.123, zeta = 0.020, frequency of decaying oscillation is 145.5 rad/s (23.2 Hz)

Mode	Lamda (m)	Tau (s)	Freq (Hz)	Wave speed (rad/s)	Theoretical (rad/s)	Difference (rad/s)	Difference %
2	84.6	0.624	1.60	135.58	124.6	(10.99)	8.10
3	56.4	0.624	1.60	90.38		34.20	37.84
4	42.3	0.624	1.60	67.79		56.80	83.79
5	33.84	0.624	1.60	54.23		70.36	129.74

Mode	Lamda (m)	Tau (s)	Freq (Hz)	Wave speed (rad/s)	Theoretical (rad/s)	Difference (rad/s)	Difference %
2	84.6	0.528	1.89	160.23	124.6	(35.64)	22.24
3	56.4	0.528	1.89	106.82		17.77	16.64
4	42.3	0.528	1.89	80.11		44.48	55.52
5	33.84	0.528	1.89	64.09		60.50	94.39

Mode	Lamda (m)	Tau (s)	Freq (Hz)	Wave speed (rad/s)	Theoretical (rad/s)	Difference (rad/s)	Difference %
2	84.6	0.456	2.19	185.53	124.6	(60.94)	32.85
3	56.4	0.456	2.19	123.68		0.90	0.73
4	42.3	0.456	2.19	92.76		31.83	34.31
5	33.84	0.456	2.19	74.21		50.38	67.89

Conductor is excited in first mode but eventually vibrates in third mode
Experimental and theoretical wave number agree favourably at 124 rad/s within $0.73 \leq \varepsilon \leq 16.64$

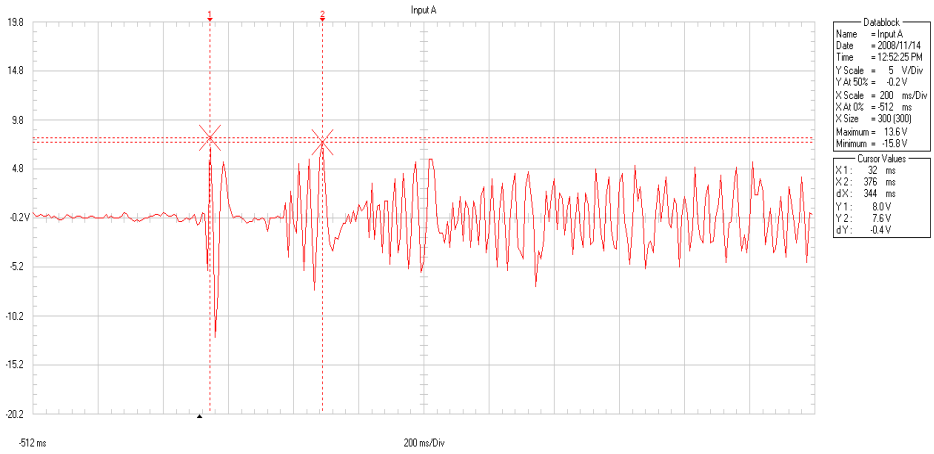

Figure 72: Excitation at 1/4 span measured from load end, cable tension = 20.8 kN

Table 37: Calculated results from data of Figure72

Mode	Lamda (m)	Tau (s)	Freq (Hz)	Wave speed (rad/s)	Theoretical (rad/s)	Difference (rad/s)	Difference %
2	84.6	0.344	2.91	245.93	124.6	(121.34)	49.34
3	56.4	0.344	2.91	163.95		(39.36)	24.01
4	42.3	0.344	2.91	122.97		1.62	1.32
5	33.84	0.344	2.91	98.37		26.22	26.65

Mode	Lamda (m)	Tau (s)	Freq (Hz)	Wave speed (rad/s)	Theoretical (rad/s)	Difference (rad/s)	Difference %
2	84.6	0.328	3.05	257.93	124.6	(133.34)	51.70
3	56.4	0.328	3.05	171.95		(47.36)	27.54
4	42.3	0.328	3.05	128.96		(4.37)	3.39
5	33.84	0.328	3.05	103.17		21.42	20.76

Mode	Lamda (m)	Tau (s)	Freq (Hz)	Wave speed (rad/s)	Theoretical (rad/s)	Difference (rad/s)	Difference %
2	84.6	0.304	3.29	278.29	124.6	(153.70)	55.23
3	56.4	0.304	3.29	185.53		(60.94)	32.85
4	42.3	0.304	3.29	139.14		(14.56)	10.46
5	33.84	0.304	3.29	111.32		13.27	11.92

Conductor is excited in first mode and continues vibrating in fourth mode
Experimental and theoretical wave number agree favourably at 124 rad/s within $1.32 \leq \varepsilon \leq 10.46$

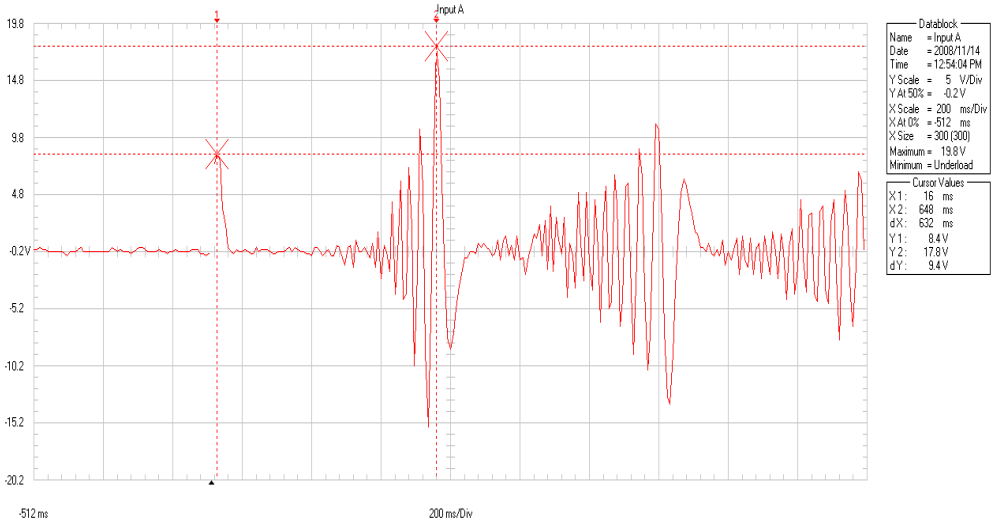

Figure 73: Excitation at 1/2 span, cable tension = 20.8 kN

Table 38: Calculated results from data of Figure 73

Mode	Lamda (m)	Tau (s)	Freq (Hz)	Wave speed (rad/s)	Theoretical (rad/s)	Difference (rad/s)	Difference %
2	84.6	0.632	1.58	133.86	124.6	(9.27)	6.93
3	56.4	0.632	1.58	89.24		35.35	39.61
4	42.3	0.632	1.58	66.93		57.66	86.15
5	33.84	0.632	1.58	53.54		71.04	132.68

Mode	Lamda (m)	Tau (s)	Freq (Hz)	Wave speed (rad/s)	Theoretical (rad/s)	Difference (rad/s)	Difference %
2	84.6	0.632	1.58	133.86	124.6	(9.27)	6.93
3	56.4	0.632	1.58	89.24		35.35	39.61
4	42.3	0.632	1.58	66.93		57.66	86.15
5	33.84	0.632	1.58	53.54		71.04	132.68

Mode	Lamda (m)	Tau (s)	Freq (Hz)	Wave speed (rad/s)	Theoretical (rad/s)	Difference (rad/s)	Difference %
2	84.6	0.584	1.71	144.86	124.6	(20.27)	14.00
3	56.4	0.584	1.71	96.58		28.01	29.01
4	42.3	0.584	1.71	72.43		52.16	72.01
5	33.84	0.584	1.71	57.95		66.64	115.01

Conductor is excited in first mode and continues vibrating in second mode
Experimental and theoritical wave number agree favourably at 124 rad/s within $6.93 \leq \varepsilon \leq 14$

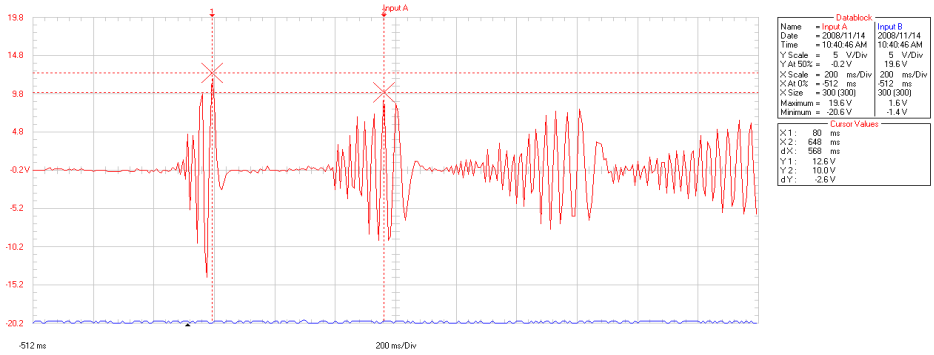

Figure 74: Excitation at $1.2\ m$ measured from load end, cable tension = 25.12 kN

Table 39: Calculated results from data of Figure 74

TERN j	PX (ms)	PY (mV)	FREQ (Hz)	ln PY	Yj	(lnPY)Yj	Yj^2	Zj	LogDec	Zeta	NatFreq (rad/s)	NatFreq (Hz)
1	632	9400.0		9.15	0	0.00	0	9.20	0.162	0.026	143	22.7
2	664	9400.0	31.3	9.15	1	9.15	1	9.04				
3	720	6800.0	17.9	8.82	2	17.65	4	8.88				
SUM		25600.0		27.12	3	26.80	5					

Using least squares method, log-dec = 0.162, zeta = 0.026, frequency of decaying oscillation is 143 rad/s (22.7Hz)

TERN j	PX (ms)	PY (mV)	FREQ (Hz)	ln PY	Yj	(lnPY)Yj	Yj^2	Zj	LogDec	Zeta	NatFreq (rad/s)	
1	1200	8000.0		8.99	0	0.00	0	8.99	0.127	0.020	175	27.8
2	1232	7200.0	31.3	8.88	1	8.88	1	8.87				
3	1272	6200.0	25.0	8.73	2	17.46	4	8.74				
SUM		21400.0		26.60	3	26.35	5					

Using least squares method, log-dec = 0.127, zeta = 0.020, frequency of decaying oscillation is 175 rad/s (27.8 Hz)

Mode	Lamda (m)	Tau (s)	Freq (Hz)	Wave speed (rad/s)	Theoretical (rad/s)	Difference (rad/s)	Difference %
2	84.6	0.568	1.76	148.94	136.9	(12.03)	8.07
3	56.4	0.568	1.76	99.30		37.62	37.89
4	42.3	0.568	1.76	74.47		62.45	83.85

Mode	Lamda (m)	Tau (s)	Freq (Hz)	Wave speed (rad/s)	Theoretical (rad/s)	Difference (rad/s)	Difference %
2	84.6	0.648	1.54	130.56	136.9	6.36	4.87
3	56.4	0.648	1.54	87.04		49.88	57.31
4	42.3	0.648	1.54	65.28		71.64	109.75
5	33.84	0.648	1.54	52.22		84.69	162.18

Mode	Lamda (m)	Tau (s)	Freq (Hz)	Wave speed (rad/s)	Theoretical (rad/s)	Difference (rad/s)	Difference %
2	84.6	0.528	1.89	160.23	136.9	(23.31)	14.55
3	56.4	0.528	1.89	106.82		30.10	28.18
4	42.3	0.528	1.89	80.11		56.80	70.90
5	33.84	0.528	1.89	64.09		72.83	113.63

Conductor is excited in first mode and continues vibrating in second mode
Experimental and theoritical wave number agree favourably at 137 rad/s within $4.87 \leq \varepsilon \leq 14.55$

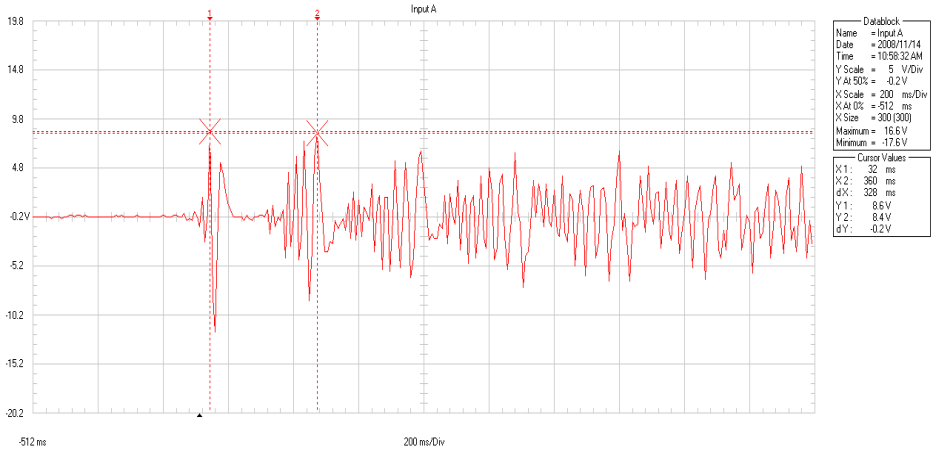

Figure 75: Excitation at 1/4 span measured from load end, cable tension = 25.12 kN

Table 40: Calculated results from data of Figure 75

Mode	Lamda (m)	Tau (s)	Freq (Hz)	Wave speed (rad/s)	Theoretical (rad/s)	Difference (rad/s)	Difference %
1	84.6	0.328	3.05	257.93	136.9	(121.01)	46.92
2	56.4	0.328	3.05	171.95		(35.03)	20.37
3	42.3	0.328	3.05	128.96		7.95	6.17
4	33.84	0.328	3.05	103.17		33.75	32.71

Mode	Lamda (m)	Tau (s)	Freq (Hz)	Wave speed (rad/s)	Theoretical (rad/s)	Difference (rad/s)	Difference %
1	84.6	0.320	3.13	264.38	136.9	(127.46)	48.21
2	56.4	0.320	3.13	176.25		(39.33)	22.32
3	42.3	0.320	3.13	132.19		4.73	3.58
4	33.84	0.320	3.13	105.75		31.17	29.47

Mode	Lamda (m)	Tau (s)	Freq (Hz)	Wave speed (rad/s)	Theoretical (rad/s)	Difference (rad/s)	Difference %
1	84.6	0.288	3.47	293.75	136.9	(156.83)	53.39
2	56.4	0.288	3.47	195.83		(58.92)	30.08
3	42.3	0.288	3.47	146.88		(9.96)	6.78
4	33.84	0.288	3.47	117.50		19.42	16.53

Mode	Lamda (m)	Tau (s)	Freq (Hz)	Wave speed (rad/s)	Theoretical (rad/s)	Difference (rad/s)	Difference %
1	84.6	0.320	3.13	264.38	136.9	(127.46)	48.21
2	56.4	0.320	3.13	176.25		(39.33)	22.32
3	42.3	0.320	3.13	132.19		4.73	3.58
4	33.84	0.320	3.13	105.75		31.17	29.47

Conductor is excited in first mode and continues vibrating in third mode
Experimental and theoretical wave number agree favourably at 137 rad/s within $3.58 \leq \varepsilon \leq 6.78$

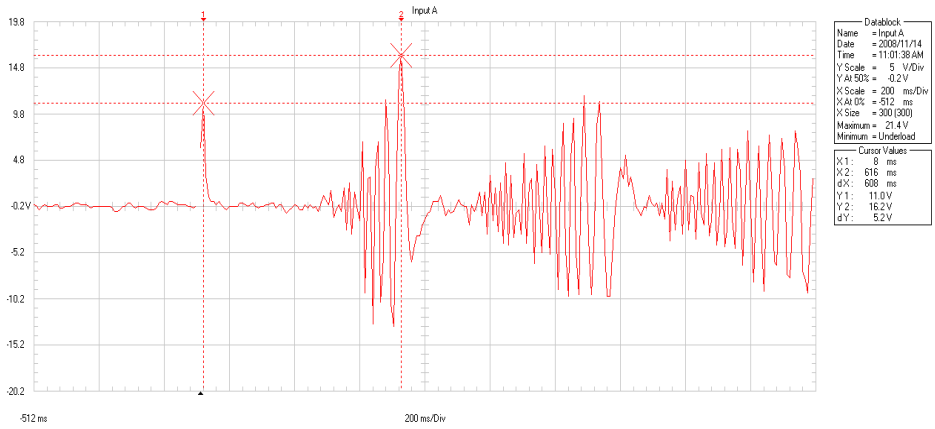

Figure 76: Excitation at 1/2 span, cable tension = 25.12 kN

Table 41: Calculated results from data of Figure 37

Mode	Lamda (m)	Tau (s)	Freq (Hz)	Wave speed (rad/s)	Theoretical (rad/s)	Difference (rad/s)	Difference %
2	84.6	0.608	1.64	139.14	136.9	(2.23)	1.60
3	56.4	0.608	1.64	92.76		44.15	47.60
4	42.3	0.608	1.64	69.57		67.34	96.80
5	33.84	0.608	1.64	55.66		81.26	146.00

Mode	Lamda (m)	Tau (s)	Freq (Hz)	Wave speed (rad/s)	Theoretical (rad/s)	Difference (rad/s)	Difference %
2	84.6	0.560	1.79	151.07	136.9	(14.15)	9.37
3	56.4	0.560	1.79	100.71		36.20	35.95
4	42.3	0.560	1.79	75.54		61.38	81.26
5	33.84	0.560	1.79	60.43		76.49	126.58

Mode	Lamda (m)	Tau (s)	Freq (Hz)	Wave speed (rad/s)	Theoretical (rad/s)	Difference (rad/s)	Difference %
2	84.6	0.504	1.98	167.86	136.9	(30.94)	18.43
3	56.4	0.504	1.98	111.90		25.01	22.35
4	42.3	0.504	1.98	83.93		52.99	63.14
5	33.84	0.504	1.98	67.14		69.77	103.92

Conductor is excited in first mode and continues vibrating in second mode
Experimental and theoretical wave number agree favourably at 137 rads/s within $1.6 \leq \varepsilon \leq 18.43$

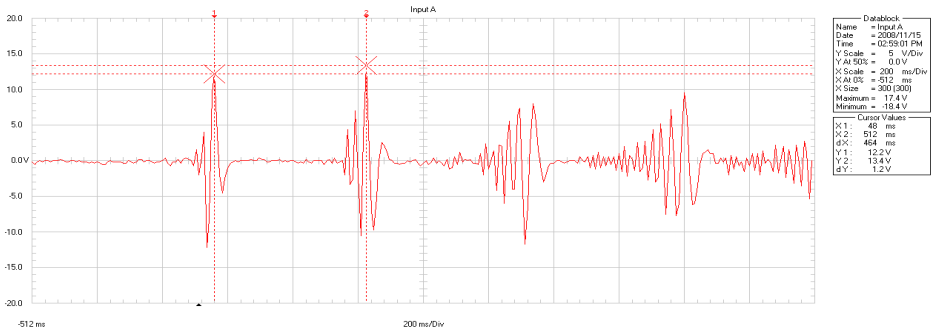

Figure 77: Excitation at $1.2\ m$ span measured from load end, cable tension = 29.86 kN

Table 42: Calculated results from data of Figure 77

TERN j	PX (ms)	PY (mV)	FREQ (Hz)	ln PY	Yj	(lnPY)Yj	Yj^2	Zj	LogDec	Zeta	NatFreq (rad/s)	NatFreq (Hz)
1	496	10600.00		9.269	0	0.0000	0	9.269	0.078	0.012	157	25.0
2	536	9800.00	25.0	9.190	1	9.2	1	9.190				
SUM		20400.0		18.459	1	9.190	1					

Using least squares method, log-dec = 0.078, zeta = 0.012, frequency of decaying oscillation is 157 rad/s (25.0 Hz)

TERN j	PX (ms)	PY (mV)	FREQ (Hz)	ln PY	Yj	(lnPY)Yj	Yj^2	Zj	LogDec	Zeta	NatFreq (rad/s)	
1	1000	11800.00		9.376	0	0.0000	0	9.376	1.369	0.213	115	18.3
2	1056	3000.00	17.9	8.006	1	8.0	1	8.006				
SUM		14800.0		17.382	1	8.006	1					

Using least squares method, log-dec = 1.369, zeta = 0.213, frequency of decaying oscillation is 115 rad/s (18.3 Hz)

TERN j	PX (ms)	PY (mV)	FREQ (Hz)	ln PY	Yj	(lnPY)Yj	Yj^2	Zj	LogDec	Zeta	NatFreq (rad/s)	
1	1464	7800.00		8.962	0	0.0000	0	8.962	0.262	0.042	112	17.9
2	1520	6000.00	17.9	8.700	1	8.7	1	8.700				
SUM		13800.0		17.661	1	8.700	1					

Using least squares method, log-dec = 0.262, zeta = 0.042, frequency of decaying oscillation is 112 rad/s (17.9 Hz)

Mode	Lamda (m)	Tau (s)	Freq (Hz)	Wave speed (rad/s)	Theoretical (rad/s)	Difference (rad/s)	Difference %
2	84.6	0.464	2.16	182.33	149.3	(33.05)	18.13
3	56.4	0.464	2.16	121.55		27.73	22.81
4	42.3	0.464	2.16	91.16		58.11	63.75
5	33.84	0.464	2.16	72.93		76.35	104.68

Mode	Lamda (m)	Tau (s)	Freq (Hz)	Wave speed (rad/s)	Theoretical (rad/s)	Difference (rad/s)	Difference %
2	84.6	0.512	1.95	165.23	149.3	(15.96)	9.66
3	56.4	0.512	1.95	110.16		39.12	35.51
4	42.3	0.512	1.95	82.62		66.66	80.68
5	33.84	0.512	1.95	66.09		83.18	125.86

Mode	Lamda (m)	Tau (s)	Freq (Hz)	Wave speed (rad/s)	Theoretical (rad/s)	Difference (rad/s)	Difference %
2	84.6	0.464	2.16	182.33	149.3	(33.05)	18.13
3	56.4	0.464	2.16	121.55		27.73	22.81
4	42.3	0.464	2.16	91.16		58.11	63.75
5	33.84	0.464	2.16	72.93		76.35	104.68

Conductor is excited in first mode and continues vibrating in second mode
Experimental and theoretical wave number agree favourably at 149 rad/s within $9.66 \leq \varepsilon \leq 18.13$

Figure 78: Excitation at 1/4 span measured from load end, cable tension = 29.86 kN

Table 43: Calculated results from data of Figure 78

Mode	Lamda (m)	Tau (s)	Freq (Hz)	Wave speed (rad/s)	Theoretical (rad/s)	Difference (rad/s)	Difference %
2	84.6	0.248	4.03	341.13	149.3	(191.85)	56.24
3	56.4	0.248	4.03	227.42		(78.14)	34.36
4	42.3	0.248	4.03	170.56		(21.29)	12.48
5	33.84	0.248	4.03	136.45		12.83	9.40

Mode	Lamda (m)	Tau (s)	Freq (Hz)	Wave speed (rad/s)	Theoretical (rad/s)	Difference (rad/s)	Difference %
2	84.6	0.248	4.03	341.13	149.3	(191.85)	56.24
3	56.4	0.248	4.03	227.42		(78.14)	34.36
4	42.3	0.248	4.03	170.56		(21.29)	12.48
5	33.84	0.248	4.03	136.45		12.83	9.40

Mode	Lamda (m)	Tau (s)	Freq (Hz)	Wave speed (rad/s)	Theoretical (rad/s)	Difference (rad/s)	Difference %
2	84.6	0.192	5.21	440.63	149.3	(291.35)	66.12
3	56.4	0.192	5.21	293.75		(144.47)	49.18
4	42.3	0.192	5.21	220.31		(71.04)	32.24
5	33.84	0.192	5.21	176.25		(26.97)	15.30

Conductor is excited in first mode and continues vibrating in fifth mode
Experimental and theoretical wave number agree favourably at 149 rad/s within $9.40 \leq \varepsilon \leq 15.30$

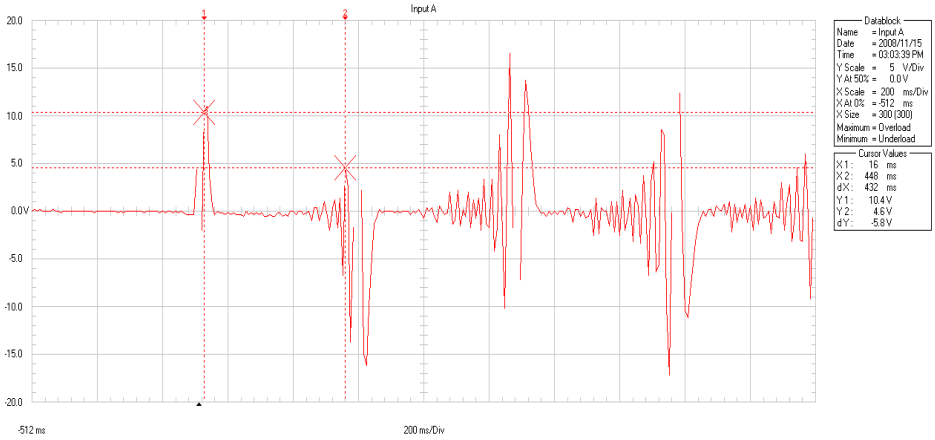

Figure 79: Excitation at 1/2 span, cable tension = 29.86 kN

Table 44: Calculated results from data of Figure 79

Mode	Lamda (m)	Tau (s)	Freq (Hz)	Wave speed (rad/s)	Theoretical (rad/s)	Difference (rad/s)	Difference %
2	84.6	0.424	2.36	199.53	149.3	(50.25)	25.19
3	56.4	0.424	2.36	133.02		16.26	12.22
4	42.3	0.424	2.36	99.76		49.51	49.63
5	33.84	0.424	2.36	79.81		69.47	87.04

Mode	Lamda (m)	Tau (s)	Freq (Hz)	Wave speed (rad/s)	Theoretical (rad/s)	Difference (rad/s)	Difference %
2	84.6	0.504	1.98	167.86	149.3	(18.58)	11.07
3	56.4	0.504	1.98	111.90		37.37	33.40
4	42.3	0.504	1.98	83.93		65.35	77.86
5	33.84	0.504	1.98	67.14		82.13	122.33

Mode	Lamda (m)	Tau (s)	Freq (Hz)	Wave speed (rad/s)	Theoretical (rad/s)	Difference (rad/s)	Difference %
2	84.6	0.520	1.92	162.69	149.3	(13.42)	8.25
3	56.4	0.520	1.92	108.46		40.82	37.63
4	42.3	0.520	1.92	81.35		67.93	83.51
5	33.84	0.520	1.92	65.08		84.20	129.39

Mode	Lamda (m)	Tau (s)	Freq (Hz)	Wave speed (rad/s)	Theoretical (rad/s)	Difference (rad/s)	Difference %
2	84.6	0.384	2.60	220.31	149.3	(71.04)	32.24
3	56.4	0.384	2.60	146.88		2.40	1.64
4	42.3	0.384	2.60	110.16		39.12	35.51
5	33.84	0.384	2.60	88.13		61.15	69.39

Conductor is excited in first mode, vibrates in second mode twice and then in third mode
Experimental and theoretical wave number agree favourably at 149 rad/s within $1.64 \leq \varepsilon \leq 12.22$

Tension: 20.73 kN

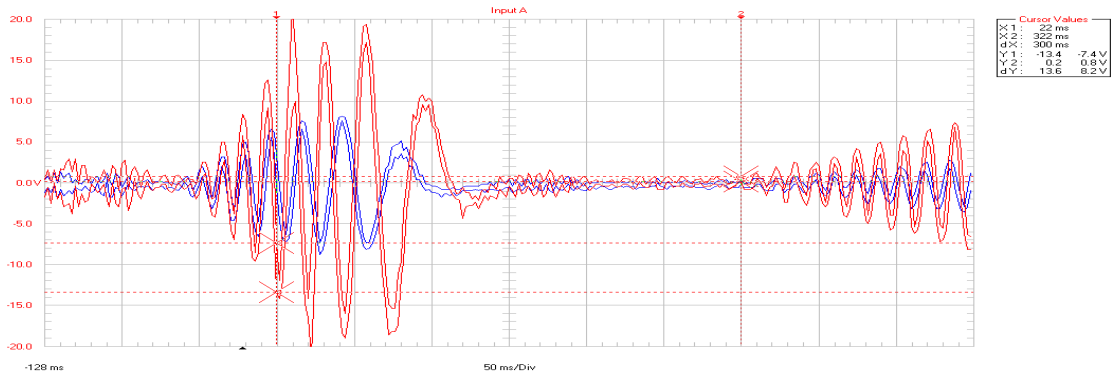

Figure 80: Excitation at $1.2\ m$ span

Table 45: Calculated results from data of Figure 80

x	dx	v	r	delta	zeta	time	f
80	0	19.4					
116	36	10.8	1.796	0.586	0.0928	0.036	28

Mode	Lambda	Tau	Freq	Wave speed	Theoretical	Difference	Difference %
2	84.6	3.56E-01	2.81E+00	2.3764E+02	124.3791	-1.1326E+02	-4.7661E+01
3	56.4	3.56E-01	2.81E+00	1.5843E+02		-3.4048E+01	-2.1491E+01
4	42.3	3.56E-01	2.81E+00	1.1882E+02		5.5588E+00	4.6784E+00
5	33.84	3.56E-01	2.81E+00	9.5056E+01		2.9323E+01	3.0848E+01

Tension: 20.73 kN

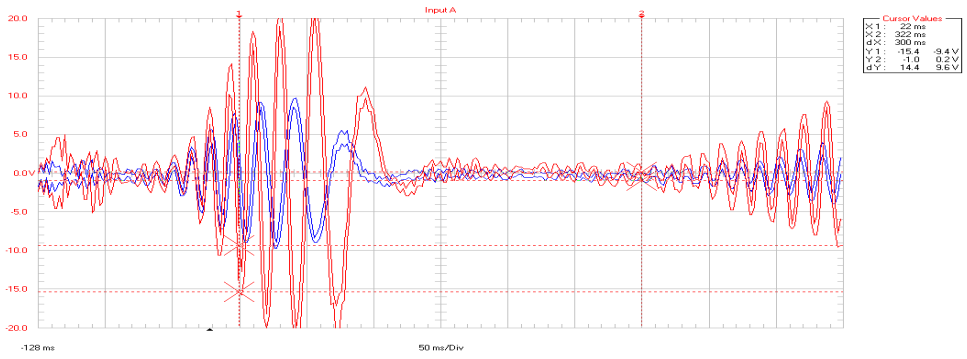

Figure 81: Excitation at $1.2\ m$ span

Table 46: Calculated results from data of Figure 81

x	dx	v	r	delta	zeta	time	f
80	0	22					
116	36	11.2	1.964	0.6751	0.107	0.036	28

Mode	Lambda	Tau	Freq	Wave speed	Theoretical	Difference	Difference %
2	84.6	3.80E-01	2.63E+00	2.2263E+02	124.3791	-9.8253E+01	-4.4132E+01
3	56.4	3.80E-01	2.63E+00	1.4842E+02		-2.4042E+01	-1.6199E+01
4	42.3	3.80E-01	2.63E+00	1.1132E+02		1.3063E+01	1.1735E+01
5	33.84	3.80E-01	2.63E+00	8.9053E+01		3.5326E+01	3.9669E+01

Tension: 20.73 kN

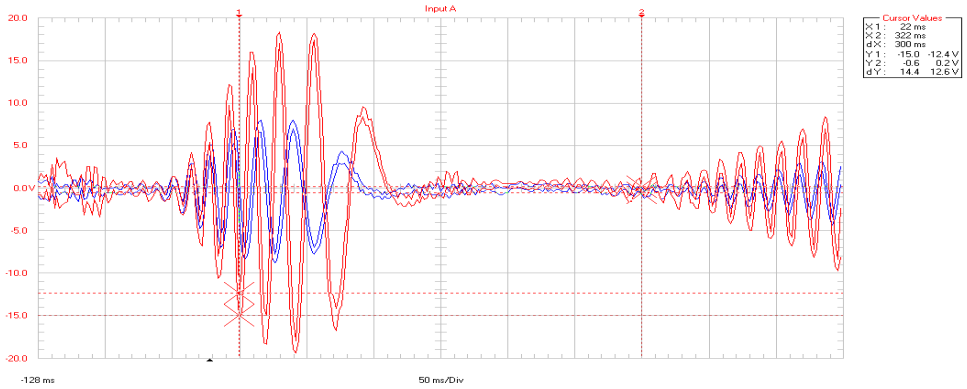

Figure 82: Excitation at $1.2\ m$ span

Table 47: Calculated results from data of Figure 82

x	dx	v	r	delta	zeta	time	f
52	0	18.4					
78	26	18.2	1.010989	0.01097	0.001739	0.026	
114	36	9.6	1.895833	0.6396	0.101281	0.031	32

Mode	Lambda	Tau	Freq	Wave speed	Theoretical	Difference	Difference %
2	84.6	3.48E-01	2.87E+00	2.4310E+02	124.3791	-1.1872E+02	-4.8837E+01
3	56.4	3.48E-01	2.87E+00	1.6207E+02		-3.7690E+01	-2.3255E+01
4	42.3	3.48E-01	2.87E+00	1.2155E+02		2.8273E+00	2.3260E+00
5	33.84	3.48E-01	2.87E+00	9.7241E+01		2.7138E+01	2.7908E+01

Tension: 20.73 kN

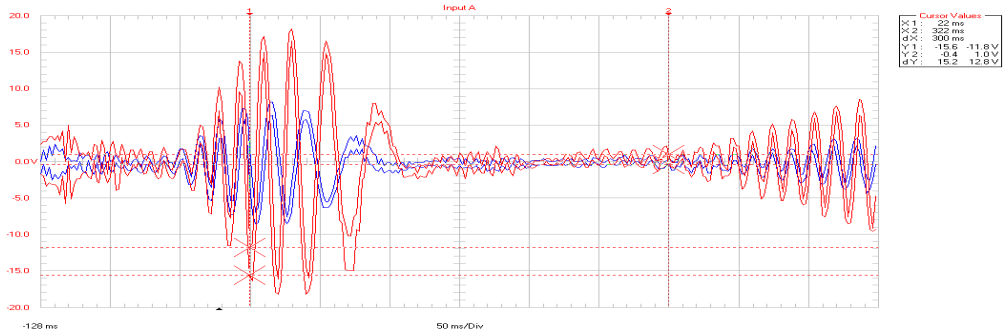

Figure 83: Excitation at $1.2\ m$ span

Table 48: Calculated results from data of Figure 83

x	dx	v	r	delta	zeta	time	f
52	0	18.2					
76	24	16.6	1.096386	0.0920189	0.014644	0.024	
112	36	8	2.075	0.72996115	0.115401	0.03	33

Mode	Lambda	Tau	Freq	Wave speed	Theoretical	Difference	Difference %
2	84.6	3.58E-01	2.79E+00	2.3631E+02	124.3791	-1.1193E+02	-4.7367E+01
3	56.4	3.58E-01	2.79E+00	1.5754E+02		-3.3163E+01	-2.1050E+01
4	42.3	3.58E-01	2.79E+00	1.1816E+02		6.2226E+00	5.2664E+00
5	33.84	3.58E-01	2.79E+00	9.4525E+01		2.9854E+01	3.1583E+01

Tension: 20.73 kN

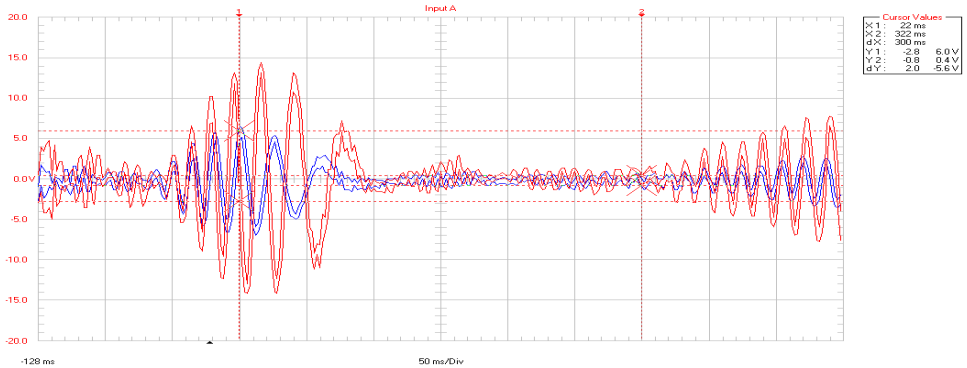

Figure 84: Excitation at $1.2\ m$ span

Table 49: Calculated results from data of Figure 84

x	dx	v	r	delta	zeta	time	f
38	0	14.4					
62	24	13.2	1.090909	0.08701138	0.013847	0.024	
98	36	7.2	1.833333	0.6061358	0.096024	0.03	33

Mode	Lambda	Tau	Freq	Wave speed	Theoretical	Difference	Difference %
2	84.6	3.56E-01	2.81E+00	2.3764E+02	124.3791	-1.1326E+02	-4.7661E+01
3	56.4	3.56E-01	2.81E+00	1.5843E+02		-3.4048E+01	-2.1491E+01
4	42.3	3.56E-01	2.81E+00	1.1882E+02		5.5588E+00	4.6784E+00
5	33.84	3.56E-01	2.81E+00	9.5056E+01		2.9323E+01	3.0848E+01

Tension: 25.11 kN

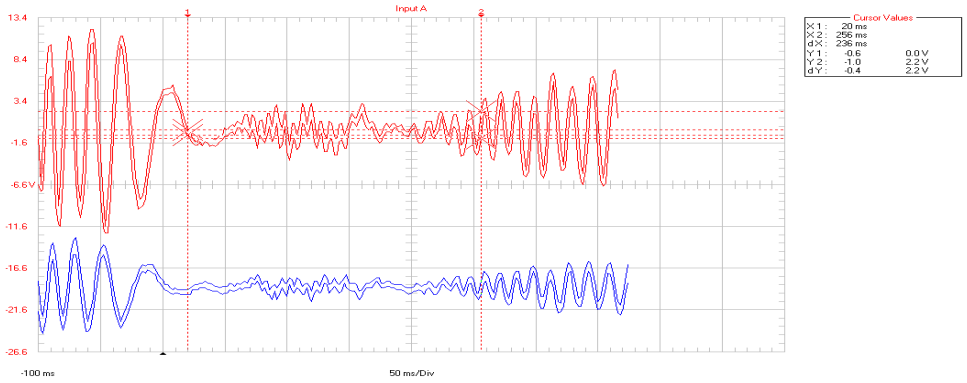

Figure 85: Excitation at $1.2\ m$ span

Table 50: Calculated results from data of Figure 85

x	dx	v	r	delta	zeta	time	f
-56	0	12					
-32	24	11.2	1.071429	0.06899287	0.01098	0.024	
8	40	5.4	2.074074	0.72951482	0.115331	0.032	31

Mode	Lambda	Tau	Freq	Wave speed	Theoretical	Difference	Difference %
2	84.6	3.18E-01	3.14E+00	2.6604E+02	136.8898	-1.2915E+02	-4.8545E+01
3	56.4	3.18E-01	3.14E+00	1.7736E+02		-4.0469E+01	-2.2817E+01
4	42.3	3.18E-01	3.14E+00	1.3302E+02		3.8709E+00	2.9100E+00
5	33.84	3.18E-01	3.14E+00	1.0642E+02		3.0475E+01	2.8638E+01

Tension: 25.11 kN

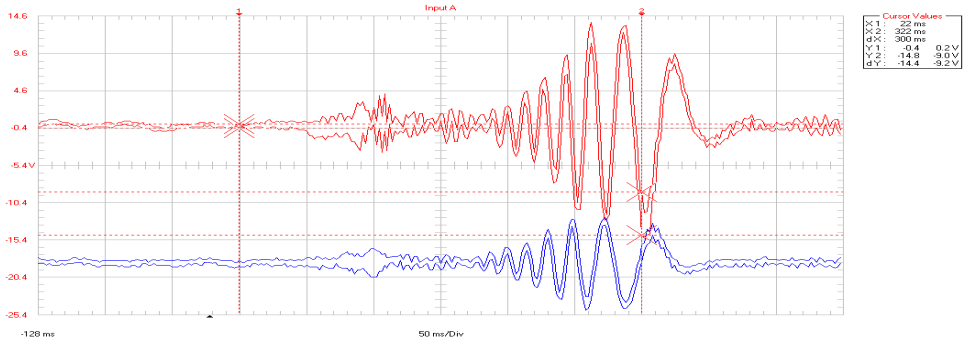

Figure 86: Excitation at $1.2\ m$ span

Table 51: Calculated results from data of Figure 86

x	dx	v	r	delta	zeta	time	f
284	0	13.8					
310	26	13.4	1.029851	0.02941389	0.004681	0.026	
346	36	9.6	1.395833	0.33349161	0.053002	0.031	32

Mode	Lambda	Tau	Freq	Wave speed	Theoretical	Difference	Difference %
2	84.6	3.18E-01	3.14E+00	2.6604E+02	136.8898	-1.2915E+02	-4.8545E+01
3	56.4	3.18E-01	3.14E+00	1.7736E+02		-4.0469E+01	-2.2817E+01
4	42.3	3.18E-01	3.14E+00	1.3302E+02		3.8709E+00	2.9100E+00
5	33.84	3.18E-01	3.14E+00	1.0642E+02		3.0475E+01	2.8638E+01

Tension: 25.11 kN

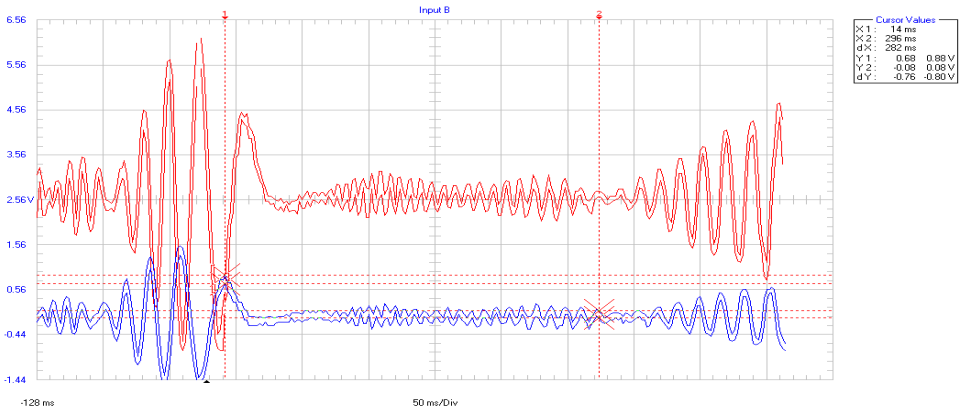

Figure 87: Excitation at $1.2\ m$ span

Table 52: Calculated results from data of Figure 87

x	dx	v	r	delta	zeta	time	f
-4	0	17.6					
26	30	9.4	1.87234	0.62718921	0.099327	0.03	33

Mode	Lambda	Tau	Freq	Wave speed	Theoretical	Difference	Difference %
2	84.6	3.74E-01	2.67E+00	2.2620E+02	136.8898	-8.9313E+01	-3.9484E+01
3	56.4	3.74E-01	2.67E+00	1.5080E+02		-1.3912E+01	-9.2256E+00
4	42.3	3.74E-01	2.67E+00	1.1310E+02		2.3788E+01	2.1033E+01
5	33.84	3.74E-01	2.67E+00	9.0481E+01		4.6408E+01	5.1291E+01

Tension: 25.11 kN

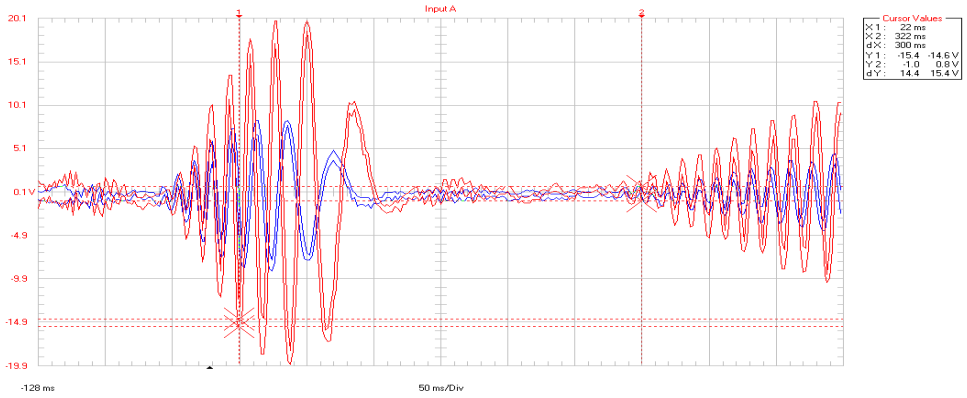

Figure 88: Excitation at $1.2\ m$ span

Table 53: Calculated results from data of Figure 88

x	dx	v	r	delta	zeta	time	f
48	0	19.8					
72	24	19.8	1	0	0	0.024	
108	36	10.6	1.868	0.6248	0.098956	0.03	33

Mode	Lambda	Tau	Freq	Wave speed	Theoretical	Difference	Difference %
2	84.6	3.50E-01	2.86E+00	2.4171E+02	136.8898	-1.0482E+02	-4.3367E+01
3	56.4	3.50E-01	2.86E+00	1.6114E+02		-2.4253E+01	-1.5051E+01
4	42.3	3.50E-01	2.86E+00	1.2086E+02		1.6033E+01	1.3266E+01
5	33.84	3.50E-01	2.86E+00	9.6686E+01		4.0204E+01	4.1582E+01

Tension: 25.11 kN

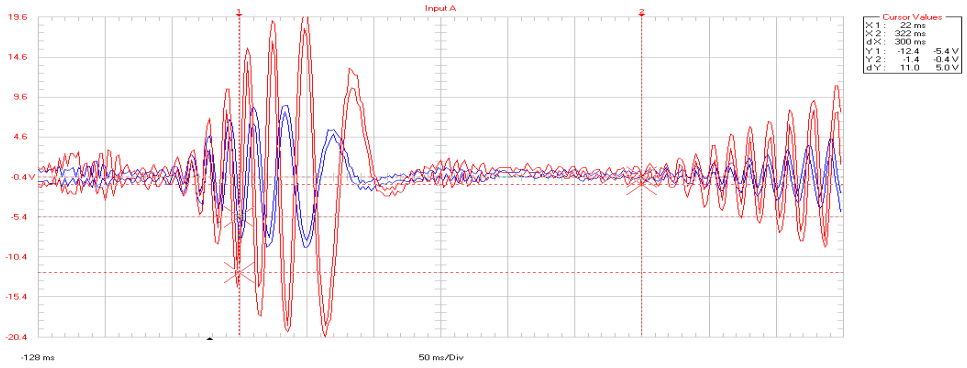

Figure 89: Excitation at $1.2\ m$ **span**

Table 54: Calculated results from data of Figure 89

x	dx	v	r	Delta	zeta	time	f
70		20.4					
104	34	13.2	1.545455	0.43531807	0.069117	0.034	29

Mode	Lambda	Tau	Freq	Wave speed	Theoretical	Difference	Difference %
2	84.6	3.52E-01	2.84E+00	2.4034E+02	136.8898	-1.0345E+02	-4.3044E+01
3	56.4	3.52E-01	2.84E+00	1.6023E+02		-2.3338E+01	-1.4565E+01
4	42.3	3.52E-01	2.84E+00	1.2017E+02		1.6719E+01	1.3913E+01
5	33.84	3.52E-01	2.84E+00	9.6136E+01		4.0753E+01	4.2391E+01

Tension: 29.56 kN

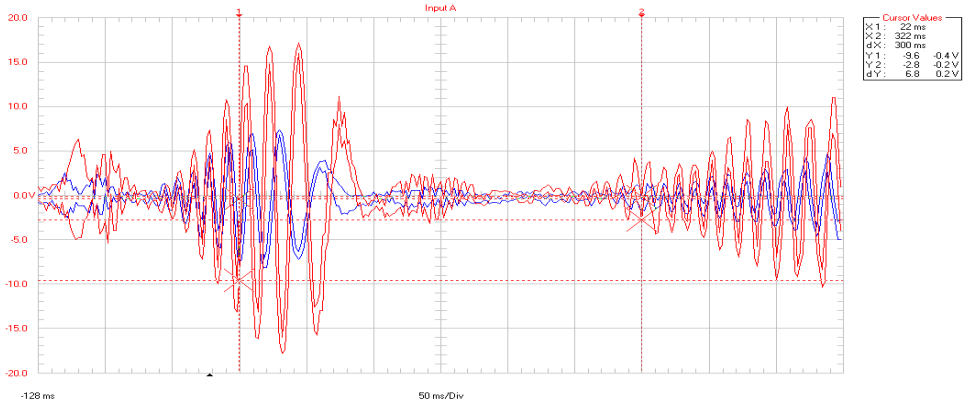

Figure 90: Excitation at $1.2\ m$ **span**

Table 55: Calculated results from data of Figure 90

x	dx	v	r	delta	zeta	time	f
66		17.2					
96	30	11.2	1.535714	0.42899561	0.068118	0.03	33

Mode	Lambda	Tau	Freq	Wave speed	Theoretical	Difference	Difference %
2	84.6	3.18E-01	3.14E+00	2.6604E+02	148.5251	-1.1751E+02	-4.4171E+01
3	56.4	3.18E-01	3.14E+00	1.7736E+02		-2.8833E+01	-1.6257E+01
4	42.3	3.18E-01	3.14E+00	1.3302E+02		1.5506E+01	1.1657E+01
5	33.84	3.18E-01	3.14E+00	1.0642E+02		4.2110E+01	3.9571E+01

Tension: 29.56 kN

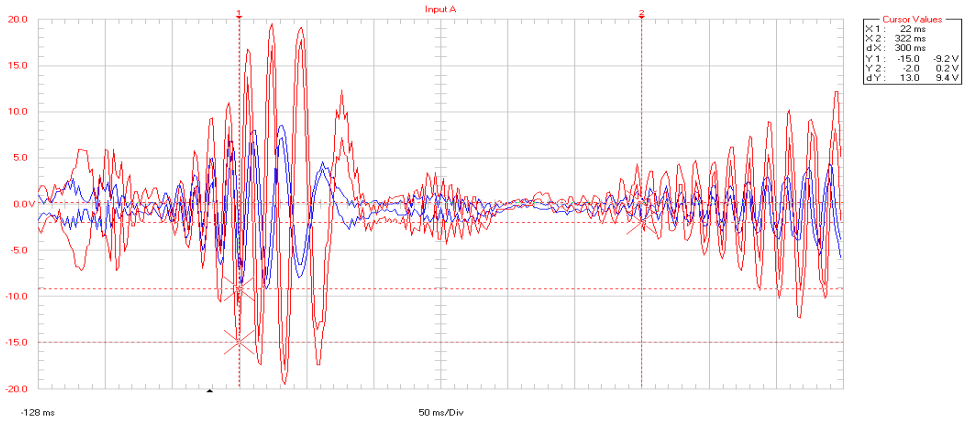

Figure 91: Excitation at $1.2\ m$ span

Table 56: Calculated results from data of Figure 91

x	dx	v	r	delta	zeta	time	f
46		19.6					
68	22	19.2	1.020833	0.02061929	0.003282	0.022	
98	30	12.4	1.548387	0.43721381	0.069417	0.026	38

Mode	Lambda	Tau	Freq	Wave speed	Theoretical	Difference	Difference %
2	84.6	3.00E-01	3.33E+00	2.8200E+02	148.5251	-1.3347E+02	-4.7332E+01
3	56.4	3.00E-01	3.33E+00	1.8800E+02		-3.9475E+01	-2.0997E+01
4	42.3	3.00E-01	3.33E+00	1.4100E+02		7.5251E+00	5.3369E+00
5	33.84	3.00E-01	3.33E+00	1.1280E+02		3.5725E+01	3.1671E+01

Tension: 29.56 kN

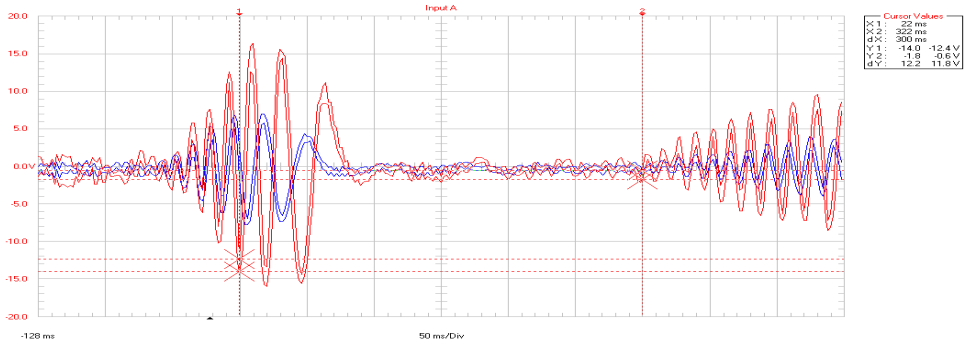

Figure 92: Excitation at $1.2\ m$ **span**

Table 57: Calculated results from data of Figure 92

x	dx	v	r	delta	zeta	time	f
32		16.4					
52	20	15.6	1.051282	0.05001042	0.007959	0.02	
86	34	11.2	1.392857	0.33135714	0.052664	0.027	37

Mode	Lambda	Tau	Freq	Wave speed	Theoretical	Difference	Difference %
2	84.6	3.12E-01	3.21E+00	2.7115E+02	148.5251	-1.2263E+02	-4.5225E+01
3	56.4	3.12E-01	3.21E+00	1.8077E+02		-3.2244E+01	-1.7837E+01
4	42.3	3.12E-01	3.21E+00	1.3558E+02		1.2948E+01	9.5504E+00
5	33.84	3.12E-01	3.21E+00	1.0846E+02		4.0064E+01	3.6938E+01

Tension: 29.56 kN

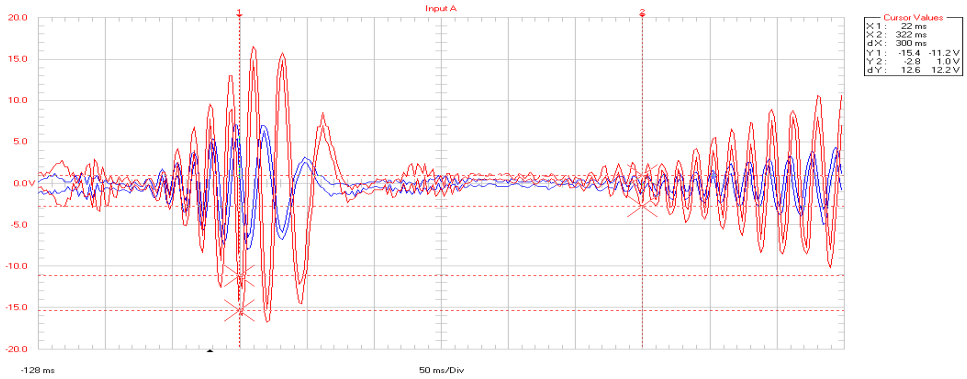

Figure 93: Excitation at $1.2\ m$ **span**

Table 58: Calculated results from data of Figure 93

x	dx	v	r	delta	zeta	time	f
32		16.6					
52	20	15.8	1.050633	0.04939276	0.007861	0.02	
84	32	8.6	1.837209	0.60824774	0.096355	0.026	38

Mode	Lambda	Tau	Freq	Wave speed	Theoretical	Difference	Difference %
2	84.6	3.18E-01	3.14E+00	2.6604E+02	148.5251	-1.1751E+02	-4.4171E+01
3	56.4	3.18E-01	3.14E+00	1.7736E+02		-2.8833E+01	-1.6257E+01
4	42.3	3.18E-01	3.14E+00	1.3302E+02		1.5506E+01	1.1657E+01
5	33.84	3.18E-01	3.14E+00	1.0642E+02		4.2110E+01	3.9571E+01

Tension: 29.56 kN

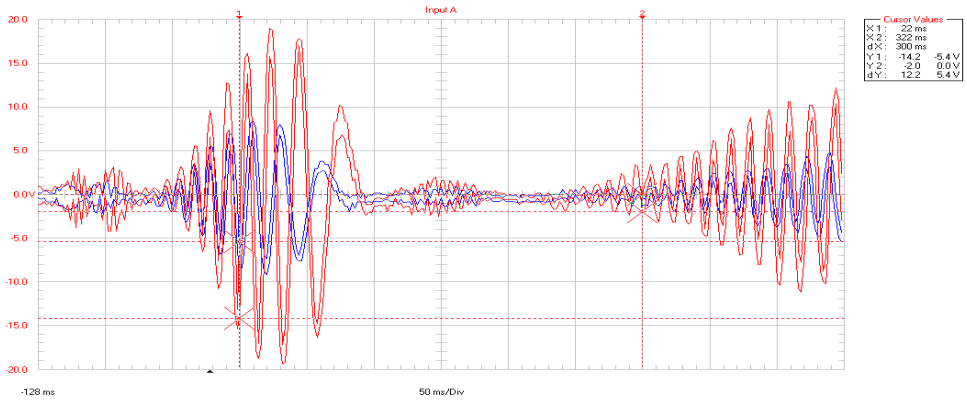

Figure 94: Excitation at $1.2\ m$ span

Table 59: Calculated results from data of Figure 94

x	dx	v	r	delta	Zeta	time	f
44		19					
66	22	17.8	1.067416	0.06524052	0.010383	0.022	
96	30	10.2	1.745098	0.55681074	0.088273	0.026	38

Mode	Lambda	Tau	Freq	Wave speed	Theoretical	Difference	Difference %
2	84.6	3.00E-01	3.33E+00	2.8200E+02	148.5251	-1.3347E+02	-4.7332E+01
3	56.4	3.00E-01	3.33E+00	1.8800E+02		-3.9475E+01	-2.0997E+01
4	42.3	3.00E-01	3.33E+00	1.4100E+02		7.5251E+00	5.3369E+00
5	33.84	3.00E-01	3.33E+00	1.1280E+02		3.5725E+01	3.1671E+01

APPENDIX II

RESULTS FOR FORCED VIBRATION METHOD ON TERN CONDUCTOR

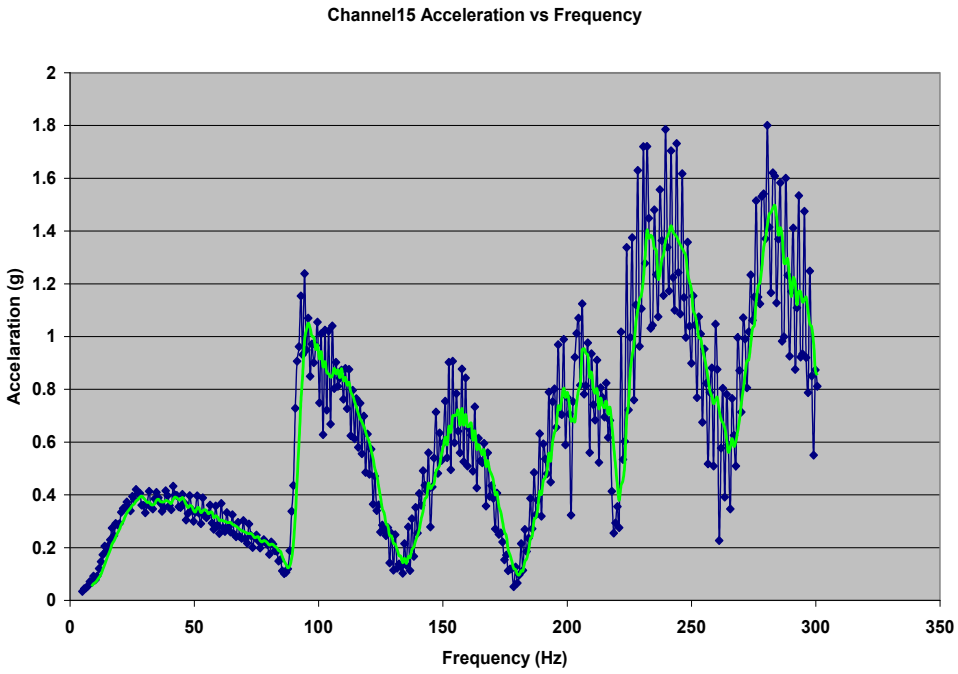

Figure 95: Graph showing acceleration (G) versus frequency (Hz)

Table 60: Data for Figure 95

25.11 kN channel 15	
F (Hz)	G (m/s^2)
41.489	0.433
94.361	1.238
153.936	0.907
206.064	1.124
239.574	1.785
280.532	1.800

Table 61: Data collected from Figure 95

25.11 kN channel 15

Resonance frequency	Acceleration	Half-power	Half-power	Band-width	Quality factor	Exciting force	Damping factor	Viscous damping
f_n	a	f_1	f_2	Δf	Q	F_o	ζ	c
41.490	0.433	18.4	67.6	49.15	0.8	570.4	0.592	35008.2
94.361	1.238	91.4	104.0	12.66	7.5	184.7	0.067	9016.8
153.936	0.907	148.7	160.6	11.92	12.9	78.0	0.039	8486.9
206.064	1.124	203.1	213.5	10.43	19.8	63.2	0.025	7426.3
239.574	1.785	235.9	247.0	11.17	21.4	92.6	0.023	7956.2
280.532	1.800	278.3	295.4	17.13	16.4	122.2	0.031	12197.9

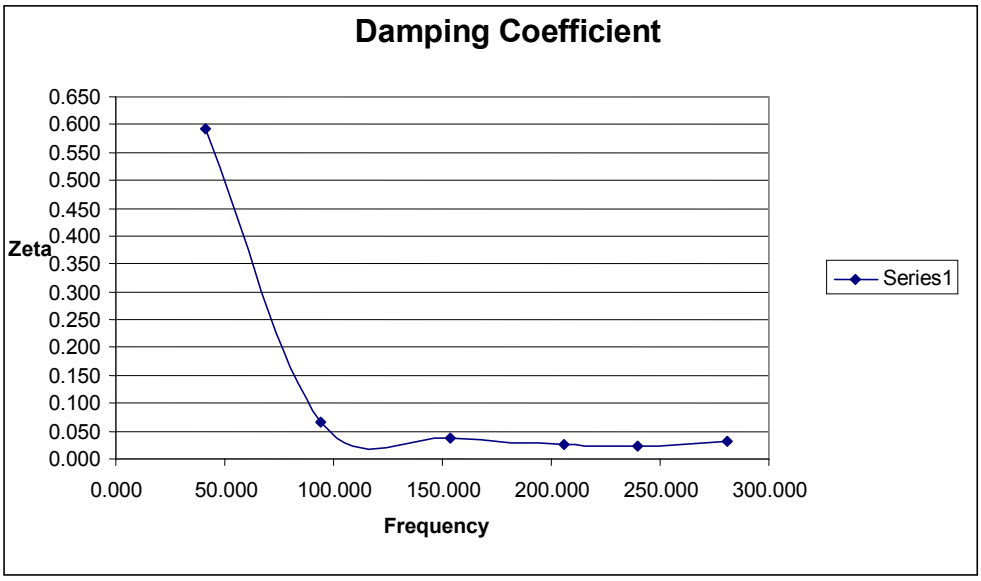

Figure 96: Graph showing damping factor (ς) versus frequency f_n (Hz)

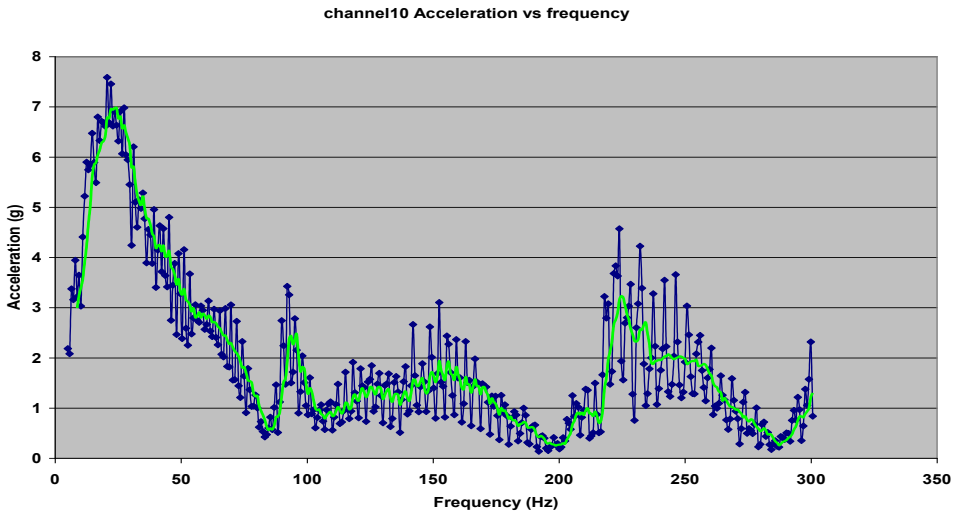

Figure 97: Graph showing acceleration (G) versus frequency (Hz)

Table 62: Data for Figure 97

25.11 kN channel 10			
F (Hz)	G (m/s^2)	V (m/s)	d (mm)
20.638	7.587	0.574	8.850
92.128	3.425	0.0547	0.2005
152.447	3.103	0.0318	0.0663
223.936	4.573	0.0319	0.0453
232.128	4.225	0.0284	0.0390

Table 63: Data for Figure 97

25.11 kN channel 10

Resonance frequency	Acceleration	Half-power	Half-power	Band-width	Quality factor	Exciting force	Damping factor	Viscous damping
f_n	a	f_1	f_2	Δf	Q	F_o	ζ	c
20.638	7.587	12.4	31.1	18.62	1.1	7611.3	0.451	13260.6
92.128	3.425	90.0	95.9	5.87	15.7	242.6	0.032	4179.0
152.447	3.103	148.7	157.2	8.45	18.0	191.2	0.028	6016.7
223.936	4.573	218.0	229.1	11.17	20.0	253.7	0.025	7956.2

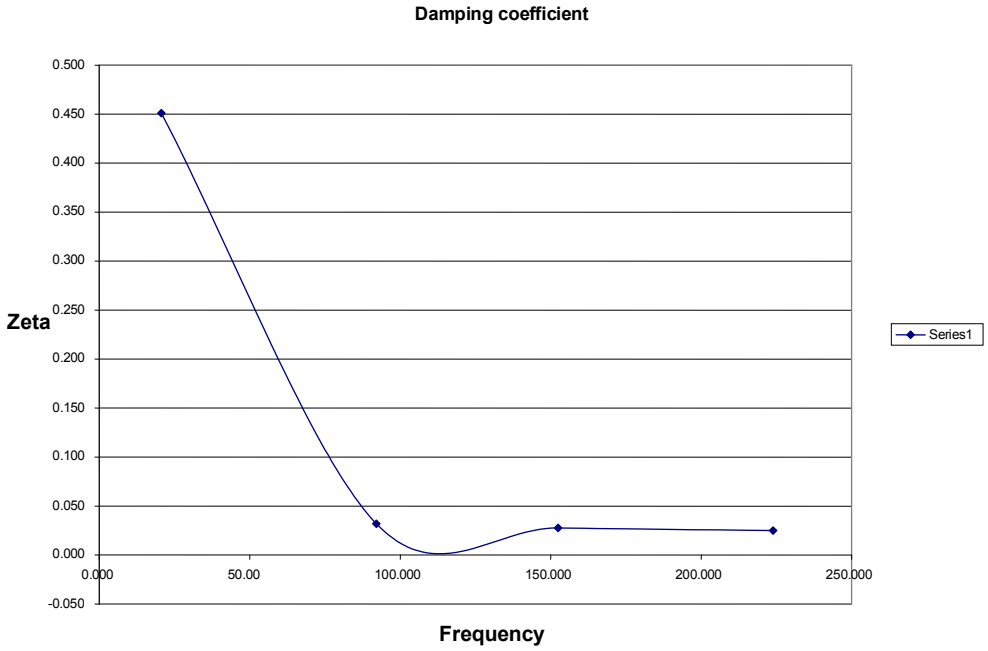

Figure 98: Graph showing damping factor (ς) versus frequency f_n (Hz)

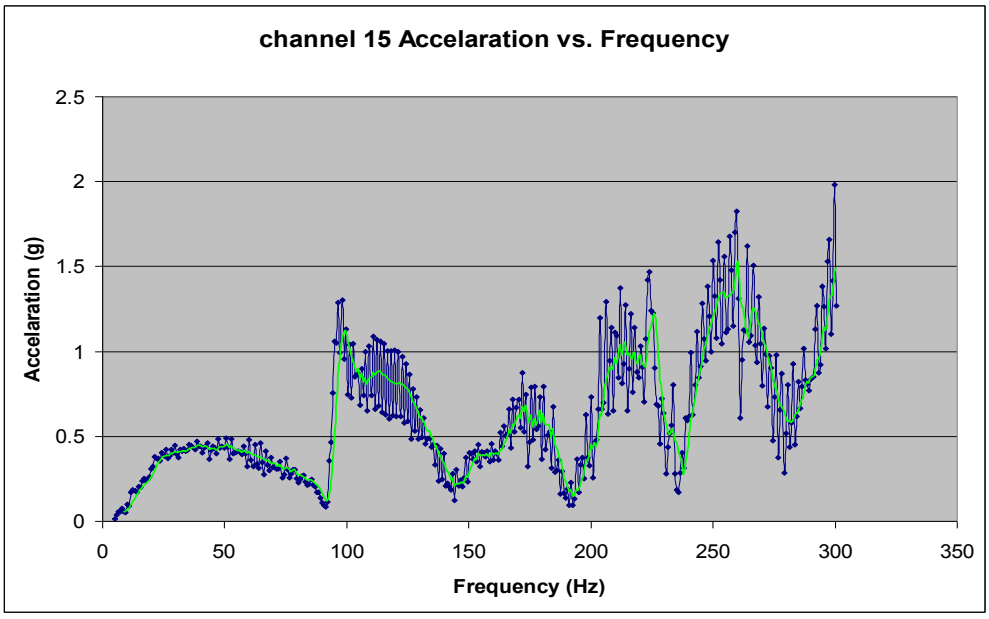

Figure 99: Graph showing acceleration (G) versus frequency (Hz)

Table 64: Data for Figure 99

29.56 kN channel 15			
f_n (Hz)	a (G)	V (m/s)	d (mm)
50.426	0.488	0.0151	0.0954
98.085	1.301	0.0207	0.0671
171.808	0.876	0.00795	0.0147
212.021	1.372	0.0101	0.0152
223.936	1.465	0.01023	0.0145
259.681	1.827	0.0110	0.0135

Table 65: Data for Figure 99

29.56 kN channel 15

Resonance frequency	Acceleration	Half-power	Half-power	Band-width	Quality factor	Exciting force	Damping factor	Damping coefficient
$f_{n\,(Hz)}$	a (G)	f_1	f_2	Δf	Q	$F_{o\,(N)}$	ζ	C (Ns/m)
50.426	0.489	21.4	75.0	53.62	0.9	577.6	0.532	38190.7
98.085	1.301	95.1	124.1	29.04	3.4	428.2	0.148	20687.0
171.809	0.876	166.6	184.5	17.89	9.6	101.4	0.052	12742.8
223.936	1.468	203.8	226.2	22.34	10.0	162.9	0.050	15912.5
259.681	1.827	245.5	268.6	23.09	11.2	180.6	0.044	16443.1

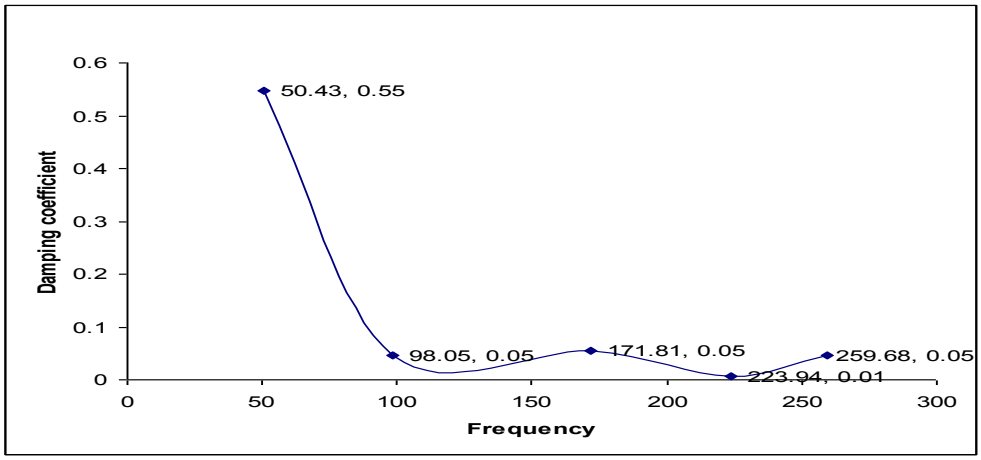

Figure 100: Graph showing damping factor (ς) versus frequency f_n (Hz)

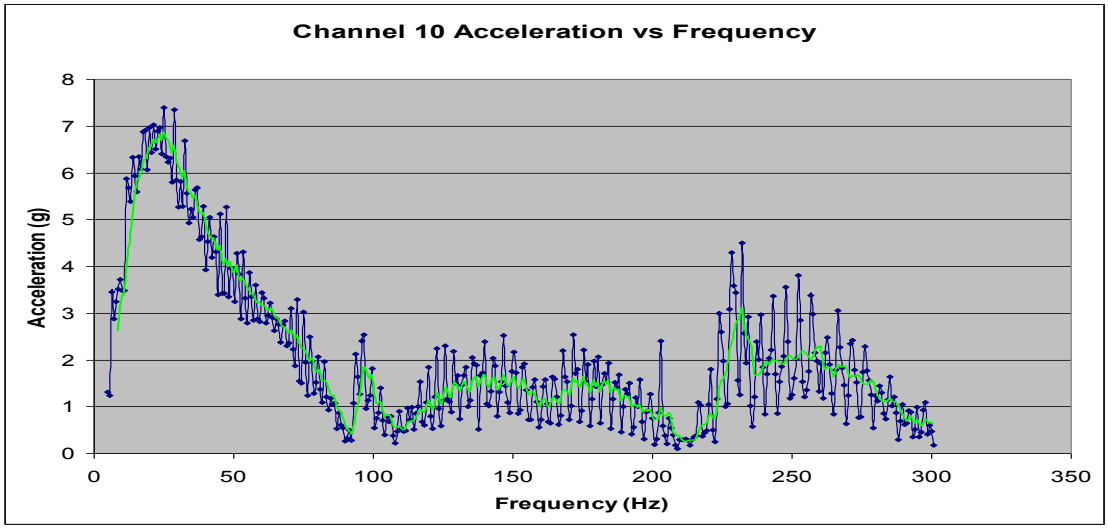

Figure 101: Graph showing acceleration (G) versus frequency f_n (Hz)

Table 66: Data for Figure 101

29.56 kN channel 10			
F (Hz)	G (m/s^2)	V (m/s)	d (mm)
25.106	7.393	0.460	5.827
96.596	2.545	0.0411	0.136
146.489	2.529	0.0269	0.0584
171.809	2.535	0.0230	0.0427
232.128	4.506	0.0303	0.0415
252.234	3.803	0.0235	0.0297

Table 67: Data for Figure 101

29.56 kN channel 10

Resonance frequency	Acceleration	Half-power	Half-power	Band-width	Quality factor	Exciting force	Damping factor	Viscous damping
f_n	a	f_1	f_2	Δf	Q	F_o	ζ	c
25.106	7.393	11.7	47.4	35.75	0.7	11705.8	0.712	25460.7
96.596	2.545	93.6	99.6	5.96	16.2	174.5	0.031	4243.1
146.489	2.529	119.7	153.2	33.51	4.4	643.4	0.114	23869.5
171.809	2.535	168.1	184.5	16.38	10.5	268.8	0.048	11669.4
232.128	4.506	228.4	232.9	4.47	52.0	96.5	0.010	3182.5

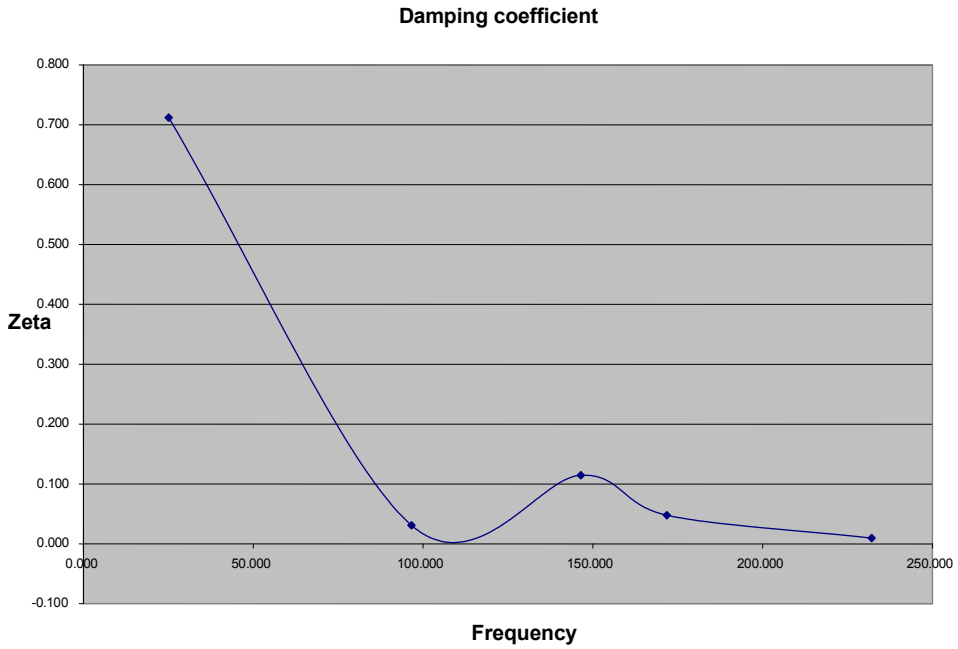

Figure 102: Graph showing damping factor (ς) versus frequency f_n (Hz)

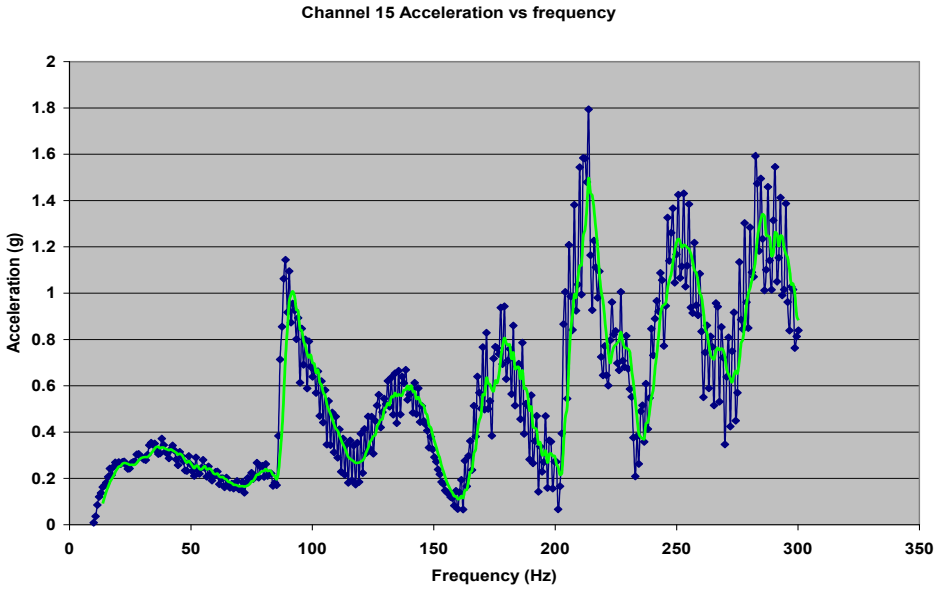

Figure 103: Graph showing acceleration (G) versus frequency f_n (Hz)

Table 68: Data for Figure 103

20.73 kN channel 15			
F (Hz)	G (m/s^2)	V (m/s)	d (mm)
38.060	0.371	0.0152	0.127
89.011	1.144	0.0201	0.0717
138.486	0.669	0.00754	0.0173
179.099	0.943	0.00822	0.0146
213.805	1.793	0.0131	0.0195
227.096	1.005	0.00691	0.00968
252.941	1.430	0.0088	0.0111
282.478	1.592	0.0088	0.00991

Table 69: Data for Figure 103

20.59 kN channel 15

Resonance frequency	Acceleration	Half-power	Half-power	Band-width	Quality factor	Exciting force	Damping factor	Viscous damping
f_n	a	f_1	f_2	Δf	Q	F_o	ζ	c
38.060	0.371	19.6	57.3	37.66	1.0	408.3	0.495	26824.7
89.011	1.144	87.5	97.1	9.60	9.3	137.2	0.054	6838.0
138.486	0.669	166.5	192.4	25.84	5.4	138.8	0.093	18408.3
213.805	1.793	207.9	214.5	6.65	32.2	62.0	0.016	4733.9
252.941	1.430	243.3	260.3	16.98	14.9	106.8	0.034	12097.5
282.478	1.592	275.8	295.0	19.20	14.7	120.3	0.034	13675.2

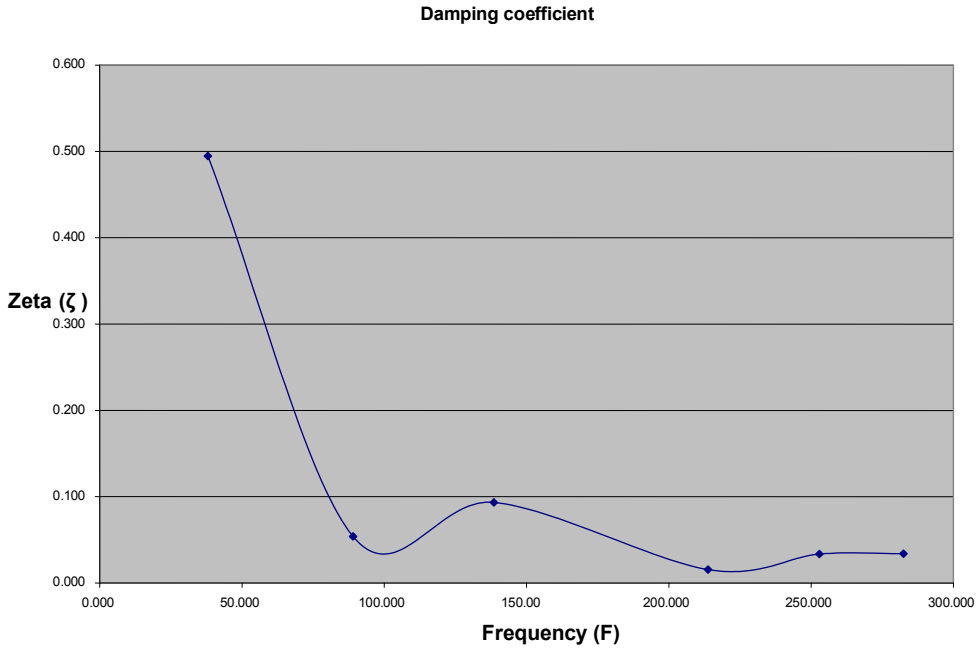

Figure 104: Graph showing damping factor (ς) versus frequency f_n (Hz)

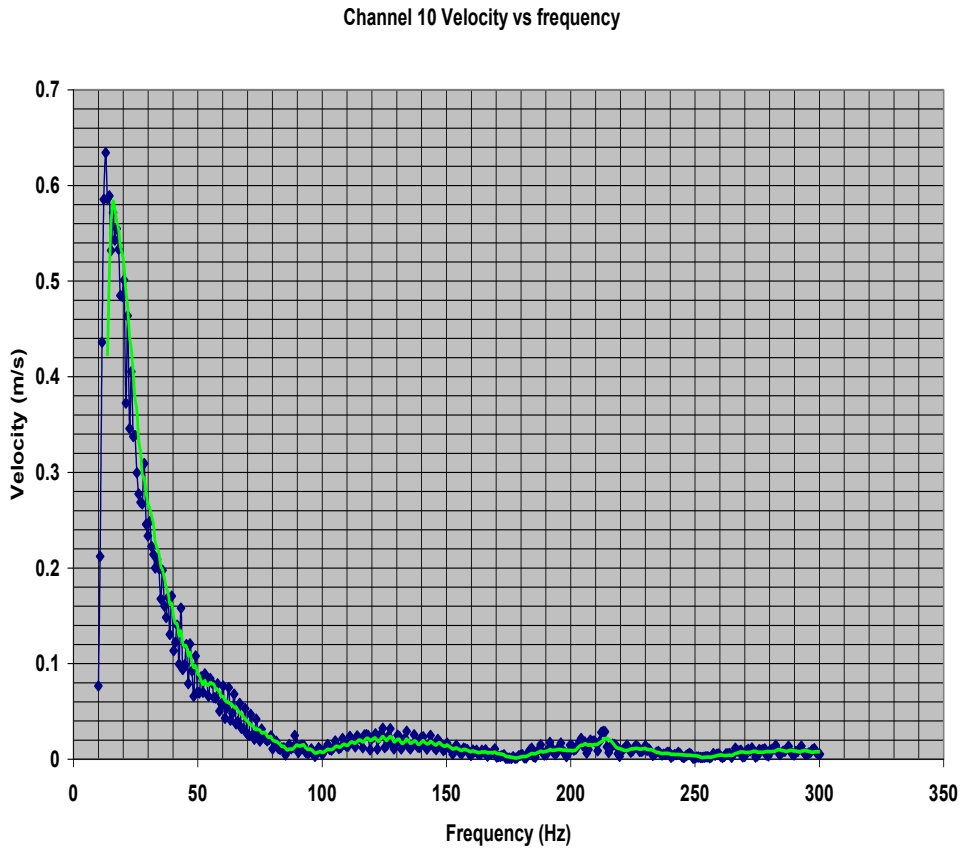

Figure 105: Graph showing acceleration (G) versus frequency f_n (Hz)

Table 70: Data for Figure 105

20.73 kN channel 10			
F (Hz)	G (m/s^2)	V (m/s)	d (mm)
12.954	7.6816	0.634	15.583
75.720	0.218	0.0313	0.132
89.011	0.158	0.0248	0.0888
124.45	0.0804	0.0324	0.0829
213.8047	0.0273	0.0288	0.0427
282.478	0.0156	0.0145	0.0164

APPENDIX III

RESULTS FOR FREE VIBRATION METHOD ON AERO-Z IEC62219-REV240609 CONDUCTOR

Tension 24.01 kN without mass absorber dampers

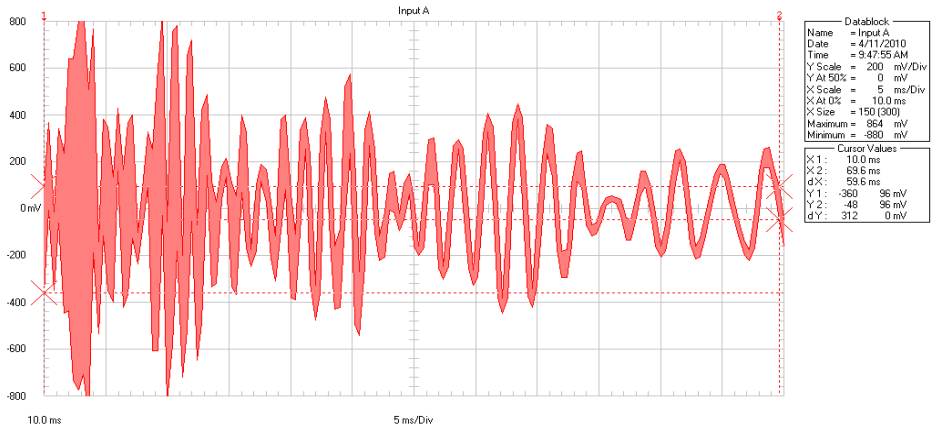

Figure 106: Excitation at $1.2\ m$ measured from load end, cable tension = 24.01 kN

Table 71: Calculated results from data of Figure 106

Aero-Z II	PX	PY	FREQ	ln PY	Yj	(lnPY)Yj	Yj^2	b	a	Zj	LogDec	Zeta	Period	NatFrec	NatFreq
j	(ms)	(mV)	(Hz)											(rad/s)	(Hz)
1	34.8	576		6.4	0	0.0	0	6.36	-0.5	6.36	0.50	0.079	0.0016	3927	625
2	36.4	416	625	6.0	1	6.0	1			5.87					
3	38.4	160	500	5.1	2	10.2	4			5.37					
4	39.6	152	833	5.0	3	15.1	9			4.88					
SUM		1304		22.5	6	31.3	14								

Using least squares method, log-dec = 0.495, zeta = 0.079, frequency of decaying oscillation = 3927 rad/s (625 Hz)

Aero-Z II	PX	PY	FREQ	ln PY	Yj	(lnPY)Yj	Yj^2			Zj	LogDec	Zeta		NatFrec	NatFreq
j	(ms)	(mV)	(Hz)											(rad/s)	(Hz)
1	48.4	448		6.1	0	0.0	0	6.37	-0.66	6.37	0.66	0.105	0.0025	2480	394.7
2	50.8	360	417	5.9	1	5.9	1			5.71					
3	53.6	248	357	5.5	2	11.0	4			5.05					
4	56	56	417	4.0	3	12.1	9			4.39					
SUM		1112		21.5	6	29.0	14								

Using least squares method, log-dec = 0.661, zeta = 0.105, frequency of decaying oscillation = 2480.2rad/s (394.7Hz)

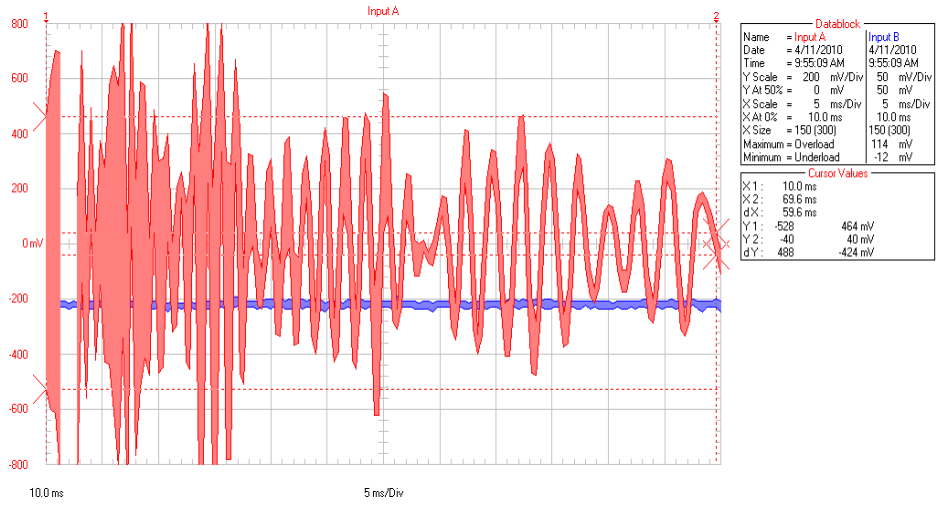

Figure 107: Excitation at $1.2\ m$ measured from load end, cable tension = 24.01 kN

Table 72: Calculated results from data of Figure 107

Aero-Z II j	PX (ms)	PY (mV)	FREQ (Hz)	ln PY	Yj	(lnPY)Y.	Yj^2	b	a	Zj	LogDec	Zeta	Period	NatFreq (rad/s)	NatFreq (Hz)
1	16.8	880		6.78	0	0.00	0	6.89	-0.244	6.89	0.244	0.039	0.001	6041.5	961.5
2	17.6	872	1250	6.77	1	6.77	1			6.65					
3	18.4	592	1250	6.38	2	12.77	4			6.40					
4	19.6	488	833.3	6.19	3	18.57	9			6.16					
5	20.8	400	833.3	5.99	4	23.97	16			5.92					
6	22	264	833.3	5.58	5	27.88	25			5.67					
SUM		3496		37.69	15	89.95	55								

Using least squares method, log-dec = 0.244, zeta = 0.039, frequency of decaying oscillation = 6041rad/s (962Hz)

Aero-Z II j	PX (ms)	PY (mV)	FREQ (Hz)	ln PY	Yj	(lnPY)Y.	Yj^2			Zj	LogDec	Zeta		NatFreq (rad/s)	NatFreq (Hz)
1	24.4	840		6.73	0	0.00	0	6.87	-0.288	6.87	0.288	0.046	0.0014	4488.0	714.3
2	25.6	808	833.3	6.69	1	6.69	1			6.58					
3	26.8	672	833.3	6.51	2	13.02	4			6.29					
4	28	328	833.3	5.79	3	17.38	9			6.01					
5	30	312	500.0	5.74	4	22.97	16			5.72					
SUM		2960		31.47	10	60.07	30								

Using least squares method, log-dec = 0.288, zeta = 0.046, frequency of decaying oscillation = 4488 rad/s (714Hz)

Tension 24.01 kN with one mass absorber damper

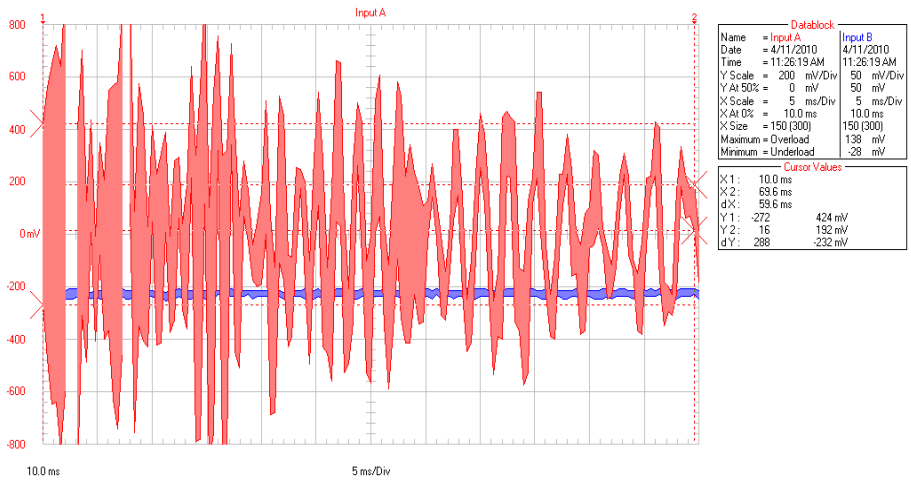

Figure 108: Excitation at $1.2\ m$ measured from load end, cable tension = 24.01 kN

Table 73: Calculated results from data of Figure 108

Aero-Z IE j	PX (ms)	PY (mV)	FREQ (Hz)	ln PY	Yj	(lnPY)Yj	Yj^2	b	a	Zj	LogDec	Zeta	Period	NatFreq (rad/s)	NatFreq (Hz)
1	36	664		6.50	0	0.0	0	6.6	-0.161	6.56	0.16	0.026	0.002	3272	520.8
2	38.8	504	357	6.22	1	6.2	1			6.40					
3	40.8	608	500	6.41	2	12.8	4			6.24					
4	42.4	584	625.0	6.37	3	19.1	9			6.08					
5	43.6	344	833.3	5.84	4	23.4	16			5.92					
6	45.6	272	500.0	5.61	5	28.0	25			5.75					
SUM		2976		36.9	15	89.5	55								

Using least squares method, log-dec = 0.166, zeta = 0.026, frequency of decaying oscillation = 3272.5 rad/s (520.8 Hz)

Aero-Z IE j	PX (ms)	PY (mV)	FREQ (Hz)	ln PY	Yj	(lnPY)Yj	Yj^2			Zj	LogDec	Zeta		NatFreq (rad/s)	NatFreq (Hz)
1	55.2	544		6.30	0	0.0	0	6.2	-0.185	6.22	0.19	0.029	0.003	2356	375.0
2	58	384	357.1	5.95	1	6.0	1			6.03					
3	60.4	320	416.7	5.77	2	11.5	4			5.85					
4	63.2	312	357.1	5.74	3	17.2	9			5.66					
SUM		1560		23.8	6	34.7	14								

Using least squares method, log-dec = 0.661, zeta = 0.105, frequency of decaying oscillation = 2480.2rad/s (394.7Hz)

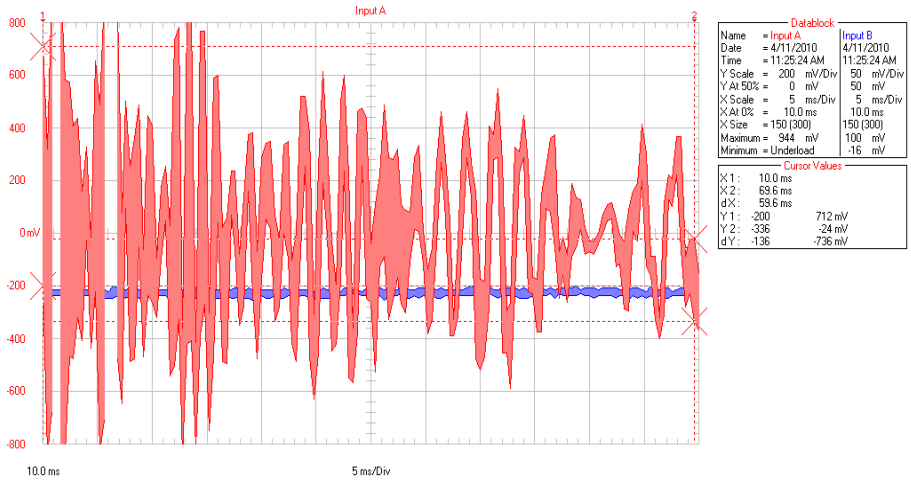

Figure 109: Excitation at $1.2\ m$ measured from load end, cable tension = 24.01 kN

Table 74: Calculated results from data of Figure 109

Aero-Z j	PX (ms)	PY (mV)	FREQ (Hz)	ln PY	Yj	(lnPY)Yj	Yj^2	b	a	Zj	LogDec	Zeta		NatFreq (rad/s)	NatFreq (Hz)
1	35.6	616		6.4	0	0.0	0	6.48	-0.142	6.48	0.142	0.023	0.0022	2856.0	454.5
2	37.6	600	500	6.4	1	6.4	1			6.34					
3	39.2	480	625	6.2	2	12.3	4			6.20					
4	41.2	488	500	6.2	3	18.6	9			6.06					
5	44.4	336	313	5.8	4	23.3	16			5.92					
SUM		2520		31	10	60.6	30								

Using least squares method, log-dec = 0.142, zeta = 0.023, frequency of decaying oscillation = 2856 rad/s (454.6 Hz)

Aero-Z j	PX (ms)	PY (mV)	FREQ (Hz)	ln PY	Yj	(lnPY)Yj	Yj^2			Zj	LogDec	Zeta		NatFreq (rad/s)	NatFreq (Hz)
1	51.6	552		6.3	0	0.0	0	6.46	-0.390	6.46	0.390	0.062	0.0026	2416.6	384.6
2	54	448	417	6.1	1	6.1	1			6.07					
3	56.8	376	357	5.9	2	11.9	4			5.68					
4	58.4	192	625	5.3	3	15.8	9			5.29					
5	62	120	278	4.8	4	19.1	16			4.90					
SUM		1688		28.4	10	52.9	30								

Using least squares method, log-dec = 0.390, zeta = 0.062, frequency of decaying oscillation = 2416.6 rad/s (384.6 Hz)

Tension 24.01 kN with two mass absorber dampers

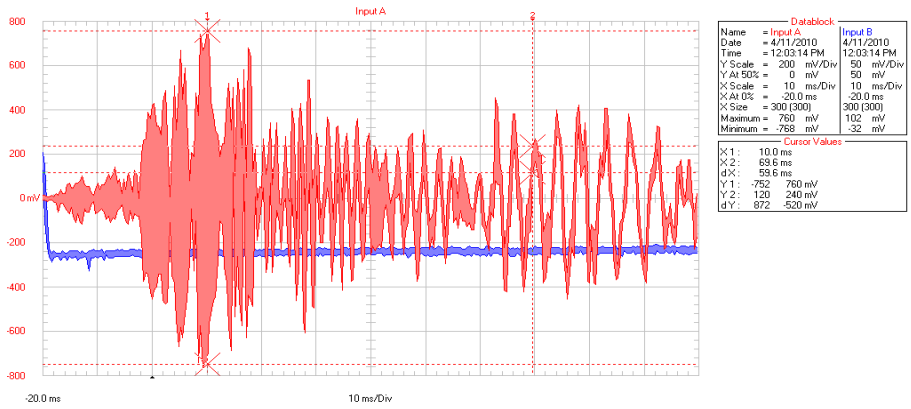

Figure 110: Excitation at $1.2\ m$ measured from load end, cable tension = 24.01 kN

Table 75: Calculated results from data of Figure 110

Aero-Z 1 j	PX (ms)	PY (mV)	FREQ (Hz)	ln PY	Yj	(lnPY)Y	Yj^2	b	a	Zj	LogDec	Zeta	Period	NatFreq (rad/s)	NatFreq (Hz)
1	28.4	536		6.28	0	0.0	0	6.06	-0.074	6.06	0.074	0.012	0.002	3491	555.6
2	30	296	625	5.69	1	5.7	1			5.98					
3	32	368	500	5.91	2	11.8	4			5.91					
4	34	328	500.0	5.79	3	17.4	9			5.83					
5	35.6	296	625.0	5.69	4	22.8	16			5.76					
6	37.6	360	500.0	5.89	5	29.4	25			5.69					
7	39.6	296		5.69	6	34.1	36								
8	40.8	240		5.48	7	38.4	49								
9	42.8	224		5.41	8	43.3	64								
SUM		2944		51.835	36	202.9	204								

Using least squares method, log-dec = 0.074, zeta = 0.012, frequency of decaying oscillation = 3491 rad/s (555.6 Hz)

Aero-Z 1 j	PX (ms)	PY (mV)	FREQ (Hz)	ln PY	Yj	(lnPY)Y	Yj^2			Zj	LogDec	Zeta		NatFreq (rad/s)	NatFreq (Hz)
1	49	312		5.74	0	0.0	0	5.72	-0.210	5.72	0.210	0.033	0.003	2285	363.6
2	52.8	232	263.2	5.45	1	5.4	1			5.51					
3	54.8	192	500.0	5.26	2	10.5	4			5.30					
4	56.4	192	625.0	5.26	3	15.8	9			5.09					
5	60	120	277.8	4.79	4	19.1	16			4.88					
SUM		1048		26.492	10	50.9	30								

Using least squares method, log-dec = 0.210, zeta = 0.033, frequency of decaying oscillation = 2285 rad/s (363.6 Hz)

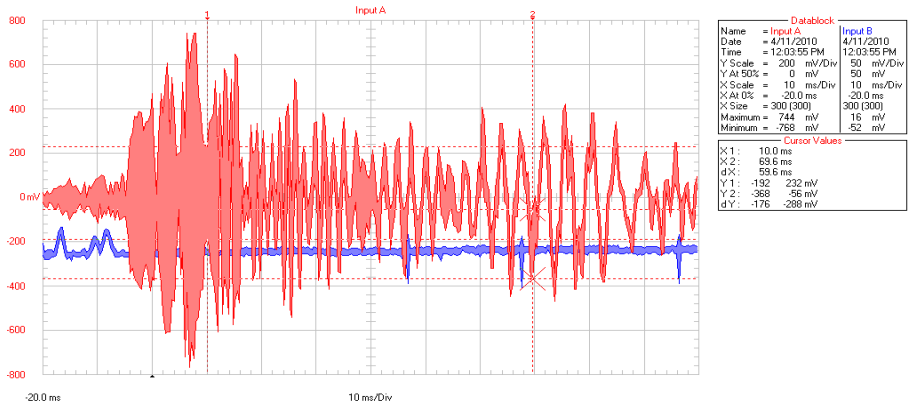

Figure 111: Excitation at $1.2\ m$ measured from load end, cable tension = 24.01 kN

Table 76: Calculated results from data of Figure 111

Aero-Z : j	PX (ms)	PY (mV)	FREQ (Hz)	ln PY	Yj	(lnPY)Yj	Yj^2	b	a	Zj	LogDec	Zeta	Period	NatFreq (rad/s)	NatFreq (Hz)
1	26.4	520		6.25	0	0.0	0	6.002	-0.08	6.00	0.077	0.012	0.0017	3665	583.3
2	27.6	232	833	5.45	1	5.4	1			5.93					
3	30	344	417	5.84	2	11.7	4			5.85					
4	31.2	384	833	5.95	3	17.9	9			5.77					
5	33.2	272	500	5.61	4	22.4	16			5.70					
6	35.2	360	500	5.89	5	29.4	25			5.62					
7	37.2	304		5.72	6	34.3	36								
8	38.4	176		5.17	7	36.2	49								
SUM		2592		45.87	28	157.3	140								

Using least squares method, log-dec = 0.077, zeta = 0.12, frequency of decaying oscillation = 3665 rad/s (583.3 Hz)

Aero-Z : j	PX (ms)	PY (mV)	FREQ (Hz)	ln PY	Yj	(lnPY)Yj	Yj^2			Zj	LogDec	Zeta		NatFreq (rad/s)	NatFreq (Hz)
1	47.2	344		5.84	0	0.0	0	5.818	-0.26	5.82	0.261	0.042	0.0024	2618	416.7
2	50	232	357	5.45	1	5.4	1			5.56					
3	52.4	232	417	5.45	2	10.9	4			5.30					
4	54.4	144	500	4.97	3	14.9	9			5.03					
SUM		952		21.704	6	31.2	14								

Using least squares method, log-dec = 0.261, zeta = 0.042, frequency of decaying oscillation = 2618 rad/s (416.7Hz)

Tension 27.02 kN without mass absorber dampers

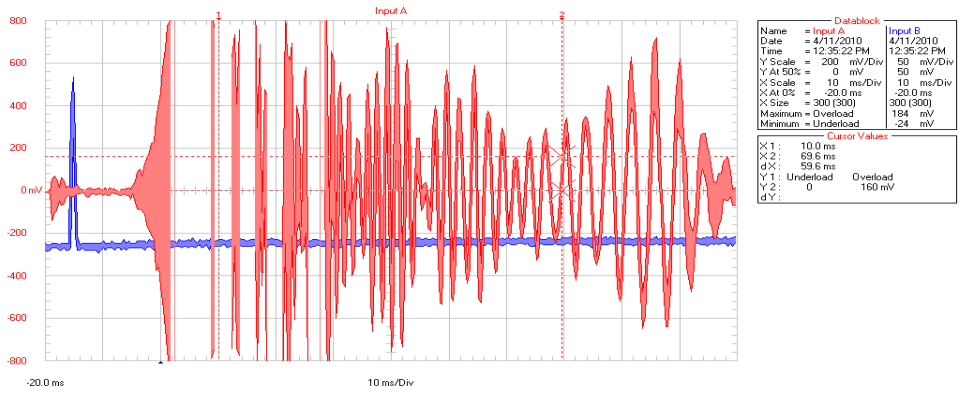

Figure 112: Excitation at $1.2\ m$ measured from load end, cable tension = 27.02 kN

Table 77: Calculated results from data of Figure 112

Aero-Z I. j	PX (ms)	PY (mV)	FREQ (Hz)	ln PY	Yj	(lnPY)Y	Yj^2	b	a	Zj	LogDec	Zeta		NatFreq (rad/s)	NatFreq (Hz)
1	39.2	768		6.64	0	0.00	0	7.15	-0.69	7.15	0.694	0.110	0.0017	3696.0	588.2
2	41.2	696	500	6.55	1	6.55	1			6.46					
3	42.8	616	625	6.42	2	12.85	4			5.76					
4	44.8	248	500	5.51	3	16.54	9			5.07					
5	46	40	833	3.69	4	14.76	16			4.37					
SUM		2368		28.81	10	50.69	30								

Using least squares method, log-dec = 0.694, zeta = 0.110, frequency of decaying oscillation = 3696 rad/s (588.2 Hz)

Aero-Z I. j	PX (ms)	PY (mV)	FREQ (Hz)	ln PY	Yj	(lnPY)Y	Yj^2			Zj	LogDec	Zeta		NatFreq (rad/s)	NatFreq (Hz)
1	54.4	592		6.38	0	0.00	0	6.39	-0.42	6.39	0.416	0.066	0.002	2618.0	416.7
2	56.8	376	417	5.93	1	5.93	1			5.98					
3	59.2	296	417	5.69	2	11.38	4			5.56					
4	61.6	160	417	5.08	3	15.23	9			5.15					
SUM		1424		23.08	6	32.54	14								

Using least squares method, log-dec = 0.416, zeta = 0.066, frequency of decaying oscillation = 2618.0rad/s (416.7Hz)

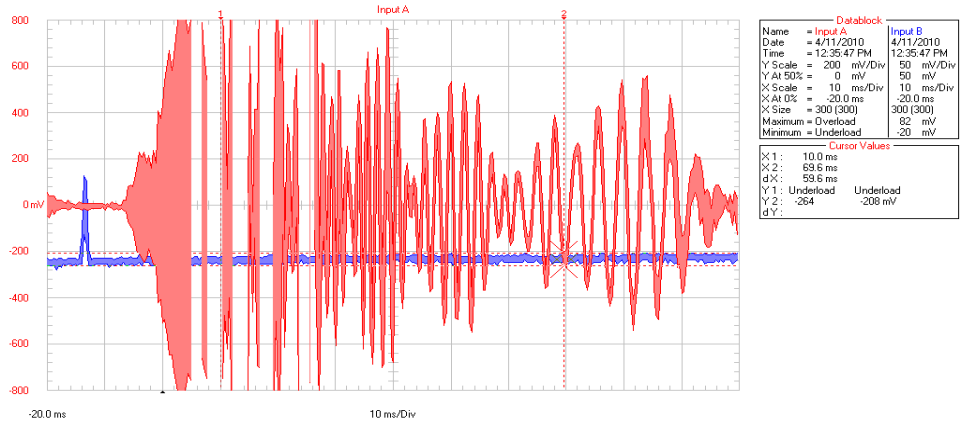

Figure 113: Excitation at $1.2\ m$ measured from load end, cable tension = 27.02 kN

Table 78: Calculated results from data of Figure 113

Aero-Z I. j	PX (ms)	PY (mV)	FREQ (Hz)	ln PY	Yj	(lnPY)Yj	Yj^2	b	a	Zj	LogDec	Zeta		NatFreq (rad/s)	NatFreq (Hz)
1	38.8	768		6.64	0	0.00	0	6.73	-0.647	6.73	0.647	0.102	0.0016	3927	625.0
2	40.8	552	500	6.31	1	6.31	1			6.08					
3	42.4	184	625	5.21	2	10.43	4			5.43					
4	43.6	128	833	4.85	3	14.56	9			4.78					
SUM		1632		23.02	6	31.30	14								

Using least squares method, log-dec = 0.647, zeta = 0.102, frequency of decaying oscillation = 3927.0rad/s (625Hz)

Aero-Z I. j	PX (ms)	PY (mV)	FREQ (Hz)	ln PY	Yj	(lnPY)Yj	Yj^2			Zj	LogDec	Zeta		NatFreq (rad/s)	NatFreq (Hz)
1	50	536		6.28	0	0.00	0	6.53	-0.357	6.53	0.357	0.057	0.0023	2732	434.8
2	52.4	528	417	6.27	1	6.27	1			6.17					
3	54.8	480	417	6.17	2	12.35	4			5.82					
4	57.2	232	417	5.45	3	16.34	9			5.46					
5	59.2	136	500	4.91	4	19.65	16			5.10					
SUM		1912		29.09	10	54.608	30								

Using least squares method, log-dec = 0.375, zeta = 0.057, frequency of decaying oscillation = 2731.8 rad/s (434.8 Hz)

Tension 27.02 kN with one mass absorber damper

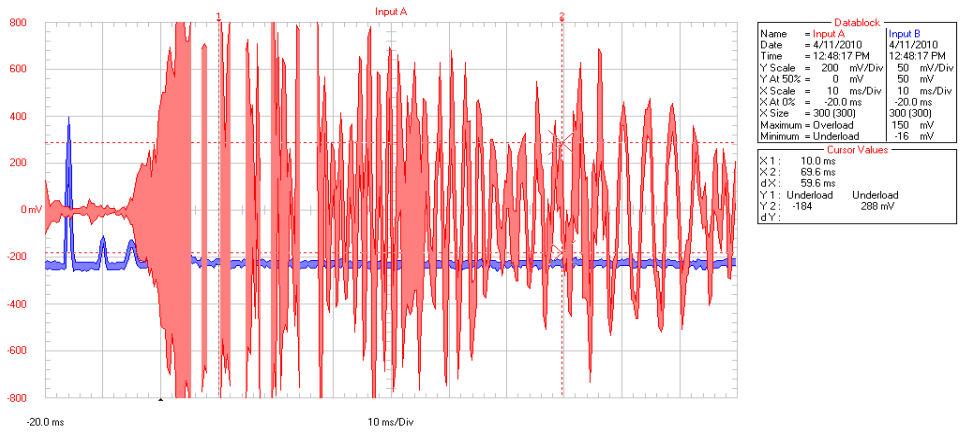

Figure 114: Excitation at $1.2\ m$ measured from load end, cable tension = 27.02 kN

Table 79: Calculated results from data of Figure 114

Aero-Z j	PX (ms)	PY (mV)	FREQ (Hz)	ln PY	Yj	(lnPY)Y	Yj^2	b	a	Zj	LogDec	Zeta	Period	NatFrec (rad/s)	NatFreq (Hz)
1	36.4	784		6.66	0	0.0	0	12.31	-1.38	12.31	1.380	0.21	0.002	4134	658
2	37.6	592	833	6.38	1	6.4	1			10.93					
3	39.6	696	500	6.55	2	13.1	4			9.55					
4	41.2	664	625	6.50	3	19.5	9			8.17					
5	42.8	488	625	6.19	4	24.8	16			6.79					
6	44	632	833	6.45	5	32.2	25			5.41					
7	45.6	480		6.17	6	37.0	36								
SUM		4336		44.90	21	133.0	91								

Using least squares method, log-dec = 1.380, zeta = 0.21, frequency of decaying oscillation = 4134 rad/s (658 Hz)

Aero-Z j	PX (ms)	PY (mV)	FREQ (Hz)	ln PY	Yj	(lnPY)Y	Yj^2			Zj	LogDec	Zeta		NatFrec (rad/s)	NatFreq (Hz)
1	50.4	680		6.52	0	0.0	0	6.60	-0.25	6.60	0.251	0.04	0.003	2513	400
2	52.8	632	417	6.45	1	6.4	1			6.35					
3	55.2	472	417	6.16	2	12.3	4			6.10					
4	57.6	304	417	5.72	3	17.2	9			5.85					
5	60.4	280	357	5.63	4	22.5	16			5.59					
SUM		2368		30.48	10	58.5	30								

Using least squares method, log-dec = 0.251, zeta = 0.040, frequency of decaying oscillation = 2513 rad/s (400 Hz)

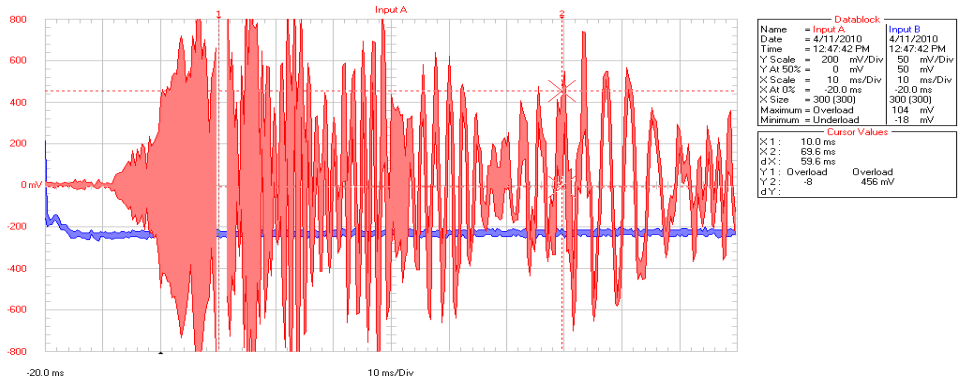

Figure 115: Excitation at $1.2\ m$ measured from load end, cable tension = 27.02 kN

Table 80: Calculated results from data of Figure 115

Aero-Z l j	PX (ms)	PY (mV)	FREQ (Hz)	ln PY	Yj	(lnPY)Yj	Yj^2	b	a	Zj	LogDec	Zeta	Period	NatFreq (rad/s)	NatFreq (Hz)
1	23.2	904		6.81	0	0.00	0	6.81	-0.216	6.81	0.216	0.034	0.0014	4620	735
2	24.4	848	833	6.74	1	6.74	1			6.60					
3	25.6	592	833	6.38	2	12.77	4			6.38					
4	23.2	336	-416.7	5.82	3	17.45	9			6.17					
5	28.4	448	192.3	6.10	4	24.42	16			5.95					
6	30	328	625.0	5.79	5	28.97	25			5.74					
SUM		3456		37.648	15	90.35	55								

Using least squares method, log-dec = 0.216, zeta = 0.034, frequency of decaying oscillation = 4620 rad/s (735 Hz)

Aero-Z l j	PX (ms)	PY (mV)	FREQ (Hz)	ln PY	Yj	(lnPY)Yj	Yj^2	b	a	Zj	LogDec	Zeta	Period	NatFreq (rad/s)	NatFreq (Hz)
1	38.4	828		6.72	0	0.00	0	2.63	-0.168	2.63	0.168	0.027	0.0026	2417	385
2	40	440	625	6.09	1	6.09	1			2.46					
3	43.6	592	278	6.38	2	12.77	4			2.29					
SUM		1860		19.189	3	18.85	5								

Using least squares method, log-dec = 0.168, zeta = 0.027, frequency of decaying oscillation =2417 rad/s (385 Hz)

Tension 27.02 kN with two mass absorber dampers

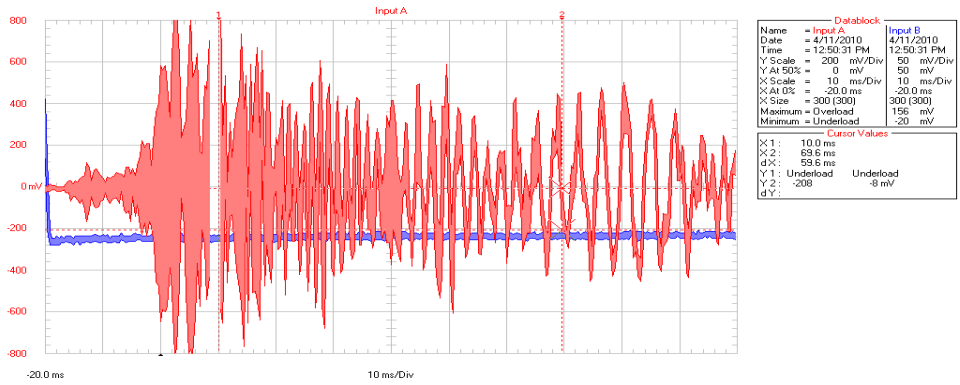

Figure 116: Excitation at $1.2\ m$ measured from load end, cable tension = 27.02 kN

Table 81: Calculated results from data of Figure 116

Aero-Z j	PX (ms)	PY (mV)	FREQ (Hz)	ln PY	Yj	(lnPY)Yj	Yj^2	b	a	Zj	LogDec	Zeta	Period	NatFreq (rad/s)	NatFreq (Hz)
1	27.6	608		6.41	0	0.00	0	11.87	-1.38	11.87	1.38	0.21	0.0017	3740	595.24
2	29.2	496	625	6.21	1	6.21	1			10.49					
3	30.8	440	625	6.09	2	12.17	4			9.11					
4	32.4	392	625	5.97	3	17.91	9			7.73					
5	34	432	625	6.07	4	24.27	16			6.35					
6	36	352	500	5.86	5	29.32	25			4.97					
7	37.6	280		5.63	6	33.81	36								
SUM		3000		42.24	21	123.69	91								

Using least squares method, log-dec = 1.380, zeta = 0.21, frequency of decaying oscillation = 3740 rad/s (595.2 Hz)

Aero-Z j	PX (ms)	PY (mV)	FREQ (Hz)	ln PY	Yj	(lnPY)Yj	Yj^2			Zj	LogDec	Zeta		NatFreq (rad/s)	NatFreq (Hz)
1	49.6	592		6.38	0	0.00	0	6.3444	-0.30	6.34	0.30	0.047	0.0023	2732	435
2	51.6	384	500	5.95	1	5.95	1			6.05					
3	54.4	344	357	5.84	2	11.68	4			5.75					
4	56.8	224	417	5.41	3	16.23	9			5.45					
5	58.8	176	500	5.17	4	20.68	16			5.16					
SUM		1720		28.76	10	54.55	30								

Using least squares method, log-dec = 0.297, zeta = 0.047, frequency of decaying oscillation = 2731.8 rad/s (434.8 Hz)

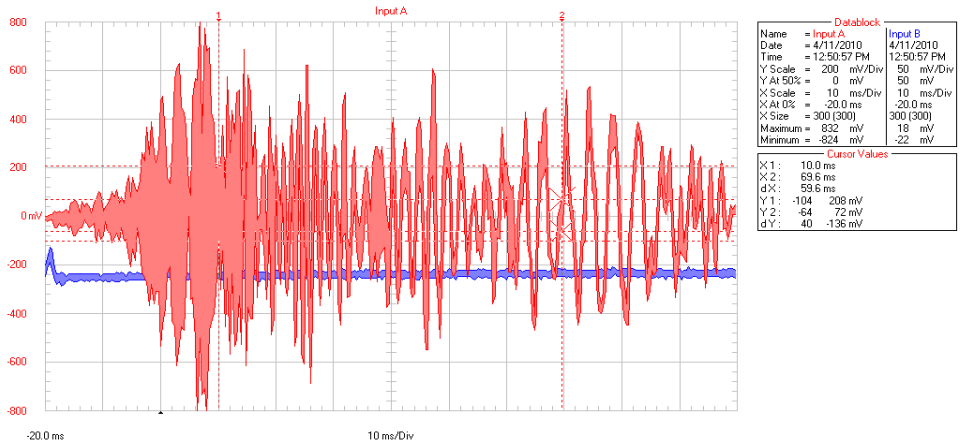

Figure 117: Excitation at $1.2\ m$ measured from load end, cable tension = 27.02 kN

Table 82: Calculated results from data of Figure 117

Aero-Z I j	PX (ms)	PY (mV)	FREQ (Hz)	ln PY	Yj	(lnPY)Yj	Yj^2	b	a	Zj	LogDec	Zeta	Period	NatFreq (rad/s)	NatFreq (Hz)
1	25.6	624		6.44	0	0.00	0	11.7	-1.39	11.74	1.39	0.22	0.0016	3927	625
2	26.8	376	833	5.93	1	5.93	1			10.35					
3	28.4	408	625	6.01	2	12.02	4			8.96					
4	30	296	625	5.69	3	17.07	9			7.57					
5	32	512	500	6.24	4	24.95	16			6.19					
6	33.6	280	625	5.63	5	28.17	25			4.80					
7	35.6	208		5.34	6	32.03	36								
SUM		2704		41.28	21	120.18	91								

using least squares method, log-dec = 1.39, zeta = 0.22, frequency of decaying oscillation = 3927 rad/s (625 Hz)

Aero-Z I j	PX (ms)	PY (mV)	FREQ (Hz)	ln PY	Yj	(lnPY)Yj	Yj^2			Zj	LogDec	Zeta		NatFreq (rad/s)	NatFreq (Hz)
1	47.2	608		6.41	0	0.00	0	6.38	-0.47	6.38	0.47	0.074	0.0024	2618	417
2	49.6	304	417	5.72	1	5.72	1			5.91					
3	52	304	417	5.72	2	11.43	4			5.44					
4	54.4	128	417	4.85	3	14.56	9			4.97					
SUM		1344		22.70	6	31.71	14								

Using least squares method, log-dec = 0.467, zeta = 0.074, frequency of decaying oscillation = 2618 rad/s (416.7Hz)

APPENDIX IV

RESULTS FOR FORCED VIBRATION METHOD ON AERO-Z IEC62219-REV240609 CONDUCTOR

Tension 24.01 kN without mass absorber dampers

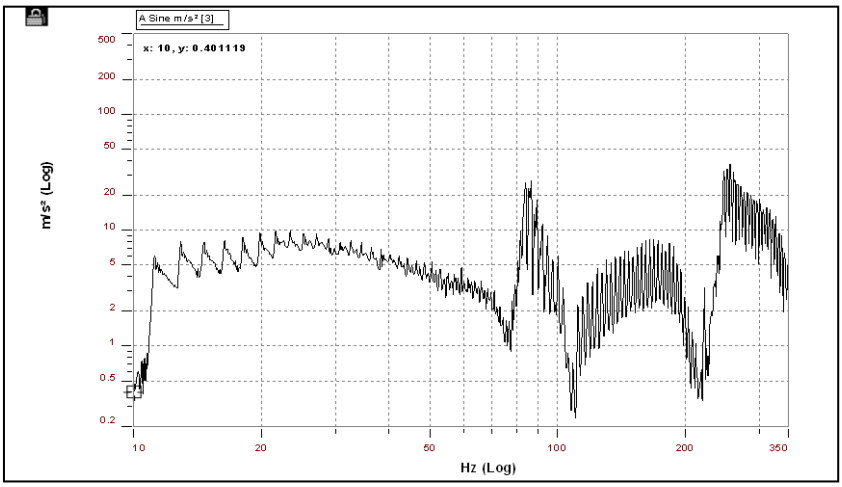

Figure 118: Sweep test from spectral dynamic viewer
(Data extracted from the accelerometer positioned at mid-span)

Figure 118 shows the results from the sweep test plotted by the spectral dynamic viewer of the PUMA system for a cable tension of 24.01kN. The results were captured from the accelerometer positioned at mid-span of the Aero-Z IEC62219-REV240609 conductor.

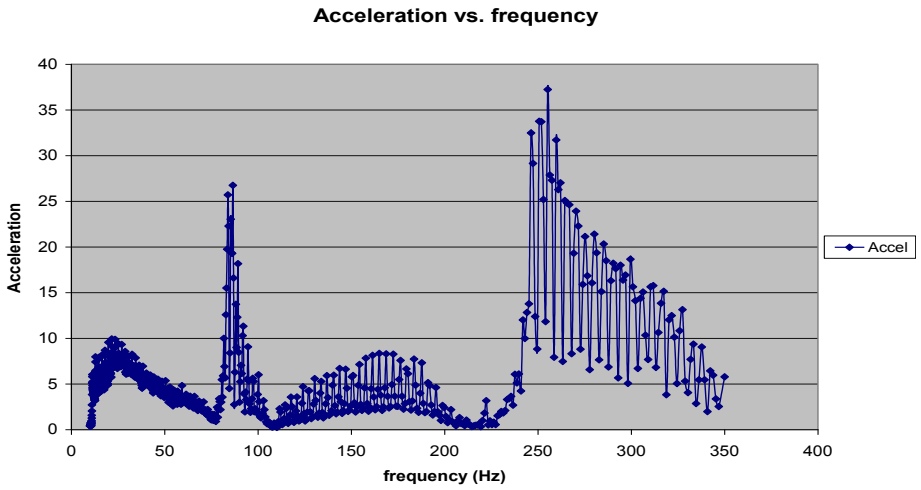

Figure 119: Sweep test extracted from Microsoft Excel data
(Channel 15 represents data from the accelerometer at mid-span)

Figure 119 is a graph of acceleration versus frequency obtained from the results of the spreadsheet data extracted from the PUMA system for a cable tension of 29.56 kN. The same graph appears in the spectral dynamic viewer as shown in Figure 118. This spreadsheet graph is more amenable to analysis (see Section 6.3.1).

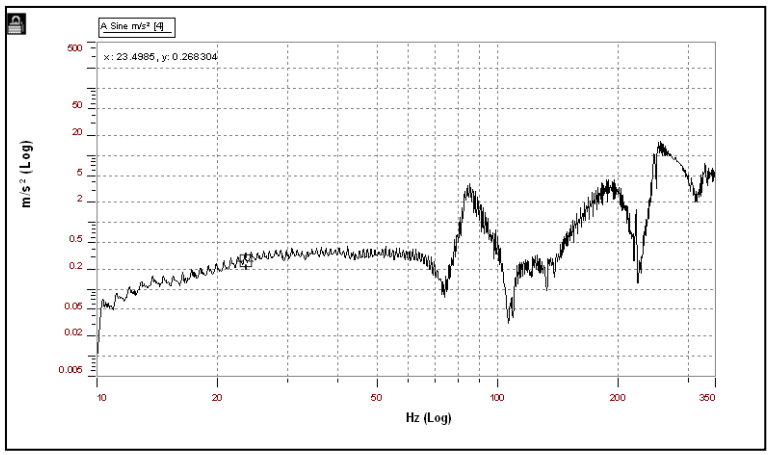

Figure 120: Sweep test from spectral dynamic viewer
(Data extracted from the accelerometer positioned at end-span)

Figure 120 shows the results from the sweep test plotted by the spectral dynamic viewer of the PUMA system for a cable tension of 24.01kN. The results were captured from the accelerometer positioned at end-span of the Aero-Z IEC62219-REV240609 conductor.

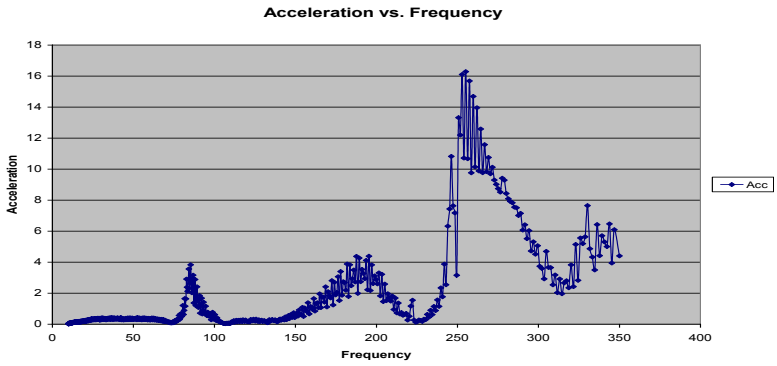

Figure 121: Sweep test extracted from Microsoft Excel data
(Channel 15 represents data from the accelerometer at end-span)

Figure 121 is a graph of acceleration versus frequency obtained from the results of the spreadsheet data extracted from the PUMA system for a cable tension of 29.56 kN. The same graph appears in the spectral dynamic viewer as shown in Figure 120. This spreadsheet graph is more amenable to analysis (see Section 6.3.1).

Tension 24.01 kN with one mass absorber damper

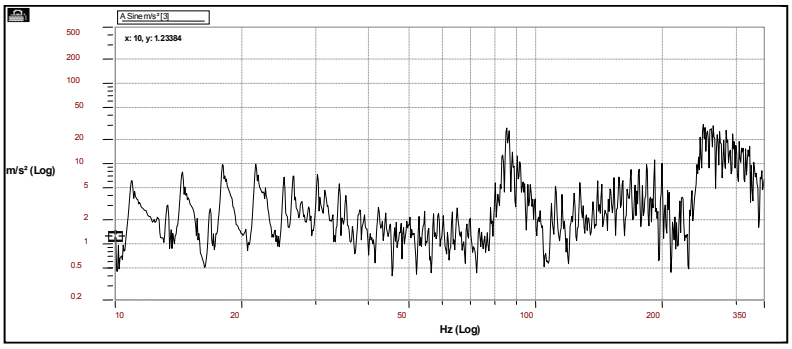

Figure 122: Sweep test from spectral dynamic viewer
(Data extracted from the accelerometer positioned at mid-span)

Figure 122 shows the results from the sweep test plotted by the spectral dynamic viewer of the PUMA system for a cable tension of 24.01kN. The results were captured from the accelerometer positioned at mid-span of the Aero-Z IEC62219-REV240609 conductor.

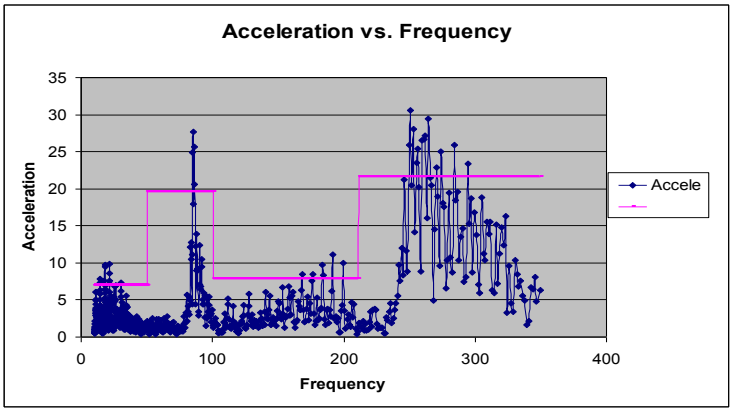

Figure 123: Sweep test extracted from Microsoft Excel data
(Channel 15 represents data from the accelerometer at mid-span)

Figure 123 is a graph of acceleration versus frequency obtained from the results of the spreadsheet data extracted from the PUMA system for a cable tension of 29.56 kN. The same graph appears in the spectral dynamic viewer as shown in Figure 122. This spreadsheet graph is more amenable to analysis (see Section 6.3.1).

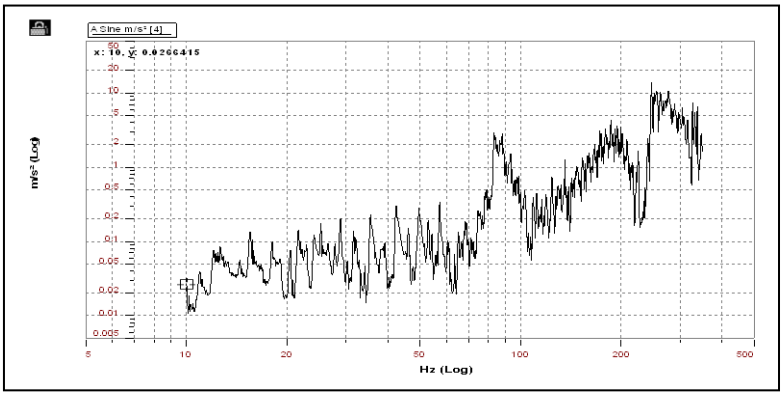

Figure 124: Sweep test from spectral dynamic viewer
(Data extracted from the accelerometer positioned at end-span)

Figure 124 shows the results from the sweep test plotted by the spectral dynamic viewer of the PUMA system for a cable tension of 24.01kN. The results were captured from the accelerometer positioned at end-span of the Aero-Z IEC62219-REV240609 conductor.

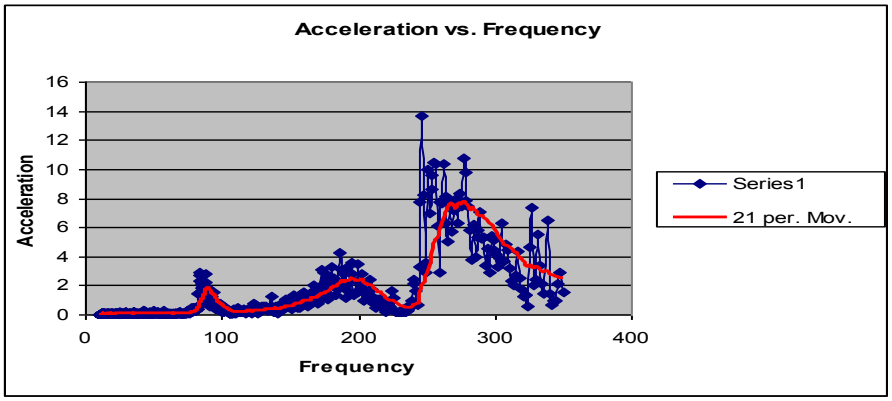

Figure 125: Sweep test extracted from Microsoft Excel data
(Channel 15 represents data from the accelerometer at mid-span)

Figure 125 is a graph of acceleration versus frequency obtained from the results of the spreadsheet data extracted from the PUMA system for a cable tension of 29.56 kN. The same graph appears in the spectral dynamic viewer as shown in Figure 124. This spreadsheet graph is more amenable to analysis (see Section 6.3.1).

Tension 24.01 kN with two mass absorber dampers

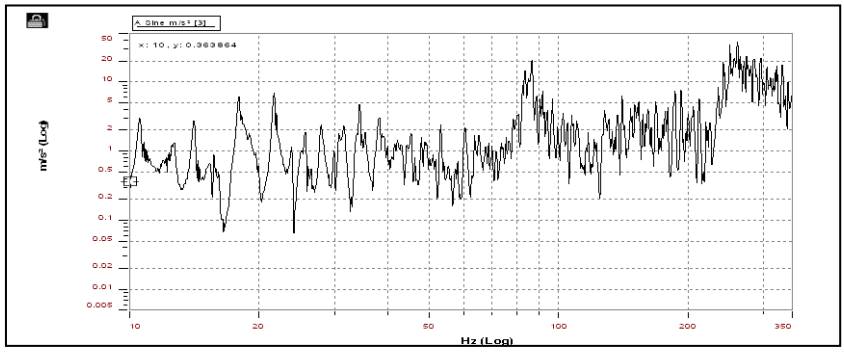

Figure 126: Sweep test from spectral dynamic viewer
(Data extracted from the accelerometer positioned at mid-span)

Figure 126 shows the results from the sweep test plotted by the spectral dynamic viewer of the PUMA system for a cable tension of 24.01kN. The results were captured from the accelerometer positioned at mid-span of the Aero-Z IEC62219-REV240609 conductor.

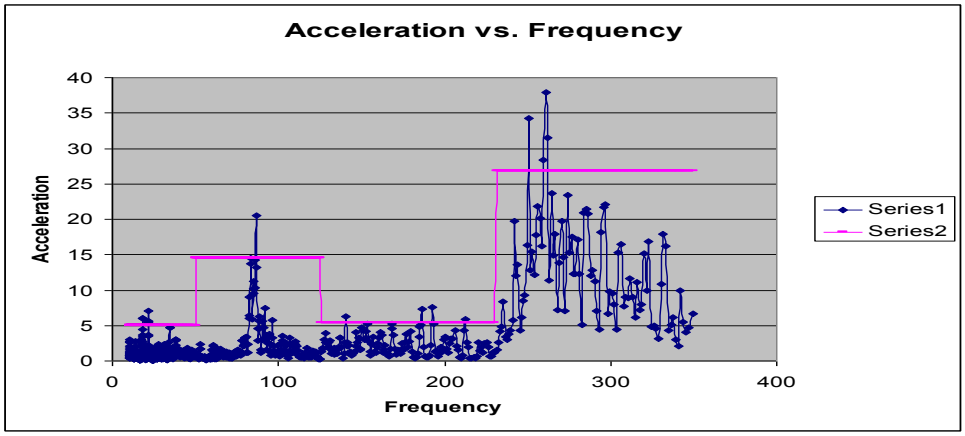

Figure 127: Sweep test extracted from Microsoft Excel data
(Channel 15 represents data from the accelerometer at mid-span)

Figure 127 is a graph of acceleration versus frequency obtained from the results of the spreadsheet data extracted from the PUMA system for a cable tension of 29.56 kN. The same graph appears in the spectral dynamic viewer as shown in Figure 126. This spreadsheet graph is more amenable to analysis (see Section 6.3.1).

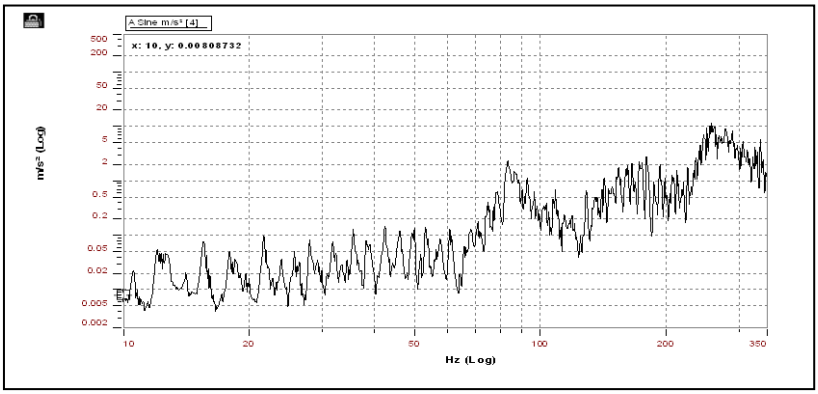

Figure 128: Sweep test from spectral dynamic viewer
(Data extracted from the accelerometer positioned at end-span)

Figure 128 shows the results from the sweep test plotted by the spectral dynamic viewer of the PUMA system for a cable tension of 24.01kN. The results were captured from the accelerometer positioned at end-span of the Aero-Z IEC62219-REV240609 conductor.

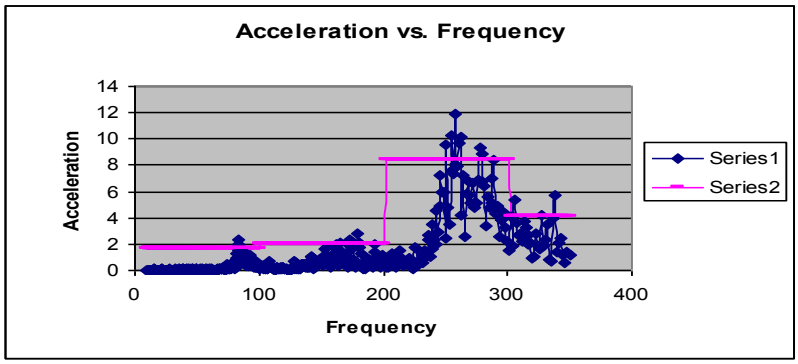

Figure 129: Sweep test extracted from Microsoft Excel data
(Channel 15 represents data from the accelerometer at mid-span)

Figure 129 is a graph of acceleration versus frequency obtained from the results of the spreadsheet data extracted from the PUMA system for a cable tension of 29.56 kN. The same graph appears in the spectral dynamic viewer as shown in Figure 128. This spreadsheet graph is more amenable to analysis (see Section 6.3.1).

Tension 27.02 kN without mass absorber dampers

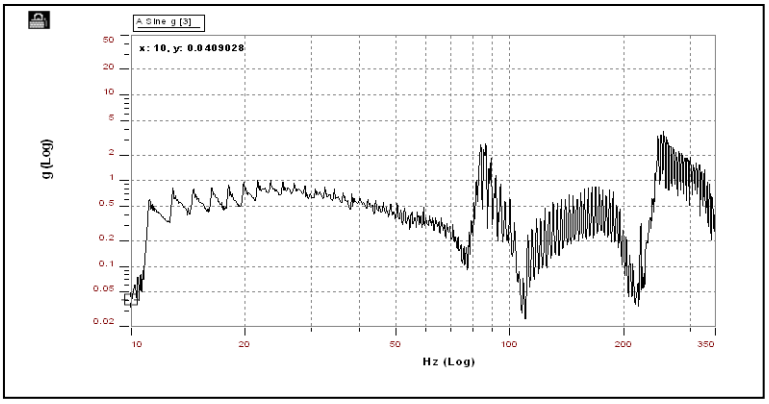

Figure 130: Sweep test from spectral dynamic viewer
(Data extracted from the accelerometer positioned at mid-span)

Figure 130 shows the results from the sweep test plotted by the spectral dynamic viewer of the PUMA system for a cable tension of 27.02kN. The results were captured from the accelerometer positioned at mid-span of the Aero-Z IEC62219-REV240609 conductor.

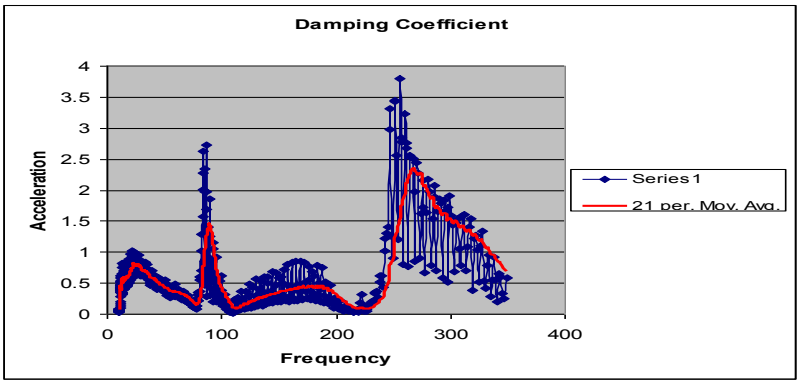

Figure 131: Sweep test extracted from Microsoft Excel data
(Channel 15 represents data from the accelerometer at mid-span)

Figure 131 is a graph of acceleration versus frequency obtained from the results of the spreadsheet data extracted from the PUMA system for a cable tension of 29.56 kN. The same graph appears in the spectral dynamic viewer as shown in Figure 130. This spreadsheet graph is more amenable to analysis (see Section 6.3.1).

Tension 27.02 kN with one mass absorber damper

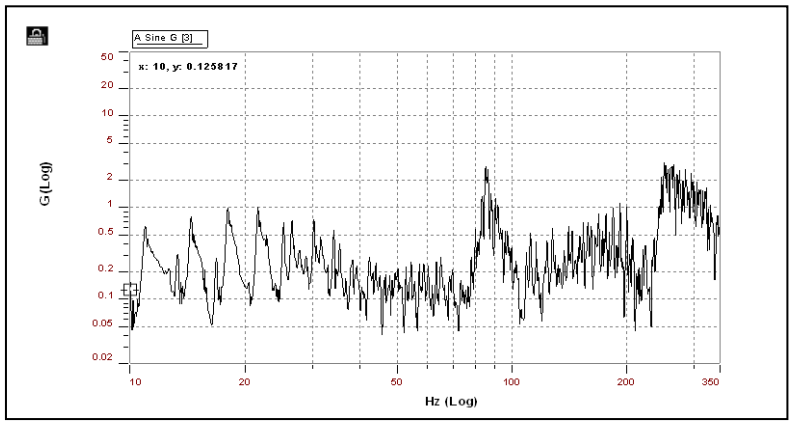

Figure 132: Sweep test from spectral dynamic viewer
(Data extracted from the accelerometer positioned at mid-span)

Figure 132 shows the results from the sweep test plotted by the spectral dynamic viewer of the PUMA system for a cable tension of 24.01kN. The results were captured from the accelerometer positioned at mid-span of the Aero-Z IEC62219-REV240609 conductor.

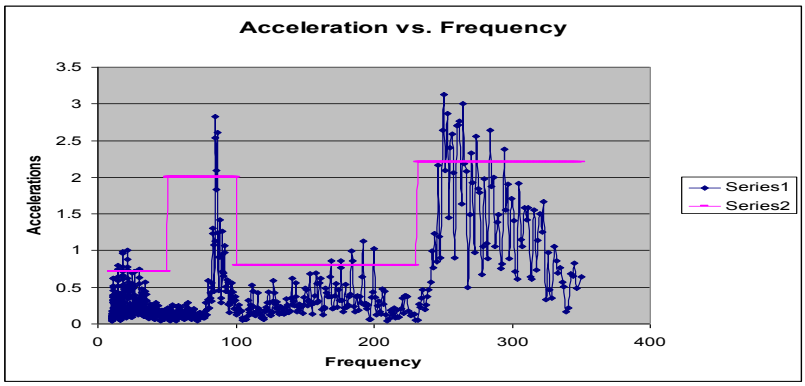

Figure 133: Sweep test extracted from Microsoft Excel data
(Channel 15 represents data from the accelerometer at mid-span)

Figure 133 is a graph of acceleration versus frequency obtained from the results of the spreadsheet data extracted from the PUMA system for a cable tension of 29.56 kN. The same graph appears in the spectral dynamic viewer as shown in Figure 132. This spreadsheet graph is more amenable to analysis (see Section 6.3.1).

Tension 27.02 kN with two dampers

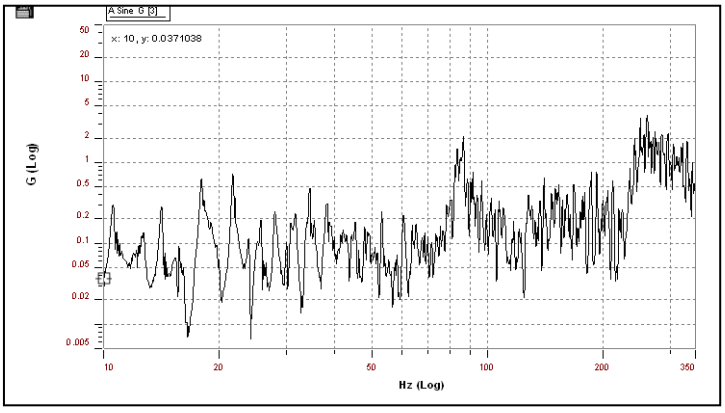

Figure 134: Sweep test from spectral dynamic viewer
(Data extracted from the accelerometer positioned at mid-span)

Figure 134 shows the results from the sweep test plotted by the spectral dynamic viewer of the PUMA system for a cable tension of 27.02kN. The results were captured from the accelerometer positioned at mid-span of the Aero-Z IEC62219-REV240609 conductor.

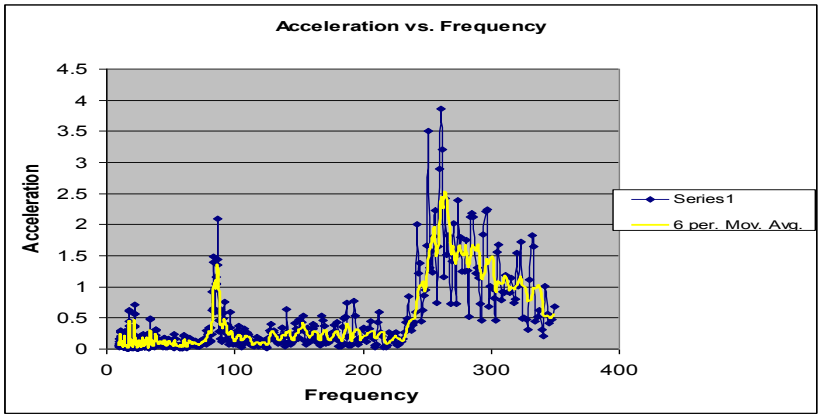

Figure 135: Sweep test extracted from Microsoft Excel data
(Channel 15 represents data from the accelerometer at mid-span)

Figure 135 is a graph of acceleration versus frequency obtained from the results of the spreadsheet data extracted from the PUMA system for a cable tension of 29.56 kN. The same graph appears in the spectral dynamic viewer as shown in Figure 134. This spreadsheet graph is more amenable to analysis (see Section 6.3.1).

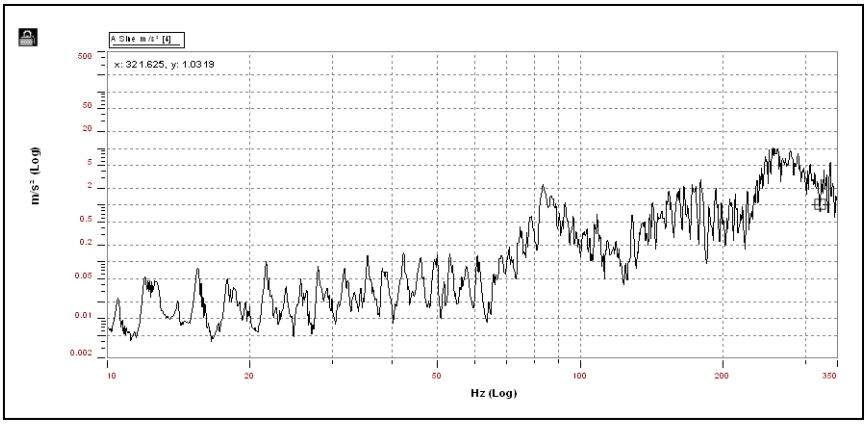

Figure 136: Sweep test from spectral dynamic viewer
(Data extracted from the accelerometer positioned at mid-span)

Figure 136 shows the results from the sweep test plotted by the spectral dynamic viewer of the PUMA system for a cable tension of 27.0kN. The results were captured from the accelerometer positioned at end-span of the Aero-Z IEC62219-REV240609 conductor.

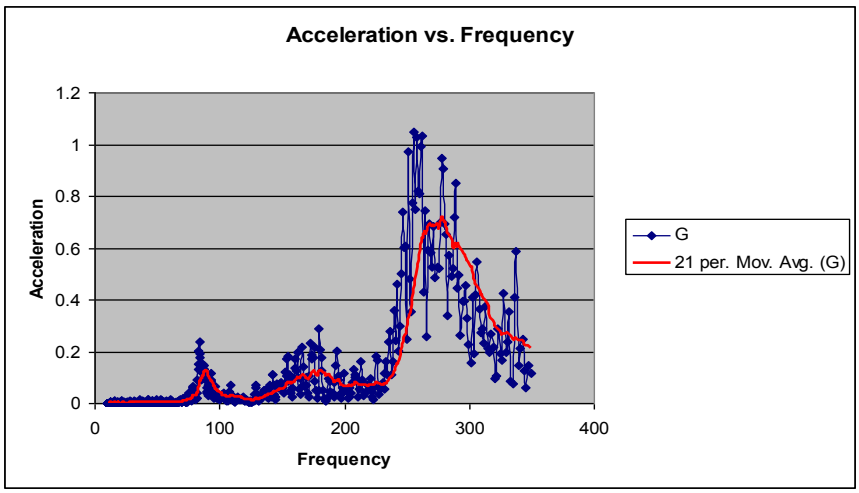

Figure 137: Sweep test extracted from Microsoft Excel data
(Channel 15 represents data from the accelerometer at mid-span)

Figure 137 is a graph of acceleration versus frequency obtained from the results of the spreadsheet data extracted from the PUMA system for a cable tension of 29.56 kN. The same graph appears in the spectral dynamic viewer as shown in Figure 136. This spreadsheet graph is more amenable to analysis (see Section 6.3.1).

APPENDIX V

CALCULATION OF RESULTS FOR INITIAL CONFIGURATION OF CONDUCTOR

From Figure 7, the initial conductor configurations may be calculated as detailed below.

For a **parabolic cable**:

At mid-span: Using equation (3.8)

$$T_{\max} = wl_A\sqrt{1+(l_A/2h_A)^2}$$

$$20730 = 1.34\times 9.81\times 42.3\sqrt{1+(42.3/(2\times h_A)^2}$$

$$\therefore h_{\max} = h_A = 56.7\,cm \text{ at midspan}$$

At ¼ span: Deriving the expression using equations (3.5) and (3.8) we find that

$$h_A = h_{\max} - y_A = h_{\max} - \frac{wx_A^2}{2T_0} \qquad (1)$$

$$h_{1/4} = h_{\max} - \frac{wx_{1/4}^2}{2T_0}$$

$$= 0.567 - \frac{(1.34\times 9.81)21.15^2}{2(20730)}$$

$$= 42.5\,cm$$

Similarly, at ⅛ span:

$$h_{1/8} = h_{\max} - \frac{wx_{3/8}^2}{2T_0}$$

$$= 0.567 - \frac{(1.34\times 9.81)31.725^2}{2(20730)}$$

$$= 24.8cm$$

For **catenary cable**:

At mid-span: Using equation (3.14) $h_{\max} = y$ at mid-span

$$h_{\max} = \frac{T_0}{\mu}\left(\cosh\frac{\mu x}{T_0} - 1\right)$$

$$h_{\max} = \frac{20730}{(1.34\times 9.81)}\left(\cosh\frac{(1.34\times 9.81)42.3}{20730} - 1\right)$$

$$\therefore h_{\max} = 56.7\,cm$$

At ¼ span: Deriving the expression using equation (3.14) we find that

$$h_A = h_{\max} - y_A = h_{\max} - \frac{T_0}{\mu}\left(\cosh\frac{\mu x_A}{T_0} - 1\right) \qquad (2)$$

$$h_{1/4} = h_{\max} - \frac{T_0}{\mu}\left(\cosh\frac{\mu x_{1/4}}{T_0} - 1\right)$$

$$= 0.567 - \frac{20730}{(1.34\times 9.81)}\left(\cosh\frac{(1.34\times 9.81)21.15}{20730} - 1\right)$$

$$= 42.5\,cm$$

At ⅛ span: Using equation (2)

$$h_{1/8} = h_{\max} - \frac{T_0}{\mu}\left(\cosh\frac{\mu x_{3/4}}{T_0} - 1\right)$$
$$= 0.567 - \frac{20730}{(1.34\times 9.81)}\left(\cosh\frac{(1.34\times 9.81)31.725}{20730} - 1\right)$$
$$= 24.8\ cm$$

$$\%\ difference = \frac{calculated - measured}{calculated}\times 100\%$$
$$= \frac{(0.567 - 0.5555)}{0.567}\times 100\% \qquad (3)$$
$$= 2.03\%$$

Other calculated results appear in Table 83:

Table 83: Initial configurations – Calculated results

Position	Position (m)		Tension (N)	
Span	84.6	20730	25110	29560
		Sag (m)	Sag (m)	Sag (m)
1/2 Span	42.3	0.567	0.468	0.398
% difference at 1/2 Span		2.03	1.18	2.38
1/4 Span	21.2	0.426	0.351	0.298
% difference at 1/4 Span		3.88	2.70	1.00
1/8 Span	10.6	0.248	0.205	0.174
% difference at 1/8 Span		9.88	11.22	17.40
Max Tension (N)		20737	25116	29565
Max Length (m) at x=L	84.6	84.641	84.628	84.620
Parabolic cable				
		Sag (m)	Sag (m)	Sag (m)
1/2 Span	42.3	0.567	0.468	0.398
1/4 Span	21.2	0.425	0.351	0.298
1/8 Span	10.6	0.248	0.205	0.174

As shown in Tables 5 and 83, the measured and calculated configurations are in good agreement, with a smallest error of $\varepsilon = 1.00\%$ and largest error of $\varepsilon = 11.22\%$. In general, the difference is smallest at mid-span.